Homeostasis drives intense microbial trace metal processing on marine particles

Pavla Debeljak, Stéphane Blain, Andrew Bowie, Pier Merwe, Barbara Bayer, Ingrid Obernosterer

Scientific Significance Statement Topic

In the ocean, particles represent a large reservoir of metals essential for life. Microorganisms inhabiting particles can potentially access this resource with antagonist consequences. The acquisition of some trace elements could be beneficial whereas the presence of others could be deleterious. A multi-element investigation of the microbial response embedding both perspectives is, however, still lacking. The present study provides evidence for the processing of nine particulate trace metals in multiple manners by diverse microbial communities. An overarching mechanism essential for life, homeostasis, provides a conceptual framework to explain this observation.

Scientific Significance Statement Outlet

We consider our work presents a conceptual advance in an important topic of marine biogeochemistry. The use of metatranscriptomics is key in our study as it provides insights that can presently not be obtained by any other chemical or microbiological approach. Given the Special Issue â€œLinking Metagenomics to Aquatic Microbial Ecologyâ€ published this year and the companion Editorial by D. Kirchman we think that our manuscript is timely and of interest to the readership of L&O.

Accepted MS

Homeostasis drives intense microbial trace metal processing on marine particles

Pavla Debeljak [1,2]†, Stéphane Blain [1], Andrew Bowie [3,4], Pier van der Merwe [4,5], Barbara Bayer[2]§, and Ingrid Obernosterer [1*]

[1]Sorbonne Université, CNRS, Laboratoire d'Océanographie Microbienne, LOMIC, F-66650 Banyuls/mer, France

[2]University of Vienna, Department of Functional and Evolutionary Ecology, A-1090 Vienna, Austria

[3]Antarctic Climate and Ecosystem Co-operative Research Centre, University of Tasmania, 20 Castray Esp. Battery Point, Tasmania, Australia, 7004

[4] Institute of Marine and Antarctic Studies, University of Tasmania, 20 Castray Esp., Battery Point, Tasmania, Australia, 7004

[5] Antarctic Gateway Partnership, University of Tasmania, 20 Castray Esp. Battery Point, Tasmania, Australia, 7004

† present address: Institut de Systématique, Évolution, Biodiversité (ISYEB), Muséum National d'Histoire Naturelle, CNRS, Sorbonne Université UMR7205, BC 50 – RdC, France

§ present address: University of California, Santa Barbara, Department of Ecology, Evolution and Marine Biology, Santa Barbara, CA 93106-9620, USA

* Ingrid Obernosterer

Email: ingrid.obernosterer@obs-banyuls.fr

Keywords: trace metals, particles, metal bioavailability, metal homeostasis, marine microbes

Running head: Microbial homeostasis and particulate metals

Abstract

As marine microorganisms and environmental conditions co-evolved over geological timescales, metals have been incorporated into all essential metabolic processes. In the modern ocean, metals are present from trace amounts limiting microbial growth to toxic concentrations. Dissolved trace metals are a major bioavailable reservoir. However, the acquisition of metals from marine particles remains largely unexplored. Here, we combined chemical characterization and a comparative metatranscriptomics approach to investigate the availability of nine metals of biological importance on particles collected in the region of Heard Island (Indian sector of the Southern Ocean). Elemental ratios identified particulate matter as a potential source of metals for prokaryotes. The expression of genes for the uptake of metals through various mechanisms demonstrated that particles are a bioavailable reservoir. But genes involved in the control of resistance to metal toxicity, storage, sensing and regulation were also highly expressed. Our observations suggest that homeostasis associated with a diverse prokaryotic community is the overarching mechanism that enhances the trace element processing on particles. These results provide clues that microbial activity on particles is critical in the redistribution of trace elements between different fractions and chemical forms in the ocean.

Introduction

Among the 20 chemical elements that are essential for life, half of them, iron (Fe), manganese (Mn), cobalt (Co), nickel (Ni), copper (Cu), zinc (Zn), cadmium (Cd), molybdenum (Mo), vanadium (V), and tungsten (W) are metals (Williams and Fraústo Da Silva 2003; Wackett et al. 2004). Metalloproteins, requiring metals as cofactors, account for one third of all proteins (Wackett et al. 2004). Free metal ions are part of the metallome and the concentration of a given metal in the cytoplasm is markedly constant among cells, but it varies by several orders of magnitudes when different elements are considered (Williams and Fraústo Da Silva 2003). This results from the co-evolution of microorganisms and environmental conditions (Silva and Williams 2001; Saito et al. 2003).

In the modern ocean, microorganisms face the challenge of acquiring enough metals to sustain their metabolic demand. The most striking case is Fe for which the low availability limits present microbial activity in large oceanic regions (Martin et al. 1992; Tagliabue et al. 2017). Moreover, once a metal has entered the cell, it is critical that it integrates to the right protein to form an active enzyme (Waldron and Robinson 2009). Because metal affinities of proteins tend to follow the Irving-Williams series (Irving and Williams 1948), populating a protein with a metal with low affinity (e.g. Fe, Mn) in the presence of others with higher affinity (e.g. Cu, Zn) requires elaborate strategies involving sensors, transporters and stores. Therefore, metal homeostasis is critical for the survival of cells (Andrews et al. 2003; Waldron and Robinson 2009; Chandrangsu et al. 2017) and drives an intense trafficking of metals inside the cell and between the cell and its micro-scale environment.

The main reservoir of metals in the ocean is the operationally defined dissolved pool, which contains chemical species with a size (< 200 nm) compatible with the physical transport capabilities of membrane proteins. Such transport modes include uptake of ions via divalent ion transporters (Andrews et al. 2003), reductive-oxidative pathways (Strzepek et al. 2011; Lis et al. 2015), endocytosis after concentration of metals at the cell surface (McQuaid et al. 2018), uptake of colloids (Rich and Morel 1990) or uptake of organic complexes via specific transporters for heme (Hogle et al. 2017) or siderophores (Sandy and Butler 2009). Particles (> 200 nm) contain metals that can quantitatively equal or exceed the dissolved pool as is the case for Fe (Boyd and Ellwood 2010; van der Merwe et al. 2019), and thus represent a potential source. Rendering particulate metals accessible for microorganisms requires, however, preliminary transformations.

The determination of the bioavailability of metals is challenging, as not all the chemical forms are equally available to microorganisms. This is well illustrated in the case of Fe, for which a careful definition and determination of the bioavailability in the dissolved form has been proposed (Shaked and Lis 2012). However, for other trace metals and notably for their particulate forms the bioavailability is still poorly constrained. To address this issue, different approaches were proposed with a focus on Fe. The geochemical perspective relies on leaching protocols that sequentially separate different fractions (Rauschenberg and Twining 2015). A more biologically oriented approach consists in following changes in the chemical composition and the microbial activity during incubations. For example, the release of Fe-binding ligands coupled with an increase in dissolved Fe was observed in incubations amended with particles (Boyd et al. 2010; Velasquez et al. 2016). A third perspective is to investigate the metabolic response of microbial cells in the presence of particles. The expression of microbial Fe transporters in the vicinity of a hydrothermal plume suggested Fe of hydrothermal origin to be bioavailable to prokaryotes (Li et al. 2014). Moreover, biologically mediated dissolution of particles has been observed during their

transit through the gut of protozoans (Barbeau et al. 1996) and assisted dissolution by siderophores of bacterial origin has also been demonstrated (Rubin et al. 2011).

The patchiness within marine particles likely renders trace element distribution and dynamics distinct from those occurring in surrounding seawater. Microbial communities inhabiting particles encounter and shape concentration gradients of various elements, including trace metals, at the micrometer scale (Azam and Malfatti 2007; Stocker et al. 2008). How diverse microbial taxa deal with these multiple challenges, such as the access to various chemical forms of metals, handling metal excess and toxicity, and how in turn they shape element composition are unanswered questions. By combining chemical characterization of marine particles and the 'metallo'-metatranscriptome of a diverse prokaryotic community, we provide here a novel view on the microbial processing of trace metals on marine particles. We show enhanced transport into and out of the cell, sensing and regulation of nine metals of biological importance, carried out by a diverse microbial community inhabiting this reservoir of trace elements in the ocean.

Materials and Methods

Collection and chemical characterization of *in situ* particulate matter

The present study was carried out during the Heard Earth-Ocean-Biosphere Interactions (HEOBI) cruise (8 January - 27 February 2016) aboard the Australian R/V *Investigator* (voyage: IN 2016-V01). For the determination of the metal to phosphorus ratios, suspended particles were collected at 8 sites in the vicinity of Heard and McDonald Island and in High-Nutrient-Low-Chlorophyll (HNLC) waters in the Indian Sector of the Southern Ocean (Fig. S1)(van der Merwe et al. 2019). For the incubation experiment, particles were collected on January 29th 2016 in shallow waters

(overall depth 210 m) in the vicinity of McDonald Island (53.03 S, 72.55 E) (Fig. S1) at 100 m. All samples were collected by McLane high volume *in-situ* pumps (WTS-LV) fitted with dual filter holders and high efficiency baffles to reduce sample wash off upon retrieval. Sample handling, collection and processing were performed in accordance with the GEOTRACES 'Cookbook' protocols (https://www.geotraces.org/methods-cookbook/). Suspended particles for the incubations and the trace metal analysis were collected using paired, acid washed, 142 mm, 0.8 µm Supor filters to obtain a 0.4 µm effective pore size. The paired filters were then subsampled into 47 mm diameter punches. For the experimental incubation (see below), concentrated particle suspensions were prepared by rinsing off particles from 2 filter punches with each 20 mL of 0.2 µm-filtered seawater per filter, collected following trace-metal clean protocols. The remaining punches served for chemical analyses of the particulate matter. A chemical leach was used to separate the chemically refractory trace metal component of marine suspended particles from the chemically labile fraction (van der Merwe et al. 2019). Both fractions were analyzed by HR-ICP-MS (Thermo-Fisher Element 2) (Bowie et al. 2010). In the present study we only considered the sum of both fractions.

Incubation experiments with prokaryotic communities and particles

To investigate prokaryotic activity and gene expression patterns on marine particles, on-board incubation experiments were performed. Batch cultures, containing the ambient prokaryotic community (< 0.8 µm size fraction) and 0.2 µm-filtered seawater in a ratio of 1:10 (final volume 2L), were amended with particles and incubated for 12 days. Particles were collected at 100 m in the vicinity of McDonald Island (Fig. S1) as described above. Seawater for the < 0.2 µm- and < 0.8 µm-size fractions was collected in HNLC waters south of Heard Island (54.17 S, 73.67 E) at 45 m depth (Fig. S1), using trace-metal clean procedures. The filtrations were performed with

polycarbonate (PC, Nuclepore, 47 mmm) filters treated with a mild HCl-wash (0.1 N) and several rinses with Milli-Q water. Particles were added to the cultures from the suspension described above (6.5 mL of suspension to 2L of batch culture). Batch cultures without particle addition served as controls. Five replicate particle-amended cultures were prepared and the control incubations were done in quadruplicates. To keep the particles in suspension, we used gentle magnetic stirring. The cultures were kept in PC carboys, in the dark in a temperature-controlled incubator at 8°C. All steps of the preparation of the cultures were done under a trace-metal clean laminar flow hood (ISO class 5).

During the 12d incubation period, the cultures were subsampled every 2-3 days for prokaryotic abundance and heterotrophic production, and the particle size distribution and enumeration of prokaryotes attached to individual particles was carried out at the beginning and the end of the incubation. Samples for metatranscriptomics and prokaryotic community composition were collected at the final time point of the incubation. For the differential expression analysis (see below), the metatranscriptomes of the prokaryotic community attached to particles (> 0.8 μm fraction in the particle-amended treatment) were compared to those obtained from prokaryotes in the < 0.8 μm fraction of the control, considered as bulk community in particle-free HNLC water.

Determination of particle size distribution and enumeration of heterotrophic prokaryotes

For microscopic observations of the particles and the enumeration of particle-attached cells (Fig. S2), 20 mL subsamples of the batch cultures were filtered onto 0.8 μm PC filters (Nuclepore, 25 mm), and the filters were placed on pads (Millipore) soaked with 5% paraformaldehyde (PFA) overnight at 4°C. The filters were then rinsed with 0.2 μm filtered Milli-Q water and dried prior to storage in petri dishes at -20°C. Back in the home laboratory, each filter was split into 6 pieces,

and stained with DAPI for microscopic observations using an Olympus AX70 epifluorescence microscope equipped with an image analyses system (Cottrell and Kirchman 2000). For each observation, two images were acquired. One image was obtained by bright-field microscopy, and another image using excitation with blue light. The images were then processed with the open platform scientific image analysis software Image J. The image obtained by excitation with blue light was used to count by eye the cells attached to the different particles. The image obtained from bright-field microscopy was split into three channels (green, blue and red) in Image J. The red image presented the best characteristics (brightness, contrast) for the determination of the surface area of the particles. The particles were contoured and the surface determined after calibration of the pixel size. For each replicate, at least 100 particles were observed on different randomly selected parts of the filter. For each particle, the surface area and the number of attached prokaryotic cells were recorded to estimate the size distribution of the particles and the areal cell abundance. Prokaryotic abundance of the bulk community and in the < 0.8 µm fraction were enumerated by flow cytometry. Subsamples (1.8 mL) were fixed with glutaraldehyde (1% final concentration), incubated for 30min at 4°C and stored at -80°C. Cells were stained with SYBRGreen I and enumerated on a BD FACS Canto flow cytometer equipped with an air-cooled laser, providing 15mW at 488 nm with the standard filter set-up as described previously (Obernosterer et al. 2008).

Prokaryotic heterotrophic production

Prokaryotic production was estimated by ^{3}H leucine incorporation applying the centrifugation method, with minor modifications (Obernosterer et al. 2008). Prokaryotic production was determined for the bulk community (unfiltered water from the batch cultures) and in the < 0.8 µm size fraction, the latter considered as free-living community. The difference in prokaryotic

184 heterotrophic production between these fractions was considered as particle-attached production.
185 Prior to the incubation with leucine, subsamples of each culture were filtered through a 0.8 μm
186 PC filter (Nuclepore, 25 mm diameter) that was treated with a mild HCl-wash (0.1 N) and several
187 rinses with Milli-Q water. Briefly, 1.5 mL samples were incubated with a mixture of [3,4,5-
188 ^{3}H(N)] leucine (Perkin Elmer, 123.8 Ci mmol^{-1}; 7 nM final concentration) and nonradioactive
189 leucine (13 nM final concentration). Controls were fixed with trichloroacetic acid (TCA; Sigma)
190 at a final concentration of 5%. Samples were incubated for 2-3h in the dark. Incubations were
191 terminated with TCA (5% final concentration). The radioactivity incorporated into prokaryotic
192 cells was measured aboard in a HIDEX 300 SL liquid scintillation counter.

193

194 **Sampling for metatranscriptomics and prokaryotic diversity**

195 At the final time point of the experiment, 500 mL of each of three replicate cultures were
196 sequentially filtered on 0.8 μm and 0.2 μm PC filters (Nuclepore, 47 mm), and the filters were
197 stored at -80°C until further analysis. For metatranscriptomics and prokaryotic community
198 composition, two separate filters for each biological replicate were used for the extraction of
199 RNA (metatransriptomic analysis) and DNA (amplicon sequencing). Methods for nucleic acid
200 extraction and amplicon sequencing used to describe prokaryotic community composition are
201 provided in Supplementary Materials.

202

203 **RNA Extraction with customized standards**

204 RNA was extracted according to a previously published protocol (Angel et al. 2012) with the
205 following modifications for the use of filters. Tubes containing the filters (2ml Eppendorf tubes)

were submerged in liquid nitrogen and the filters were ground into small pieces with a sterile metal spatula. To each sample, 750 µL phosphate buffer (120 mM, pH 5.5) and 250 µL TNS buffer (500 mM Tris base, 100 mM NaCl, 10% SDS), and customized RNA standards (Supplementary Materials) were added to the filter pieces, and cells were lysed with 5x freeze and thaw cycles. After centrifuging at 20 000 x g at 4°C for 3 min, the supernatant was added to a fresh tube and one volume of TE saturated phenol (pH 5.5) was added. RNA was purified using standard phenol/chloroform/isoamyl alcohol and chloroform/isoamyl alcohol purification, and the supernatant was transferred to non-stick RNase-free microfuge tubes (Eppendorf). Nucleic acids were precipitated with 30% polyethylene glycol (PEG) in 1.6 M NaCl and 2 µL glycogen (Thermo Scientific), washed once with ice-cold 75% EtOH and resuspended in low TE buffer. DNA was digested with TURBO DNase (Ambion) and purified using the RNeasy MinElute Cleanup Kit (Qiagen). Complete DNA removal was validated via PCR amplification of 30 cycles and quality of RNA was checked with Bioanalyzer RNA chip profiles (Agilent Technologies, Santa Clara, CA, USA). The Ribo-Zero Gold rRNA Removal Kit (Epidemiology) was used to remove cytoplasmic and mitochondrial ribosomal RNA and sequencing was performed in pair-end using HiSeq (3000/4000) Illumina 2 × 150 bp chemistry on one full Illumina lane by Fasteris SA. Raw sequencing reads were deposited at the European Nucleotide Archive under Project number PRJEB38529.

Metatranscriptome read processing, assembly and annotation

The metatranscriptome shotgun libraries were prepared using a strand-specific protocol. An initial round of read processing was provided by the company, using trimmomatic (Bolger et al. 2014), an integrated quality-control tool for high-throughput Illumina NGS data. The standard Illumina adapters and low-quality bases were removed with the following parameters “2:30:10

SLIDINGWINDOW:4:5", and reads without inserts or reads for which ambiguities were found were also removed, resulting in 92 - 97% of 2×150 bp paired-end reads (average 24.5 ± 4.5 Mio reads per sample). Further, we performed another round of quality control and refinement with Trim Galore v0.5.0 (https://www.bioinformatics.babraham.ac.uk/projects/trim_galore/) for automatic detection and removal of overrepresented adapters, using a phred score of 20 and a length cutoff of 50 bp. To focus on protein-coding RNAs, we computationally eliminated ribosomal RNAs and internal standards-derived reads using SortMeRNA v 2.1b (Kopylova et al. 2012). A BLASTN homology search (Altschul et al. 1990) against a custom database which consisted of representative prokaryotic rRNAs and tRNAs from NCBI RefSeq along with the template sequences of customized internal RNA standards, was also implemented using a bit score cut-off of 50 as suggested in previous studies (Satinsky et al. 2013).

Given that the same ambient prokaryotic community was used as an inoculum for all incubations, and prokaryotic genes rarely have introns, the reads from all samples were pooled together and used for co-assembly using MegaHit v1.2.7 (Li et al. 2015) with default parameters. The assembly yielded 819,328 contigs with an N50 of 577 bp. Contigs shorter than 300 bp were discarded from further analysis, and 732,369 contigs were retained. Genes were predicted using Prodigal v2.6.3(Hyatt et al. 2010). The resulting amino acid sequences (>100 aa) were taxonomically annotated by DIAMOND BLASTP against nr database (January 2019) with options "--more-sensitive -e 0.000001 -f 100 -k 1 -p 10" (Buchfink et al. 2015), and functionally annotated using eggNOG 5.0 (Huerta-Cepas et al. 2019) and GhostKOALA (Kanehisa et al. 2016b) with default parameters. The taxonomic affiliation resulted in 66% prokaryotic, 9% eukaryotic, 8% unassigned and 17% unaligned contigs. A total of 420,218 prokaryotic protein sequences were finally retrieved, among which 65 % could be assigned to KEGG orthologous (KO) groups (Kanehisa et al. 2016a).

254

255 **Gene differential expression and functional enrichment analyses**

256 Reads were mapped back to the assembled contigs using Bowtie2 (Langmead and Salzberg 2012)
257 with default parameters, resulting in an overall 54.3% recruitment rate. Reads that were aligned to
258 the selected prokaryotic gene features were counted using featureCounts
259 (http://bioinf.wehi.edu.au/featureCounts/) with the following parameters for strand specific reads
260 -F 'GTF' -t 'gene' -Q 1 -s2 -p -C (Liao et al. 2014). The R package DESeq2 (Love et al. 2014) was
261 used to perform differential expression analysis based on the count table generated by
262 'featureCounts'. One control sample had to be excluded from the further analysis as it was
263 significantly different from the triplicate set recruiting less reads than all other samples (DESeq
264 function Cooks distance). Differential expression analysis was thus calculated with a duplicate set
265 of control samples. We have used the Likelihood Ratio Test (LRT) as implemented in the
266 DESeq2 software (Love et al. 2014) to screen each gene for significant differences in normalized
267 transcript abundance between treatments (fitType: local). After adjusting for multiple testing, an
268 adjusted p-value of < 0.05 was used as threshold. The raw count data were summed by KO
269 numbers and normalized based on the count data of the internal standards by applying the
270 'controlGenes' option of the DESeq2 software to statistically test the dynamics of absolute
271 transcriptional activity as published elsewhere (Beier et al. 2018). A further normalization step
272 was performed in order to account for differences in the average feature length of each gene in
273 each sample using the 'normMatrix' option. Transcripts with a total count of less than 50 were
274 removed. Total transcripts per sample were calculated by multiplying reads of protein encoding
275 transcripts of the transcriptome library with the number of molecules of the internal standard
276 added to the samples; this value was then divided by the recovered reads of the internal standard
277 in the sequence library (Satinsky et al. 2013) as described in the Supplementary Materials.

278

279 **Metal-related transcript analysis**

280 KO numbers of metal related enzymes were retrieved by co-factor function on the bioinformatics
281 resource portal ExPASy (https://enzyme.expasy.org/enzyme-bycofactor.html). We note that this
282 co-factor function also retrieves metal transporters that are not enzymes with metals as co-factors.
283 We performed this analysis for Co^{2+}, Cob(II)alamin, cobalt cation, Cu cation, Cu^{2+}, Fe cation,
284 Fe^{2+}, Fe^{3+}, Ferriheme b, Fe-sulfur, Mo cation, Mn^{2+}, Ni^{2+}, Zn^{2+}, Cd and W. Transcripts annotated
285 for the specific KEGG were summed by treatment and relative transcript abundance was
286 calculated for taxa associated per KEGG and visualized in the R ComplexHeatmap package
287 (https://jokergoo.github.io/ComplexHeatmap-reference/book/)(Gu et al. 2016). Phylogenetic
288 groups were visualised on the family or lowest possible taxonomic level.

289

290 **Results**

291

292 Chemical analysis of the bulk particulate material collected at 8 sites in the region of Heard Island
293 (Indian sector of the Southern Ocean; Fig. S1) revealed that the ratios of Mo, Co, Cu, Ni, Zn, Mn
294 and Fe to phosphorus are in the range of or above those reported in the literature for heterotrophic
295 prokaryotes (Fig. 1a), identifying particulate matter as a potential source of these metals. The
296 particles used in the incubation experiment were sampled in the vicinity of the volcanic
297 McDonald island at 100m depth (53.03 S, 72.55 E; Fig. S1). We used microscopic observations
298 (Fig. S2) to characterize the particle surface area distribution in the range 25 to 1000 μm^2. The
299 abundance of particles decreased with surface area (Fig. 1b), while heterotrophic prokaryotes
300 determined on individual particles had an opposite trend (Fig. 1c), resulting in an overall constant
301 cell abundance per unit (μm^2) of surface area (Fig. 1d).

To investigate microbial processes on the particles, we performed an onboard experiment. The presence of particles resulted in two distinct phases of the response of the ambient prokaryotic community (< 0.8 μm size fraction). During phase 1, extending over the first 4 days of incubation, the initially high cell-specific prokaryotic production, as determined by ^{3}H leucine incorporation, decreased by 4-fold to reach values equal to those in seawater to which no particles were added (Fig. S3). Phase 1 is considered a transient microbial response to leaching products, released by particles upon their initial re-suspension in low-trace-metal seawater. During the following 8 days of the incubation (day 4 to day 12), cell-specific prokaryotic production remained stable. This second phase is considered a quasi-steady state, and was the focus of our study, including the metatranscriptomic analysis.

The particles were colonized by *in situ* prokaryotic communities and areal cell abundances did not change between the initial and the final time points of the incubation (Fig. S4). Our microscopic observations allowed us to determine the volumetric abundance of cells attached to particles of 0.61±0.40 x 10^{5} mL^{-1}. This compares to a bulk prokaryotic cell abundance of 2.65±0.2 x 10^{5} mL^{-1} in the particle-free control incubations. Particle-attached cells were highly active throughout the incubation period (Fig. S5), and at the final time point, cell-specific production of prokaryotes attached to particles (4.43 ± 1.03 amol leucine $cell^{-1}$ d^{-1}) exceeded that of prokaryotes in the particle-free control (0.30 ± 0.08 amol leucine $cell^{-1}$ d^{-1}) by 15-fold.

The prokaryotic community composition determined at the end of the incubations revealed that *Flavobacteriaceae*, *Rhodobacteraceae* and *Oceanospirillaceae* were abundant contributors (each ≈15% relative abundance on average) to the communities attached to particles (Fig. S6), and other observed families were *Halieaceae*, *Porticoccaceae*, *Moritellaceae*, *Planctomycetaceae* and *Verrucomicrobiaceae*. *Flavobacteriaceae* were also abundant members of the community in the

326 control incubations (≈19-21 %) and relative abundances of *Rhodobacteraceae* (≈ 5 %) and
327 *Oceanospirillaceae* (≈ 4-6 %) were lower. The higher contributions of SAR11 (15-20%), SAR92
328 (7-14%) and the OM43 clade (12 %) were distinct features of the communities in particle-free
329 control incubations.

330 To explore trace metal-related microbial processes on marine particles, we compared the gene
331 expression profiles between prokaryotic communities attached to particles and communities in the
332 control incubations. We focused on transcripts of KEGG orthologous (KO) genes related to the
333 metals Zn, Mn, Cu, Co, Ni, Cd, Mo, W, and Fe (Table S1). Of the 1125 non-redundant KO genes
334 retrieved, 476 KO gene transcripts were identified in our metatranscriptomic data set of which
335 386 KO gene transcripts were enhanced (Log2fold change > 1) in the inventory of the particle-
336 attached community as compared to that of prokaryotes in particle-free incubations (Table S2).
337 We focus in the following on the KO gene transcripts involved in metal transport into and out of
338 the cell (efflux), sensing, regulation, resistance and storage of the nine metals. The numerous KO
339 gene transcripts identified had enhanced relative (Fig. 2; Fig. S7) and absolute transcript
340 abundances (Fig. S8) in the particle-attached community as compared to that in the particle-free
341 control incubations. These included transcripts for transporters of Fe^{2+}, Fe^{3+}, Zn, Mn, Ni, Cd, Mo
342 and W. Some of these transporters are weakly selective cation carriers that cannot be associated
343 to a single metal (e.g. Mn/Zn/Fe, *tro*, *mnt*, *znu*). Transporters of organically complexed Fe
344 (siderophore receptors, *fiu*, Fe^{3+} dicitrate transport, *fecA*, ferric hydroxamate transport, *fhuC*) were
345 also enhanced on particles.

346 Genes involved in efflux and resistance (Fe, *fie*, Co, Zn, Cd, *czc*, *cus, cnr*), regulation (Fe, *fur* and
347 Zn, *zur*), sensing (two component system, Cu, *cop*) and storage (ferritin, *ftn*, bacterioferritin, *dps*
348 and iron storage protein, *dps*) also revealed higher transcript abundances in the particle-attached
349 transcript inventories as compared to those in the control. A large number of genes involved in

the biosynthesis of various siderophores were detected and they revealed the highest increases (Log2fold changes of 2.5 to 10) among the metal related genes.

To determine which prokaryotic taxa were associated with the trace metal processing on particles, we assigned the taxonomy of the transcripts (Fig. 3; the taxonomic assignment in the control is provided in Fig. S9). *Rhodobacteraceae* (order *Rhodobacterales*) contributed to the transport, sensing and regulation of all 9 metals, while other prokaryotes had a reduced set of trace metal transcripts. Transport of Fe^{3+} (*afuA*, *B*, *C*) was mainly associated with *Rhodobacteraceae*, and that of Fe^{2+} (*feoB*, *efeU*) with *Porticoccaceae* (*Cellvibrionales*), *Moritellaceae* (*Alteromonadales*) and *Flavobacteriaceae (Flavobacteriales). Planctomycetaceae* (*Planctomycetales*) were particularly associated with Zn/Cd (*zip**B*) and Mo/W (*wtpC*) transport, *Halomonadaceae* (*Oceanospiralles*) with the transport of Zn and Mn (*ABC.ZM.S*), and *Deltaproteobacteria* (not assigned to the family level) to that of Ni (*ABC.PE.P*, *P1* and *ddpD*). Transcripts involved in Co/Zn/Cd efflux (*czc*, *cus*, *cnrA, B, C*) were associated with members of the *Porticoccaceae*, *Alteromonadacaea* and *Deltaproteobacteria*, whereas *Planctomycetaceae* were associated with Cu efflux (*gesA*, *mexP*). *Deltaproteobacteria* contributed to Zn/Fe regulation (*zur, fur*) and transcripts for Cu regulation (*scsB*) were dominated by *Moritellaceae*. Relative transcript abundance could vary between subunits of the same transporter complex for a given taxonomic group, which could indicate differential regulation or the temporal decoupling of the expression of the subunits within diverse taxa.

Diverse bacterial groups contributed to siderophore biosynthesis, including *Flavobacteriaceae* (*entC*, *irp1*), *Deltaproteobacteria* (*ent**D*), *Mycobacteriaceae* (*mbtB, F*, *dhbF*, *entF*) and *Streptomycetaceae* (both A*ctinomycetales*)(*enFt*, *irp1,2*, *dhbF*), *Nostocaceae* (Cyanobacteria)(*mbtE*) and *Verrucomicrobia* (not assigned to the family level)(*pchF*, *irp1*). With the exception of *Flavobacteriaceae*, taxonomic groups involved in siderophore biosynthesis were

374 distinct from those contributing to Fe-complex transport. Among these where *Rhodobacteraceae*
375 (*ABC.FEV.A, S*), *Moritellaceae (ABC.FEV. S), Oceanospirillaceae (fecA, fhuC),*
376 *Halomonadaceae (fecA, ABC.FEV.A), Alteromonadaceae (fiu, fphuc)* and *Opitutales*
377 (*Verrucomicrobia*)(*fiu*). The taxonomic groups that contributed to metal storage and sensing
378 belonged to *Deltaproteobacteria* (*bfr*), *Porticoccaceae* (*bfr*)*, Moritellaceae* (*ftn*, *bfr*),
379 *Flavobactericeae* (*ftn, dps*) and *Alteromonadaceae* (*bfr, dps*), while Fe efflux transcripts (*fieF*)
380 were assigned only to *Moritellaceae*.
381
382 **Discussion**
383
384 **The metatranscriptomic response to particulate trace metals.** We observed enhanced
385 transcript abundances of genes involved in different trace metal related processes, including
386 transport into and out of the cell, regulation and storage in particle-associated prokaryotic
387 communities from the Southern Ocean. The elevated gene transcript abundances of a variety of
388 transporters for all metals, except for Cu and Co, points to an increased uptake by particle-
389 attached cells. In the case of Fe, the uptake was further associated with extracellular mobilization
390 owing to the synthesis of different types of siderophores. Metal uptake was mediated by selective
391 transporters like those involved in the internalization of Fe-siderophores, and by weakly selective
392 cation carriers such as for Mn/Zn/Fe (*tro*, *mnt*, *znu*) and Zn/Cd (*zip*). The enhanced abundance of
393 transcripts involved in the regulation of metal uptake like *fur* (Fe) and *zur* (Zn), and in the two-
394 component system for Cu sensing (*cus*) suggests the requirement for a strong control of metal
395 transport when cells are attached to particles. Transport was also directed outward from the cell as
396 revealed by efflux pumps for Co/Zn/Cd (*czc, zit*) and Cu (*cus*), indicating the need to manage the
397 internal excess. Transcripts dedicated to Fe storage in ferritin (*ftn*) or the Fe storage protein *dps*
398 further point to the management of excess concentrations, or as a sparing or redistribution

399 strategy. This concurrent enhanced transcription of distinct metal-related genes by particle-
400 attached heterotrophic prokaryotes suggests that the involved processes are governed by an
401 overarching biological property.

402 **The role of metal homeostasis**. Homeostasis has been defined as an ensemble of cellular
403 processes maintaining suitable intracellular metal concentrations under changing external
404 conditions (Waldron and Robinson 2009). As previously described, homeostasis relies on a
405 complex network of feedbacks and feed-forwards (Williams and Fraústo Da Silva 2003) and is
406 associated with a diverse metabolic tool box including many functions for transport (inward and
407 outward), external mobilization, sensing, buffering, sparing, storage and regulation (Ma et al.
408 2009; Chandrangsu et al. 2017). This essential property further ensures the timely insertion of a
409 required metal to the protein of interest. The present study demonstrates that multiple pathways
410 associated with metal homeostasis are activated by prokaryotes inhabiting marine particles.

411

412 Homeostasis of heterotrophic prokaryotes has been extensively investigated for a few metals and
413 individual strains. The classical scenario of Fe homeostasis is that cells activate different
414 mechanisms in response to varying external conditions, and to avoid the waste of energy or toxic
415 effects the switch between processes of uptake, storage and efflux is strongly regulated (Andrews
416 et al. 2003). As a consequence, within a microbial cell, some processes, for example siderophore
417 production and uptake, can be differentially regulated over others, such as Fe storage in ferritin.
418 The description of the homeostasis of Cu (Braymer and Giedroc 2014), Zn (Braymer and Giedroc
419 2014), Ni (Macomber and Hausinger 2011) and Mn (Jakubovics and Jenkinson 2001) lead to the
420 same conclusion of a simultaneous up- and down- regulation of genes that participate in distinct
421 processes, such the acquisition and efflux of elements. Our observations of the simultaneously

higher transcript abundances of genes involved in the transport and also those involved in metal efflux and regulation seems, therefore, at odds with the concept of homeostasis.

Geochemical and biological complexity of marine particles. We propose the geochemical heterogeneity of particles inhabited by a taxonomically diverse community to resolve this apparent paradox. A large variety of individual particles, each a complex mixture of biogenic and lithogenic components, make up the pool of marine particulate matter. Metals can be found deeply enclosed in a matrix or weakly adsorbed at the surface, depending on the nature of the biogenic material, such as intact cells, aggregates or fecal pellets (Blain and Tagliabue 2016). Lithogenic material contains many fractions, presented by diverse chemical composition and degrees of crystallization (van der Merwe et al. 2019). This geochemical complexity can lead to a variety of metabolic responses that likely occur either within microstructures of individual particles or in the immediately surrounding region, the particle-sphere. In the present study, gene expression was determined after 12 days of incubation in the dark, when the activity of phytoplankton within these particles was strongly reduced due to the lack of light. The presence of active phytoplankton cells is unlikely to change the gene expression profiles of prokaryotes attached to non-living particles. Phytoplankton, notably diatoms the dominant group in the Southern Ocean, have no direct access to particulate metals, excluding the possibility of competition with prokaryotes for this resource. Our observations rather suggest that prokaryotes render a fraction of particulate metals bioavailable that could subsequently be accessible to photoautotrophs. The gene expression patterns presented here are a global response of diverse prokaryotic communities to the geochemical complexity of individual particles. We illustrate below the roles of some prokaryotic groups, each composed of diverse taxa with specific functions in trace element processing (Sun et al. 2021), and its link to homeostasis.

445 *Rhodobacteraceae* contributed to the expression of genes involved in homeostasis of several
446 metals, pointing to their prominent role in particulate trace element cycling. The metabolically
447 diverse *Roseobacter* clade contains multiple strategies to sense and react to the environment,
448 reflected in the patch-adapted life style of many members (Luo and Moran 2014; Held et al.
449 2019). A particular feature is the large repertoire of transporters including numerous pathways for
450 the acquisition of inorganic and organically complexed metals (Newton et al. 2010; Hogle et al.
451 2016). Several *Roseobacter* harbor the Fe response regulator (*irr*) (Rodionov et al. 2006) to sense
452 Fe indirectly through heme biosynthesis (Hogle et al. 2017), and the respective gene transcripts
453 were present in both treatments in the present study. Despite the overwhelming involvement of
454 *Roseobacter* to the uptake of several trace elements and the sensing of changes in their
455 concentration, this clade had minor contributions to the uptake of organically complexed Fe
456 (*ABC.FEV*).

457 The taxonomic assignments of siderophore biosynthesis genes were overall different to those for
458 uptake, indicating that siderophore bound Fe was available to nonproducing members of the
459 community (Cordero et al. 2012). This cross-feeding interaction could be an efficient strategy on
460 particles where cells are in close vicinity to each other, facilitating sensing of available Fe
461 sources. *Flavobacteriaceae* contributed to both the production of siderophores (*ent*, *irp*) and the
462 utilization of organically-bound Fe, while regulating excess through the Fe storage proteins
463 ferritin (*ftn*) and *dps*. *Flavobacteriaceae* are efficient degraders of polymeric compounds (Cottrell
464 and Kirchman 2000) enriched within particles, a functional capability that could sustain their
465 investment to the energetically costly pathway of siderophore biosynthesis. Fe-limiting conditions
466 (Boiteau et al. 2016; Debeljak et al. 2019) and Fe pulses (Sijerčić and Price 2015) were both
467 associated with enhanced siderophore production, and this process appears to be regulated by
468 cell-cell communication (McRose et al. 2018). Our observations of the various types of

siderophore biosynthesis and transporter gene transcripts indicate that a fraction of the particle-bound Fe needs to be rendered bioavailable and they illustrate the key role of diverse microbes in this process.

The higher transcript abundances for Cu were exclusively associated with efflux and resistance, but not with transport into the cell. The difference in the metal to phosphorus ratio between particulate matter and prokaryotic cells was most pronounced for Cu (Fig. 1), which indicates high and thus potentially toxic Cu concentrations within some particles. Transcripts were mostly affiliated with *Planctomycetaceae (ges, mex)* and *Flavobacteriaceae (cus*) and several families belonging to *Alteromonadales, such as Alteromonadaceae, Pseudomonadaceae* and *Psychromonodaceae (cus), and Moritellaceae (scs),* suggesting these groups make intense use of this metal under a strict homeostasis control (Posacka et al. 2019), because excess of Cu is highly toxic. Cu is required for many cellular functions, including multiple extracellular or periplasmic Cu-enzymes, like multi-copper oxidases, amine oxidases or lysine oxidases, all involved in the oxidation of diverse organic substrates. *Moritellaceae* possess a range of extracellular enzymes particularly adapted to low temperatures (Malecki et al. 2013), enabling them to exploit complex sources of organic matter, while *Alteromonadaceae* can efficiently utilize diverse labile substrates (Pedler et al. 2014). These different strategies could result in the observed higher cell-specific prokaryotic production on particles as compared to the control treatment. This enhanced metabolic activity is consistent with the idea of particles as "hotspots" (Grossart et al. 2003; Azam and Malfatti 2007) where concentrations of organic matter can be several orders of magnitude higher than in surrounding seawater. The idea that particulate organic carbon stimulated bulk prokaryotic activity is further supported by dose addition experiments identifying carbon as growth-limiting for the prokaryotic community in the control treatments (data not

492 shown). The intense intracellular Cu regulation and efflux could be a consequence of the
493 enhanced particulate organic matter processing by members with different strategies.

494 One consequence of prokaryotic heterotrophic activity is the consumption of oxygen and thus the
495 creation of gradients of oxygenated conditions within particles, resulting in heterogeneity within
496 the same or between particles that could impact the metal homeostatic response of prokaryotes in
497 different ways. Fe(II) is mainly present under low oxygen concentrations and the higher transcript
498 abundances of Fe^{2+} uptake genes by prokaryotes on particles suggests the presence of low oxygen
499 micro-niches. One process typical for low oxygen environments is denitrification, the step-wise
500 reduction of nitrate (NO_3^-) to nitrite (NO_2^-), nitric oxide (NO), nitrous oxide and eventually
501 dinitrogen gas (N_2). Genes encoding periplasmic nitrate reductase (*nap*), nitric oxide reductase
502 (*norB*) and copper-containing nitrous oxide reductase (*nosZ*) were higher expressed on particles
503 (Log2fold change: 5.2-6.2)(Table S3). Concurrently, a number of genes involved in aerobic
504 processes such as nitrification were significantly enhanced on particles (Log2Fold 1.8-2.9)(Table
505 S3). We also identified higher abundances of transcripts related to nitrogen fixation (e.g. *nif*) in
506 the particle-attached prokaryotic community than in the control (Log2Fold 3.6-9.3)(Table S3).
507 Mo and Fe are key elements of nitrogenase, catalyzing the reduction of atmospheric dinitrogen
508 (N_2) to ammonia (NH_3). The *nifH* gene was exclusively assigned to *Deltaproteobacteria* (Fig.
509 S10), containing members that carry out N_2 fixation under low oxygen concentrations (Farnelid et
510 al. 2011). Together, these observations suggest the presence of niches with varying micro-
511 environmental conditions that support aerobic and anaerobic microbial metabolisms. The
512 involved prokaryotes and their respective metal requirements could reflect the impact of such
513 niches on the overall transcriptional response.

514

Biogeochemical lessons and perspectives of the transcriptomic view of prokaryote-particle interactions. The intense trace metal processing on particles is tightly linked to the fraction of particulate metals that is bioavailable. In the case of Fe, prokaryotic degradation of sinking particles lead to the release of dissolved Fe or weak Fe ligands and the remineralization of biogenic and lithogenic Fe occurs at different length scales (Boyd et al. 2010; Bressac et al. 2019). Our results provide a novel perspective to this view. The expression of metal-related genes suggests that diverse chemical forms of dissolved Fe, including the short-lived state Fe(II), are produced and utilized by prokaryotes. Moreover, the numerous highly enriched chatecholate-type siderophore synthesis transcripts point to the production of the strongest known categories of Fe binding ligands. Such strong ligands which promote mineral dissolution (Kalinowski et al. 2000) at high dissolution rates (Akafia et al. 2014) could be released to scavenge Fe from different types of minerals, such as ilmenite as observed in the particles used here (van der Merwe et al. 2019). For metals other than Fe, knowledge on trace metal release linked to prokaryotic degradation of particles is limited (Twining et al. 2014). Our results provide clues that these processes should be significant and require further attention and quantification.

The metal-processing on particles could impact the surrounding environment. It is unlikely that the entire outward flow resulting from efflux pumps or release of ligands was entirely captured back by attached prokaryotes before dispersion by turbulence. Particles and their plumes are likely feeding the environment with a suite of regenerated dissolved metal species (Azam and Malfatti 2007; Stocker et al. 2008). Additionally, a consequence of prokaryotic activity is the transfer of a fraction of metals from an abiotic, in the form of particles, to a biotic reservoir, a starting point for a journey of metals in the microbial loop. In the light of our findings, the concept of the ferrous wheel (Kirchman 1996; Tortell et al. 1996) could be refined to pinpoint the

role of non-living particles as source of bioavailable Fe, and it could further be extended to other trace elements leading to the microbial metal wheel.

Acknowledgments

We thank M. Coffin, The PI of the Heard Earth-Ocean-Biosphere Interactions (HEOBI) voyage and the crew and scientists of the Australian R/V *Investigator* for their support during the cruise (IN 2016-V01). Thanks to the HEOBI trace-metal team for help in the collection of seawater. P. Catala carried out the flow cytometry analyses. We thank Gerhard J. Herndl for the opportunity to perform RNA extractions in the laboratory of the Microbial Oceanography Working Group in Vienna. We thank Laurie Bousquet and Sara Beier for their help and important discussions on RNA-Sequencing data analysis. The authors thank the Roscoff Bioinformatics platform ABiMS (http://abims.sb-roscoff.fr) for providing computational resources. We thank M. A. Moran and M. Landa for providing the internal standards for further *in vitro* transcription. This work was supported by the French Research program of INSU-CNRS LEFE/CYBER ("Les enveloppes fluides et l'environnement" – "Cycles biogéochimiques, environnement et ressources") of the project PACBO, the International Collaborative Program CNRS-PICS of the project FASO, the Austrian FWF grant under the number P28781-B21. The research was also supported by the Australian Research Council (DP150100345 to ARB), the Antarctic Climate and Ecosystems CRC, and Australian Antarctic Science program (AAS4338 to ARB). The HEOBI voyage shiptime was supported by the Australian Marine National Facility. The authors declare no conflict of interest. We thank two referees whose comments and suggestions helped improve a previous version of the manuscript.

562 **References**

563 Akafia, M. M., J. M. Harrington, J. R. Bargar, and O. W. Duckworth. 2014. Metal oxyhydroxide
564 dissolution as promoted by structurally diverse siderophores and oxalate. Geochimica et
565 Cosmochimica Acta **141**: 258–269. doi:10.1016/j.gca.2014.06.024
566 Altschul, S. F., W. Gish, W. Miller, E. W. Myers, and D. J. Lipman. 1990. Basic local alignment
567 search tool. Journal of Molecular Biology **215**: 403–410. doi:10.1016/S0022-
568 2836(05)80360-2
569 Andrews, S. C., A. K. Robinson, and F. Rodrigez-Quinones. 2003. Bacterial iron homeostasis.
570 FEMS Microbiology reviews **27**: 215–237.
571 Angel, R., P. Claus, and R. Conrad. 2012. Methanogenic archaea are globally ubiquitous in
572 aerated soils and become active under wet anoxic conditions. The ISME Journal **6**: 847–
573 862. doi:10.1038/ismej.2011.141
574 Azam, F., and F. Malfatti. 2007. Microbial structuring of marine ecosystems. Nat Rev Microbiol **5**:
575 782–791. doi:10.1038/nrmicro1747
576 Barbeau, K., J. W. Moffett, D. A. Caron, P. L. Croot, and D. L. Erdner. 1996. Role of protozoan
577 grazing in relieving iron limitation of phytoplankton. Nature **380**: 61–64.
578 doi:10.1038/380061a0
579 Beier, S., P. Holtermann, D. Numberger, T. Schott, L. Umlauf, and K. Jürgens. 2018. A
580 metatranscriptomics-based assessment of small-scale mixing of sulfidic and oxic waters
581 on redoxcline prokaryotic communities. Environ Microbiol 1462-2920.14499.
582 doi:10.1111/1462-2920.14499
583 Blain, S., and A. Tagliabue. 2016. Iron cycle in oceans, ISTE Ltd/John Wiley and Sons Inc.

584 Boiteau, R. M., D. R. Mende, N. J. Hawco, and others. 2016. Siderophore-based microbial
585 adaptations to iron scarcity across the eastern Pacific Ocean. Proc Natl Acad Sci USA
586 **113**: 14237–14242. doi:10.1073/pnas.1608594113
587 Bolger, A. M., M. Lohse, and B. Usadel. 2014. Trimmomatic: a flexible trimmer for Illumina
588 sequence data. Bioinformatics **30**: 2114–2120. doi:10.1093/bioinformatics/btu170
589 Bowie, A. R., A. T. Townsend, D. Lannuzel, T. A. Remenyi, and P. van der Merwe. 2010. Modern
590 sampling and analytical methods for the determination of trace elements in marine
591 particulate material using magnetic sector inductively coupled plasma–mass
592 spectrometry. Analytica Chimica Acta **676**: 15–27. doi:10.1016/j.aca.2010.07.037
593 Boyd, P. W., and M. J. Ellwood. 2010. The biogeochemical cycle of iron in the ocean. Nature
594 Geoscience **3**: 675–682. doi:10.1038/ngeo964
595 Boyd, P. W., E. Ibisanmi, S. G. Sander, K. A. Hunter, and G. A. Jackson. 2010. Remineralization of
596 upper ocean particles: Implications for iron biogeochemistry. Limnology and
597 Oceanography **55**: 1271–1288. doi:10.4319/lo.2010.55.3.1271
598 Braymer, J. J., and D. P. Giedroc. 2014. Recent developments in copper and zinc homeostasis in
599 bacterial pathogens. Current Opinion in Chemical Biology **19**: 59–66.
600 doi:10.1016/j.cbpa.2013.12.021
601 Bressac, M., C. Guieu, M. J. Ellwood, and others. 2019. Resupply of mesopelagic dissolved iron
602 controlled by particulate iron composition. Nat. Geosci. **12**: 995–1000.
603 doi:10.1038/s41561-019-0476-6
604 Buchfink, B., C. Xie, and D. H. Huson. 2015. Fast and sensitive protein alignment using
605 DIAMOND. Nature Methods **12**: 59–60. doi:10.1038/nmeth.3176

606 Chandrangsu, P., C. Rensing, and J. D. Helmann. 2017. Metal homeostasis and resistance in
607 bacteria. Nat Rev Microbiol **15**: 338–350. doi:10.1038/nrmicro.2017.15
608 Cordero, O. X., L.-A. Ventouras, E. F. DeLong, and M. F. Polz. 2012. Public good dynamics drive
609 evolution of iron acquisition strategies in natural bacterioplankton populations.
610 Proceedings of the National Academy of Sciences **109**: 20059–20064.
611 doi:10.1073/pnas.1213344109
612 Cottrell, M. T., and D. L. Kirchman. 2000. Natural assemblages of marine proteobacteria and
613 members of the cytophaga-flavobacter cluster consuming low- and high-molecular-
614 weight dissolved organic matter. Applied environmental Microbiology **66**: 1692–1697.
615 Debeljak, P., E. Toulza, S. Beier, S. Blain, and I. Obernosterer. 2019. Microbial iron metabolism as
616 revealed by gene expression profiles in contrasted Southern Ocean regimes. Environ
617 Microbiol **21**: 2360–2374. doi:10.1111/1462-2920.14621
618 Farnelid, H., A.F. Andersson, S. Bertilsson, W.A. Al-Soud, L.H. Hansen, S. Sorensen, G.F. Steward,
619 A. Hagström, and L. Riemann. 2011. Nitrogenase gene amplifications from global marine
620 surface waters are dominated by genes of non-cyanobacteria. PLosONE **6**: e19223
621 Grossart, H.-P., T. Kiorboe, K. Tang, and H. Ploug. 2003. Bacterial Colonization of Particles:
622 Growth and Interactions. Applied and Environmental Microbiology **69**: 3500–3509.
623 Gu, Z., R. Eils, and M. Schlesner. 2016. Complex heatmaps reveal patterns and correlations in
624 multidimensional genomic data. Bioinformatics **32**: 2847–2849.
625 doi:10.1093/bioinformatics/btw313
626 Held, N. A., M. R. McIlvin, D. M. Moran, M. T. Laub, and M. A. Saito. 2019. Unique Patterns and
627 Biogeochemical Relevance of Two-Component Sensing in Marine Bacteria O. Mason

[ed.]. mSystems **4**: e00317-18, /msystems/4/1/msys.00317-18.atom. doi:10.1128/mSystems.00317-18

Hogle, S. L., B. Brahamsha, and K. A. Barbeau. 2017. Direct Heme Uptake by Phytoplankton-Associated *Roseobacter* Bacteria J. Weitz [ed.]. mSystems **2**: e00124-16, /msys/2/1/e00124-16.atom. doi:10.1128/mSystems.00124-16

Hogle, S. L., J. C. Thrash, C. L. Dupont, and K. A. Barbeau. 2016. Trace Metal Acquisition by Marine Heterotrophic Bacterioplankton with Contrasting Trophic Strategies V. Müller [ed.]. Appl. Environ. Microbiol. **82**: 1613–1624. doi:10.1128/AEM.03128-15

Huerta-Cepas, J., D. Szklarczyk, D. Heller, and others. 2019. eggNOG 5.0: a hierarchical, functionally and phylogenetically annotated orthology resource based on 5090 organisms and 2502 viruses. Nucleic Acids Res. **47**: D309–D314. doi:10.1093/nar/gky1085

Hyatt, D., G.-L. Chen, P. F. LoCascio, M. L. Land, F. W. Larimer, and L. J. Hauser. 2010. Prodigal: prokaryotic gene recognition and translation initiation site identification. BMC Bioinformatics **11**: 119. doi:10.1186/1471-2105-11-119

Irving, H., and R. J. P. Williams. 1948. Order of Stability of Metal Complexes. Nature **162**: 746–747. doi:10.1038/162746a0

Jakubovics, N. S., and H. F. Jenkinson. 2001. Out of the iron age: new insights into the critical role of manganese homeostasis in bacteria. Microbiology **147**: 1709–1718. doi:10.1099/00221287-147-7-1709

Kalinowski, B. E., L. J. Liermann, S. Givens, and S. L. Brantley. 2000. Rates of bacteria-promoted solubilization of Fe from minerals: a review of problems and approaches. Chemical Geology **169**: 357–370. doi:10.1016/S0009-2541(00)00214-X

651 Kanehisa, M., Y. Sato, M. Kawashima, M. Furumichi, and M. Tanabe. 2016a. KEGG as a reference
652 resource for gene and protein annotation. Nucleic Acids Research **44**: D457–D462.
653 doi:10.1093/nar/gkv1070
654 Kanehisa, M., Y. Sato, and K. Morishima. 2016b. BlastKOALA and GhostKOALA: KEGG Tools for
655 Functional Characterization of Genome and Metagenome Sequences. J. Mol. Biol. **428**:
656 726–731. doi:10.1016/j.jmb.2015.11.006
657 Kirchman, D. L. 1996. Microbial ferrous wheel. Nature 303–304.
658 Kopylova, E., L. Noé, and H. Touzet. 2012. SortMeRNA: fast and accurate filtering of ribosomal
659 RNAs in metatranscriptomic data. Bioinformatics **28**: 3211–3217.
660 doi:10.1093/bioinformatics/bts611
661 Langmead, B., and S. L. Salzberg. 2012. Fast gapped-read alignment with Bowtie 2. Nature
662 Methods **9**: 357–359. doi:10.1038/nmeth.1923
663 Li, D., C.-M. Liu, R. Luo, K. Sadakane, and T.-W. Lam. 2015. MEGAHIT: an ultra-fast single-node
664 solution for large and complex metagenomics assembly via succinct de Bruijn graph.
665 Bioinformatics **31**: 1674–1676. doi:10.1093/bioinformatics/btv033
666 Li, M., B. M. Toner, B. J. Baker, J. A. Breier, C. S. Sheik, and G. J. Dick. 2014. Microbial iron uptake
667 as a mechanism for dispersing iron from deep-sea hydrothermal vents. Nat Commun **5**:
668 3192. doi:10.1038/ncomms4192
669 Liao, Y., G. K. Smyth, and W. Shi. 2014. featureCounts: an efficient general purpose program for
670 assigning sequence reads to genomic features. Bioinformatics **30**: 923–930.
671 doi:10.1093/bioinformatics/btt656

672 Lis, H., C. Kranzler, N. Keren, and Y. Shaked. 2015. A Comparative Study of Iron Uptake Rates and
673 Mechanisms amongst Marine and Fresh Water Cyanobacteria: Prevalence of Reductive
674 Iron Uptake. Life **5**: 841–860. doi:10.3390/life5010841
675 Love, M. I., W. Huber, and S. Anders. 2014. Moderated estimation of fold change and dispersion
676 for RNA-seq data with DESeq2. Genome Biol **15**. doi:10.1186/s13059-014-0550-8
677 Luo, H., and M. A. Moran. 2014. Evolutionary Ecology of the Marine Roseobacter Clade.
678 Microbiol. Mol. Biol. Rev. **78**: 573–587. doi:10.1128/MMBR.00020-14
679 Ma, Z., F. E. Jacobsen, and D. P. Giedroc. 2009. Coordination Chemistry of Bacterial Metal
680 Transport and Sensing. Chem. Rev. **109**: 4644–4681. doi:10.1021/cr900077w
681 Macomber, L., and R. P. Hausinger. 2011. Mechanisms of nickel toxicity in microorganisms.
682 Metallomics **3**: 1153. doi:10.1039/c1mt00063b
683 Malecki, P. H., J. E. Raczynska, C. E. Vorgias, and W. Rypniewski. 2013. Structure of a complete
684 four-domain chitinase from *Moritella marina* , a marine psychrophilic bacterium. Acta
685 Crystallogr D Biol Crystallogr **69**: 821–829. doi:10.1107/S0907444913002011
686 Martin, J. H., M. R. Gordon, and S. E. Fitzwater. 1992. Iron limitation in Antatrctic waters. Nature
687 **345**: 156–158.
688 Mazzotta, M., M. R. McIlvin, and M. A. Saito. 2020. Characterization of the Fe Metalloproteome
689 of a Ubiquitous Marine Heterotroph, Pseudoalteromonas (BB2-AT2): Multiple
690 Bacterioferritin Copies Enable Significant Fe Storage. preprint.
691 McQuaid, J. B., A. B. Kustka, M. Oborník, and others. 2018. Carbonate-sensitive phytotransferrin
692 controls high-affinity iron uptake in diatoms. Nature **555**: 534–537.
693 doi:10.1038/nature25982

694 McRose, D. L., O. Baars, M. R. Seyedsayamdost, and F. M. M. Morel. 2018. Quorum sensing and
695 iron regulate a two-for-one siderophore gene cluster in *Vibrio harveyi*. Proc Natl Acad
696 Sci USA **115**: 7581–7586. doi:10.1073/pnas.1805791115
697 van der Merwe, P., K. Wuttig, T. Holmes, T. W. Trull, Z. Chase, A. T. Townsend, K. Goemann, and
698 A. R. Bowie. 2019. High Lability Fe Particles Sourced From Glacial Erosion Can Meet
699 Previously Unaccounted Biological Demand: Heard Island, Southern Ocean. Front. Mar.
700 Sci. **6**: 332. doi:10.3389/fmars.2019.00332
701 Newton, R. J., L. E. Griffin, K. M. Bowles, and others. 2010. Genome characteristics of a
702 generalist marine bacterial lineage. ISME J **4**: 784–798. doi:10.1038/ismej.2009.150
703 Obernosterer, I., U. Christaki, D. Lefèvre, P. Catala, F. Van Wambeke, and P. Lebaron. 2008.
704 Rapid bacterial mineralization of organic carbon produced during a phytoplankton
705 bloom induced by natural iron fertilization in the Southern Ocean. Deep Sea Research
706 Part II: Topical Studies in Oceanography **55**: 777–789. doi:10.1016/j.dsr2.2007.12.005
707 Pedler, B. E., L. I. Aluwihare, and F. Azam. 2014. Single bacterial strain capable of significant
708 contribution to carbon cycling in the surface ocean. Proceedings of the National
709 Academy of Sciences **111**: 7202–7207. doi:10.1073/pnas.1401887111
710 Posacka, A. 2017. Biogeochemical cycling of copper in the Northeast Pacific Ocean : role of
711 marine heterotrophic bacteria.doi:10.14288/1.0355246
712 Posacka, A. M., D. M. Semeniuk, and M. T. Maldonado. 2019. Effects of Copper Availability on
713 the Physiology of Marine Heterotrophic Bacteria. Front. Mar. Sci. **5**: 523.
714 doi:10.3389/fmars.2018.00523

715 Rauschenberg, S., and B. S. Twining. 2015. Evaluation of approaches to estimate biogenic
716 particulate trace metals in the ocean. Marine Chemistry **171**: 67–77.
717 doi:10.1016/j.marchem.2015.01.004
718 Rich, H. W., and F. M. M. Morel. 1990. Availability of well-defined iron colloids to the marine
719 diatom *Thalassiosira weissflogii*. Limnol. Oceanogr. **35**: 652–662.
720 doi:10.4319/lo.1990.35.3.0652
721 Rodionov, D. A., M. S. Gelfand, J. D. Todd, A. R. J. Curson, and A. W. B. Johnston. 2006.
722 Computational Reconstruction of Iron- and Manganese-Responsive Transcriptional
723 Networks in α-Proteobacteria. PLoS Comput Biol **2**: e163.
724 doi:10.1371/journal.pcbi.0020163
725 Rubin, M., I. Berman-Frank, and Y. Shaked. 2011. Dust- and mineral-iron utilization by the
726 marine dinitrogen-fixer Trichodesmium. Nature Geosci **4**: 529–534.
727 doi:10.1038/ngeo1181
728 Saito, M. A., D. M. Sigman, and F. M. M. Morel. 2003. The bioinorganic chemistry of the ancient
729 ocean: the co-evolution of cyanobacterial metal requirements and biogeochemical
730 cycles at the Archean–Proterozoic boundary? Inorganica Chimica Acta **356**: 308–318.
731 doi:10.1016/S0020-1693(03)00442-0
732 Sandy, M., and A. Butler. 2009. Microbial Iron Acquisition: Marine and Terrestrial Siderophores.
733 Chemical Reviews **109**: 4580–4595. doi:10.1021/cr9002787
734 Satinsky, B. M., S. M. Gifford, B. C. Crump, and M. A. Moran. 2013. Use of Internal Standards for
735 Quantitative Metatranscriptome and Metagenome Analysis. Microbial Metagenomics,
736 Metatranscriptomics, and Metaproteomics **531**: 237–250. doi:10.1016/B978-0-12-
737 407863-5.00012-5

738 Shaked, Y., and H. Lis. 2012. Disassembling Iron Availability to Phytoplankton. Frontiers in
739 Microbiology **3**. doi:10.3389/fmicb.2012.00123
740 Sijerčić, A., and N. Price. 2015. Hydroxamate siderophore secretion by Pseudoalteromonas
741 haloplanktis during steady-state and transient growth under iron limitation. Mar. Ecol.
742 Prog. Ser. **531**: 105–120. doi:10.3354/meps11338
743 Silva, J. J. R. F. da, and R. J. P. Williams. 2001. The biological chemistry of the elements: the
744 inorganic chemistry of life, 2nd ed. Oxford University Press.
745 Stocker, R., J. R. Seymour, A. Samadani, D. E. Hunt, and M. F. Polz. 2008. Rapid chemotactic
746 response enables marine bacteria to exploit ephemeral microscale nutrient patches.
747 Proceedings of the National Academy of Sciences **105**: 4209–4214.
748 doi:10.1073/pnas.0709765105
749 Strzepek, R. F., M. T. Maldonado, K. A. Hunter, R. D. Frew, and P. W. Boyd. 2011. Adaptive
750 strategies by Southern Ocean phytoplankton to lessen iron limitation: Uptake of
751 organically complexed iron and reduced cellular iron requirements. Limnol. Oceanogr.
752 **56**: 1983–2002. doi:10.4319/lo.2011.56.6.1983
753 Sun, Y., P. Debeljak and I. Obernosterer. 2021. Microbial iron and carbon metabolism as
754 revealed by taxonomy-specific functional diversity in the Southern Ocean. ISMEJ. doi:
755 10.1038/s41396-021-00973-3
756 Tagliabue, A., A. R. Bowie, P. W. Boyd, K. N. Buck, K. S. Johnson, and M. A. Saito. 2017. The
757 integral role of iron in ocean biogeochemistry. Nature **543**: 51–59.
758 Tortell, P. D., M. T. Maldonado, and N. M. Price. 1996. The role of heterotrophic bacteria in iron-
759 limited ocean ecosystems. Nature **383**: 330–332. doi:10.1038/383330a0

760 Twining, B. S., S. D. Nodder, A. L. King, and others. 2014. Differential remineralization of major
761 and trace elements in sinking diatoms. Limnology and Oceanography **59**: 689–704.
762 Velasquez, I. B., E. Ibisanmi, E. W. Maas, P. W. Boyd, S. Nodder, and S. G. Sander. 2016.
763 Ferrioxamine Siderophores Detected amongst Iron Binding Ligands Produced during the
764 Remineralization of Marine Particles. Front. Mar. Sci. **3**. doi:10.3389/fmars.2016.00172
765 Wackett, L. P., A. G. Dodge, and L. B. M. Ellis. 2004. Microbial Genomics and the Periodic Table.
766 Applied and Environmental Microbiology **70**: 647–655. doi:10.1128/AEM.70.2.647-
767 655.2004
768 Waldron, K. J., and N. J. Robinson. 2009. How do bacterial cells ensure that metalloproteins get
769 the correct metal? Nat Rev Microbiol **7**: 25–35. doi:10.1038/nrmicro2057
770 Williams, R. J. . P., and J. J. R. Fraústo Da Silva. 2003. Evolution was Chemically Constrained.
771 Journal of Theoretical Biology **220**: 323–343. doi:10.1006/jtbi.2003.3152
772
773

774 **Figure Legends**

775 **Figure 1.** Particle characterization

776 Comparison of the metal to phosphorus ratios (mol/mol) between bulk marine particulate matter
777 and heterotrophic prokaryotes (a). Grey boxplots represent mean, first and third quartiles for total
778 trace metals in particles collected during the HEOBI cruise at 8 sites in the Indian Sector of the
779 Southern Ocean (n=55). Maroon boxplots represent mean, first and third quartiles for the ratio
780 measured in cultures of 5 different strains of heterotrophic prokaryotes (n=16, except for Mo and
781 Ni where n=1; no data for Cd and V available)(Posacka 2017; Posacka et al. 2019; Mazzotta et al.
782 2020). Size class distribution of particles (b), prokaryotic cell abundance on individual particles
783 (c) and cell abundance per surface area unit (d) in the incubation experiments. Observations are
784 from the final time point.

785

786

787 **Figure 2.** Enrichment of trace metal related gene transcripts in particle-associated prokaryotes

788 Fold changes of normalized transcript counts of KEGG orthologous genes in prokaryotic
789 communities attached to particles as compared to those in particle-free incubations (given in
790 Log2Fold). Significantly higher expressed transcripts (adjusted p-value <0.05) are indicated by an
791 asterisk (*) and genes potentially implicated in the transport of multiple metals are indicated by
792 the letter M (for multiple). Genes that are part of an ABC transporter complex are highlighted by
793 rectangular boxes.

794

795

Figure 3. Taxonomic assignment of metal-related genes

Heatmap illustrating the relative contribution of prokaryotic groups to the expression of a given KEGG orthologous (KO) gene in the particle-attached community (each KO gene sums up to 1 and 1 equals 100%). Phylogenetic groups are visualized on the family or lowest possible taxonomic level. KO gene transcripts are grouped by function: transport, efflux and sensing/regulation of 9 metals, siderophore synthesis, Fe-complex transport and Fe storage (as in Fig. 2). The full description of the KEGG abbreviations is given in Fig. 2. The full gene name of the Fe-complex transporter *bhuR_hugA_hmbR* is *tpA_hemR_IbpA_hpuB_bhuR_hugA_hmbR*. The corresponding heatmap for the control treatment is provided in Supplementary Fig. 9.

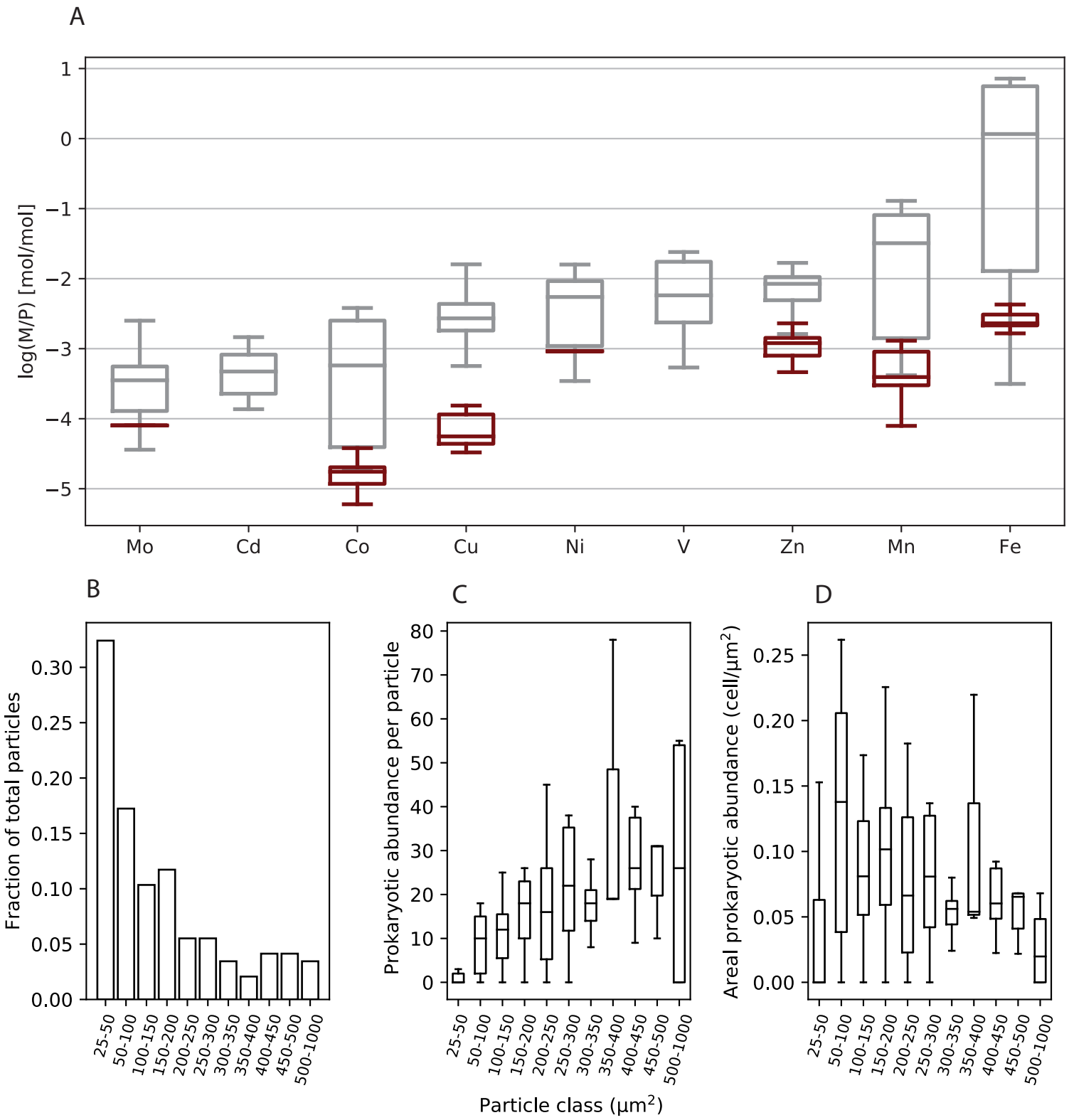
A
log(M/P) [mol/mol]
1
0
−1
−2
−3
−4
−5
Mo
Cd
Co
Cu
Ni
V
Zn
Mn
Fe
B
Fraction of total particles
0.30
0.25
0.20
0.15
0.10
0.05
0.00
C
Prokaryotic abundance per particle
80
70
60
50
40
30
20
10
0
D
Areal prokaryotic abundance (cell/µm²)
0.25
0.20
0.15
0.10
0.05
0.00
25-50
50-100
100-150
150-200
200-250
250-300
300-350
350-400
400-450
450-500
500-1000
Particle class (µm²)

Figure 1


iron(III) transport system ATP-binding protein, ABC type (afuC, fbpC)
iron(III) transport system ATP-binding protein, ABC type (afuB, fbpB)
iron(III) transport system ATP-binding protein, ABC type (afuA, fbpA)
ferrous iron transport protein B (feoB)
high-affinity iron transporter, FTR, FTH1 (efeU)
manganese/zinc/iron transport system substrate-binding protein (troA, mntA, znuA)
manganese/zinc/iron transport system substrate-binding protein (troB, mntB, znuB)
manganese/zinc/iron transport system substrate-binding protein (troC, mntC, znuC)
zinc/manganese transport system substrate-binding protein (ABC.ZM.S)
zinc transport system substrate-binding protein (znuA)
zinc transporter, ZIP family, TC.ZIP, ZRT3, ZIP2 (zupT)
zinc and cadmium transporter (zipB)
peptide/nickel transport system ATP-binding protein_ABC.PE.A (ddpD)
peptide/nickel transport system ATP-binding protein-ABC.PE.A1 (ddpF)
peptide/nickel transport system permease protein (ABC.PE.P)
peptide/nickel transport system permease protein (ABC.PE.P1)
peptide/nickel transport system substrate-binding protein (ABC.PE.S)
nickel transport system ATP-binding protein (nikE, cntF)
molybdate transport system ATP-binding protein (modC)
molybdate transport system permease protein (modB)
molybdate transport system substrate-binding protein (modA)
molybdate transport system ATP-binding protein (modF)
molybdate/tungstate transport system ATP-binding protein (wtpC)
tungstate transport system substrate-binding protein (tupA, vupA)
tungstate transport system ATP-binding protein (tupC, vupC)
ferrous-iron efflux pump (FieF)
outer membrane protein, cobalt-zinc-cadmium efflux system, heavy metal efflux system (czcC, cusC, cnrC)
cobalt-zinc-cadmium resistance protein, heavy metal efflux system protein (czcA, cusA, cnrA)
membrane fusion protein, cobalt-zinc-cadmium efflux system, heavy metal efflux system (czcB, cusB, cnrB)
membrane fusion protein, gold/copper resistance efflux system (gesA, mexP)
copper/silver efflux system membrane protein Cu(I)/Ag(I) (cusA, silA)
cobalt-zinc-cadmium efflux system protein (czcD, zitB)
Fur family transcriptional regulator, ferric uptake regulator (fur, zur, furB)
Fur family transcriptional regulator, peroxide stress response regulator (perR)
Fur family transcriptional regulator, zinc uptake regulator (zur)
suppressor for copper-sensitivity B (scsB)
two-component system, OmpR family, heavy metal sensor histidine kinase (cusS, copS, silS)
two-component system, OmpR family, copper resistance phosphate regulon response regulator (cusR)
isochorismate synthase (entC)
enterobactin synthetase component D (entD)
enterobactin synthetase component D (entF)
menaquinone-specific isochorismate synthase (menF)
nonribosomal peptide synthetase DhbF (dhbF)
yersiniabactin nonribosomal peptide synthetase, HMWP2 (irp2)
yersiniabactin nonribosomal peptide/polyketide synthase, HMWP1 (irp1)
mycobactin phenyloxazoline synthetase (mbtB)
mycobactin peptide synthetase MbtE (mbtE)
mycobactin peptide synthetase MbtF (mbtF)
nonribosomal peptide synthetase VibF (vibF)
pyochelin synthetase (pchF)
nonribosomal peptide synthetase MxcG (mxcG)
hemoglobin/transferrin/lactoferrin receptor protein, TC.FEV.OM3 (tbpA, hemR, lbpA, hpuB, bhuR, hugA, hmbR)
catecholate siderophore receptor (fiu)
Fe(3+) dicitrate transport protein (fecA)
iron complex transport system ATP-binding protein, iron-siderophore and Vit B12 transporter (ABC.FEV.A)
iron complex transport system permease protein, iron-siderophore and Vit B12 transporter (ABC.FEV.P)
iron complex transport system substrate-binding protein, iron-siderophore and Vit B12 transporter (ABC.FEV.S)
ferric hydroxamate transport systems ATP binding protein; iron-chelate-transporting ATPase (fhuC)
ferritin (ftnA, ftn)
bacterioferritin (bfr)
starvation-inducible DNA-binding protein; iron-detoxification proteins, iron storage protein (dps)
Metal Transport
Metal Efflux
Sensing regulation
Siderophore synthesis
Fe complex transport
Fe storage
0.0
2.5
5.0
7.5
10.0
Log 2 Fold change

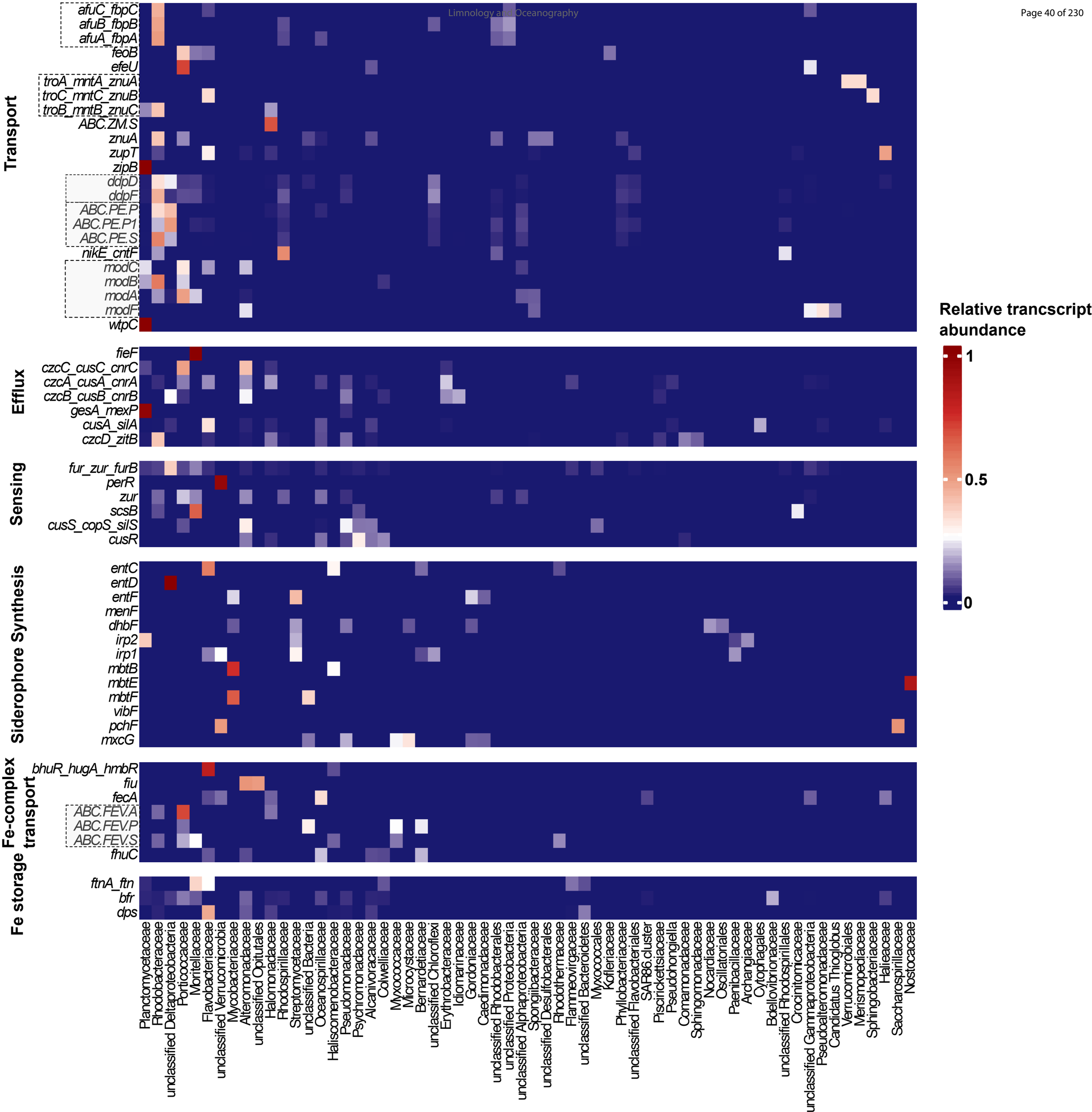
Transport
afuC_fbpC
afuB_fbpB
afuA_fbpA
feoB
efeU
troA_mntA_znuA
troC_mntC_znuB
troB_mntB_znuC
ABC.ZM.S
znuA
zupT
zipB
ddpD
ddpF
ABC.PE.P
ABC.PE.P1
ABC.PE.S
nikE_cntF
modC
modB
modA
modF
wtpC
Efflux
fieF
czcC_cusC_cnrC
czcA_cusA_cnrA
czcB_cusB_cnrB
gesA_mexP
cusA_silA
czcD_zitB
Sensing
fur_zur_furB
perR
zur
scsB
cusS_copS_silS
cusR
Siderophore Synthesis
entC
entD
entF
menF
dhbF
irp2
irp1
mbtB
mbtE
mbtF
vibF
pchF
mxcG
Fe storage
Fe-complex transport
bhuR_hugA_hmbR
fiu
fecA
ABC.FEV.A
ABC.FEV.P
ABC.FEV.S
fhuC
ftnA_ftn
bfr
dps
Planctomycetaceae
Rhodobacteraceae
unclassified Deltaproteobacteria
Porticoccaceae
Moritellaceae
Flavobacteriaceae
unclassified Verrucomicrobia
Mycobacteriaceae
Alteromonadaceae
unclassified Opitutales
Halomonadaceae
Rhodospirillaceae
Streptomycetaceae
unclassified Bacteria
Oceanospirillaceae
Haliscomenobacteraceae
Pseudomonadaceae
Psychromonadaceae
Alcanivoracaceae
Colwelliaceae
Myxococcaceae
Microcystaceae
Bernardetiaceae
unclassified Chloroflexi
Erythrobacteraceae
Idiomarinaceae
Gordoniaceae
Caedimonadaceae
unclassified Rhodobacterales
unclassified Proteobacteria
unclassified Alphaproteobacteria
Spongiibacteraceae
unclassified Desulfobacterales
Rhodothermaceae
Flammeovirgaceae
unclassified Bacteroidetes
Myxococcales
Kofleriaceae
Phyllobacteriaceae
unclassified Flavobacteriales
SAR86.cluster
Piscirickettsiaceae
Pseudohongiella
Comamonadaceae
Sphingomonadaceae
Nocardiaceae
Oscillatoriales
Paenibacillaceae
Archangiaceae
Cytophagales
Bdellovibrionaceae
unclassified Rhodospirillales
Crocinitomicaceae
unclassified Gammaproteobacteria
Pseudoalteromonadaceae
Candidatus Thioglobus
Verrucomicrobiales
Merismopediaceae
Sphingobacteriaceae
Halieaceae
Saccharospirillaceae
Nostocaceae
Relative trancscript abundance
1
0.5
0

Supplementary Material for the manuscript

Homeostasis drives intense microbial trace metal processing on marine particles

Pavla Debeljak, Stéphane Blain, Andrew Bowie, Pier van der Merwe, Barbara Bayer, and Ingrid Obernosterer*

*Corresponding author

e-mail: Ingrid.obernosterer@obs-banyuls.fr

This PDF file includes

10 Supplementary Figures

1 Supplementary Table (Suppl. Table 3)

Supplementary Methods

Other Supplementary Material

Supplementary Tables 1 and 2, provided separately in Excel format

Supplementary Figures

Fig. S1 Map of study sites.

Location of stations of the Heard Earth-Ocean-Biosphere Interactions (HEOBI) cruise (8 January - 27 February 2016), where particulate matter for the chemical analyses shown in Fig. 1a was collected. The location of the station where particles for the incubation experiment were collected is highlighted in yellow. The blue colored station is located in High-Nutrient-Low-Chlorophyll (HNLC) waters and refers to the location where seawater and the ambient prokaryotic community for the incubation experiment were sampled.

Fig. S2. Picture of particles and prokaryotic cells.

Microscopic observations of particles collected at the end of the incubation showing the attached cells clustering around particles. Observations were made with an Olympus AX70 epifluorescence microscope with excitation at 365 nm after staining with DAPI.

Fig. S3. Cell-specific microbial activity.

Cell-specific prokaryotic heterotrophic production, as determined by ^{3}H-leucine incorporation, of the ambient prokaryotic community (< 0.8 µm size fraction) over the 12-day incubation period in the particle-amended treatments (white circles) and the particle-free control (black circles). Phase 1 and phase 2 are indicated by shaded areas. Mean values ±SD of replicate biological incubations are shown (see details in Material and Methods).

Fig. S4. Particle characteristics

Size class distribution of particles (a), prokaryotic cell abundance on individual particles (b) and cell abundance per surface unit (c) in the incubation experiments. Observations are from the initial time point.

Fig. S5. Microbial activity of particle-attached cells.

Prokaryotic heterotrophic production, as determined by ^{3}H-leucine incorporation, of particle-attached cells (> 0.8 μm)(white circles) and of total cells in the control treatment (black circles). Mean values ±SD of replicate biological incubations are shown (see details in Material and Methods).

Fig. S6. Prokaryotic community composition.

Composition of prokaryotic communities attached to particles (a) and in the control (b) based on 16S rRNA sequencing. Taxonomy is shown for families with a minimum of 5% relative abundance in at least one treatment. Results for replicate incubations are shown. PA-particle attached; Ctrl-Control.

Fig. S7. Enrichment of normalized gene transcripts involved in trace-metal processing

Normalized transcript counts of metal-related KEGG orthologs in prokaryotic communities attached to particles (PA) and in communities in particle-free incubations (C). Significantly different transcripts are indicated by an asterisk (*) (adjusted p-value <0.05) and genes potentially implicated in the transport of multiple metals are indicated by the letter M (for multiple). Genes that are part of an ABC transporter complex are highlighted by rectangular boxes.

Fig. S8. Enrichment of absolute gene transcripts involved in trace-metal processing

Absolute transcript counts of metal-related KEGG orthologs in prokaryotic communities attached to particles (PA) and in communities in particle-free incubations (C). Significantly different transcripts are indicated by an asterisk (*) (adjusted p-value <0.05) and genes potentially implicated in the transport of multiple metals are indicated the letter M (for multiple). Genes that are part of an ABC transporter complex are highlighted by rectangular boxes.

Fig. S9. Taxonomic assignment of metal-related genes

Heatmap illustrating the relative contribution of prokaryotic groups to the expression of a given KEGG orthologous (KO) gene in the community in particle-free incubations (each KO gene sums up to 1 and 1 equals 100%). Phylogenetic groups are visualized on the family or if possible lowest

taxonomic level. KO gene transcripts are grouped by function: transport, efflux and sensing/regulation of 9 metals, siderophore synthesis, Fe-complex transport and Fe storage (as in Fig. 2). The full description of the KEGG abbreviations is given in Fig. 2. Grey shading indicates that the taxonomy of the respective KO genes could not be assigned.

Fig. S10. Taxonomic assignment of genes involved in the nitrogen cycle

Heatmap illustrating the relative contribution of prokaryotic groups to the expression of a given KEGG orthologous (KO) gene in the particle-attached community. (each KO gene sums up to 1 and 1 equals 100%).

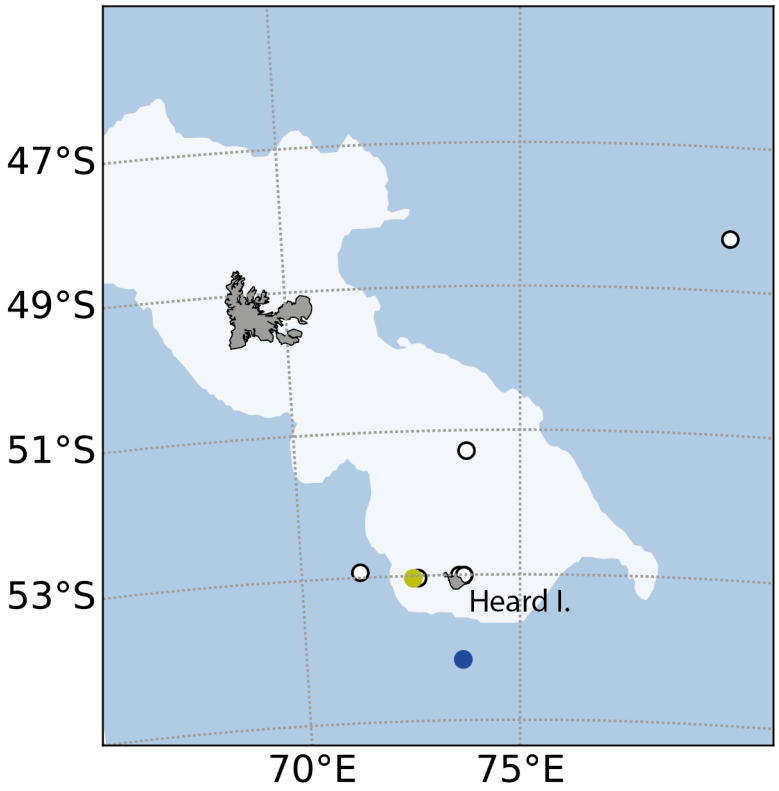

Fig. S1

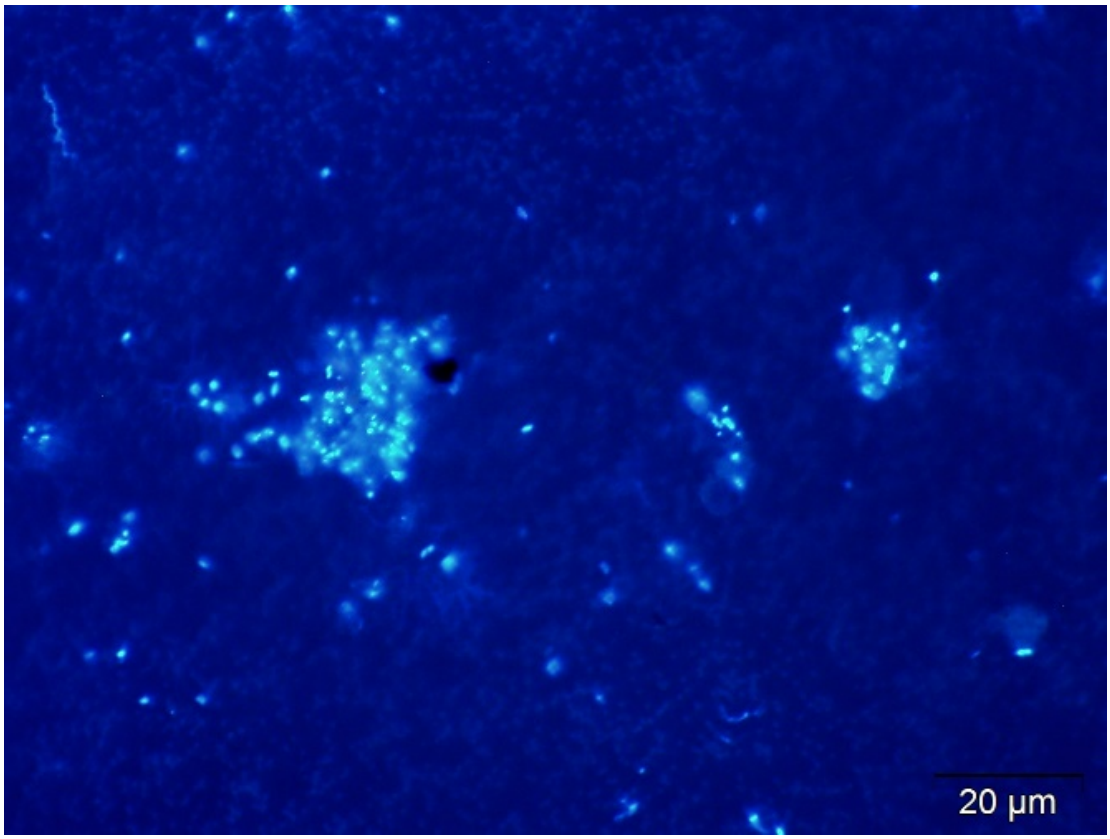

Fig. S2

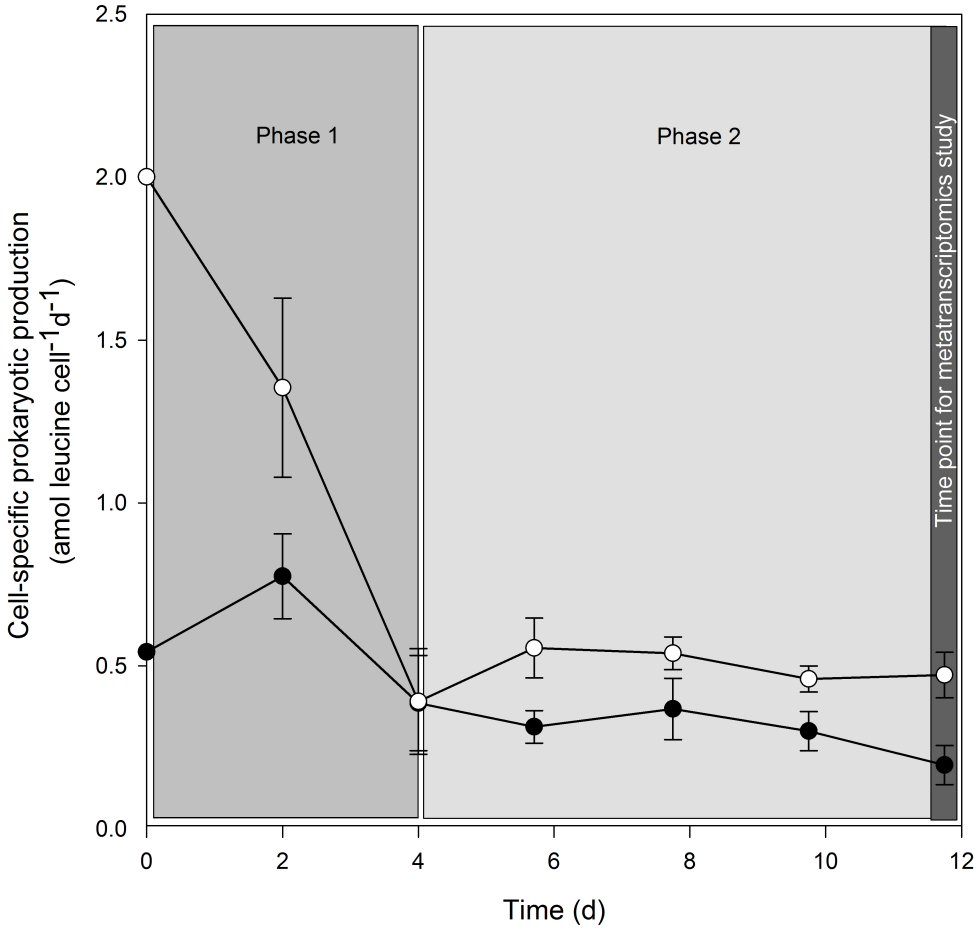
Phase 1
Phase 2
Time point for metatranscriptomics study
Cell-specific prokaryotic production
(amol leucine cell^{-1}d^{-1})
Time (d)
0.0
0.5
1.0
1.5
2.0
2.5
0
2
4
6
8
10
12

Fig. S3

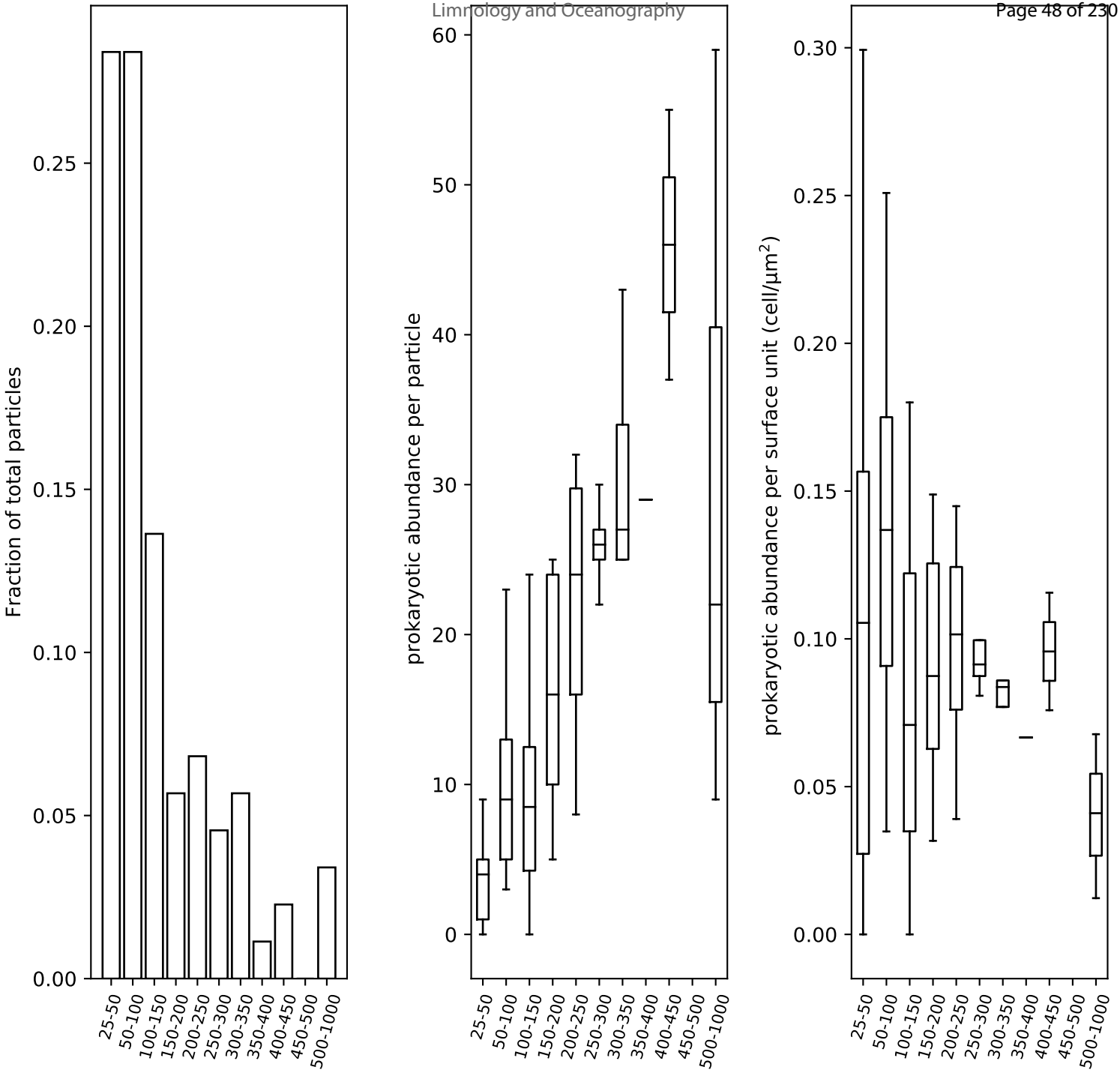
Fraction of total particles
0.00
0.05
0.10
0.15
0.20
0.25
prokaryotic abundance per particle
0
10
20
30
40
50
60
prokaryotic abundance per surface unit (cell/µm²)
0.00
0.05
0.10
0.15
0.20
0.25
0.30
25-50
50-100
100-150
150-200
200-250
250-300
300-350
350-400
400-450
450-500
500-1000
Surface class (µm²)

Fig. S4

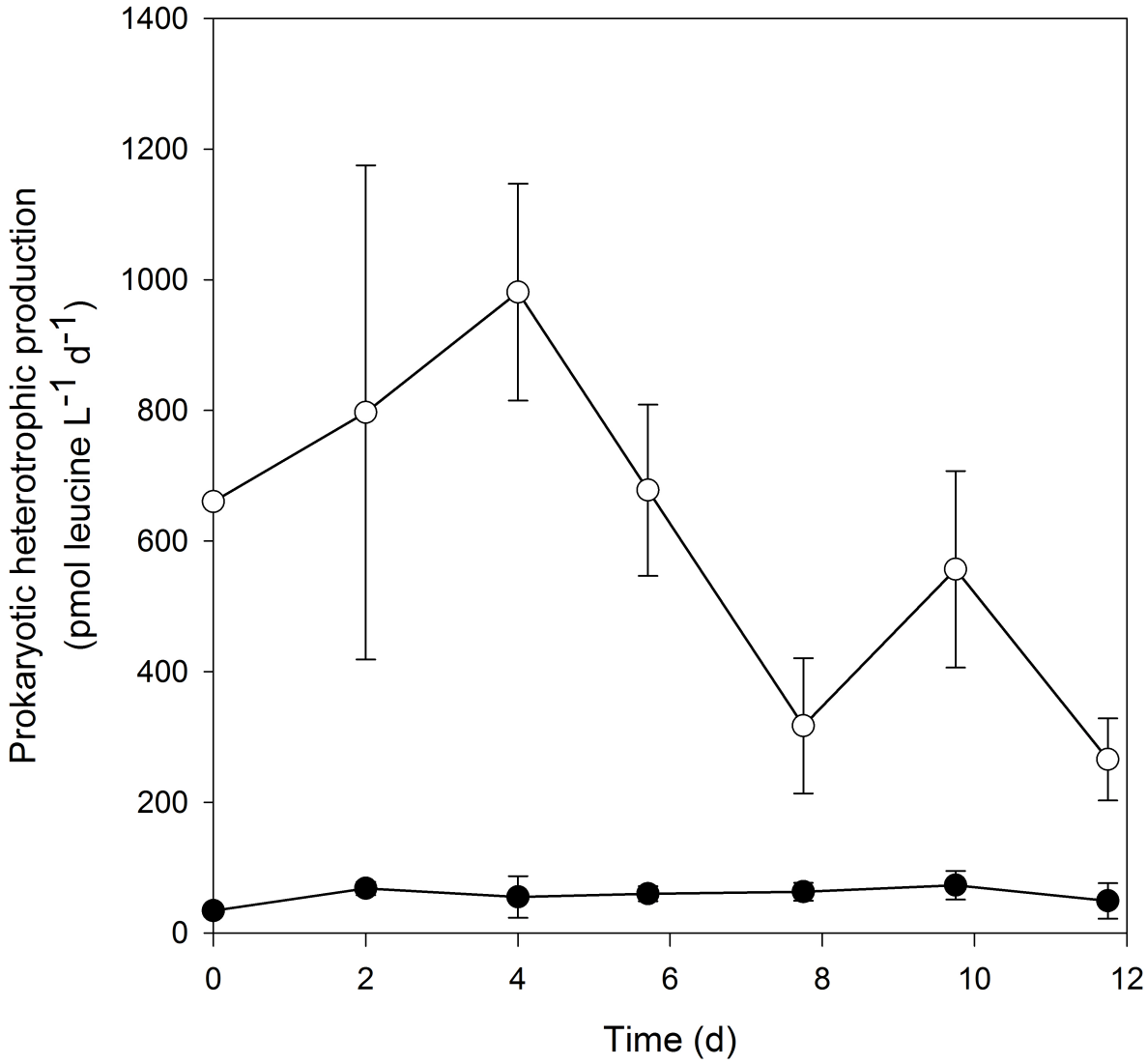
Prokaryotic heterotrophic production
(pmol leucine L-1 d-1)
1400
1200
1000
800
600
400
200
0
0
2
4
6
8
10
12
Time (d)

Fig. S5

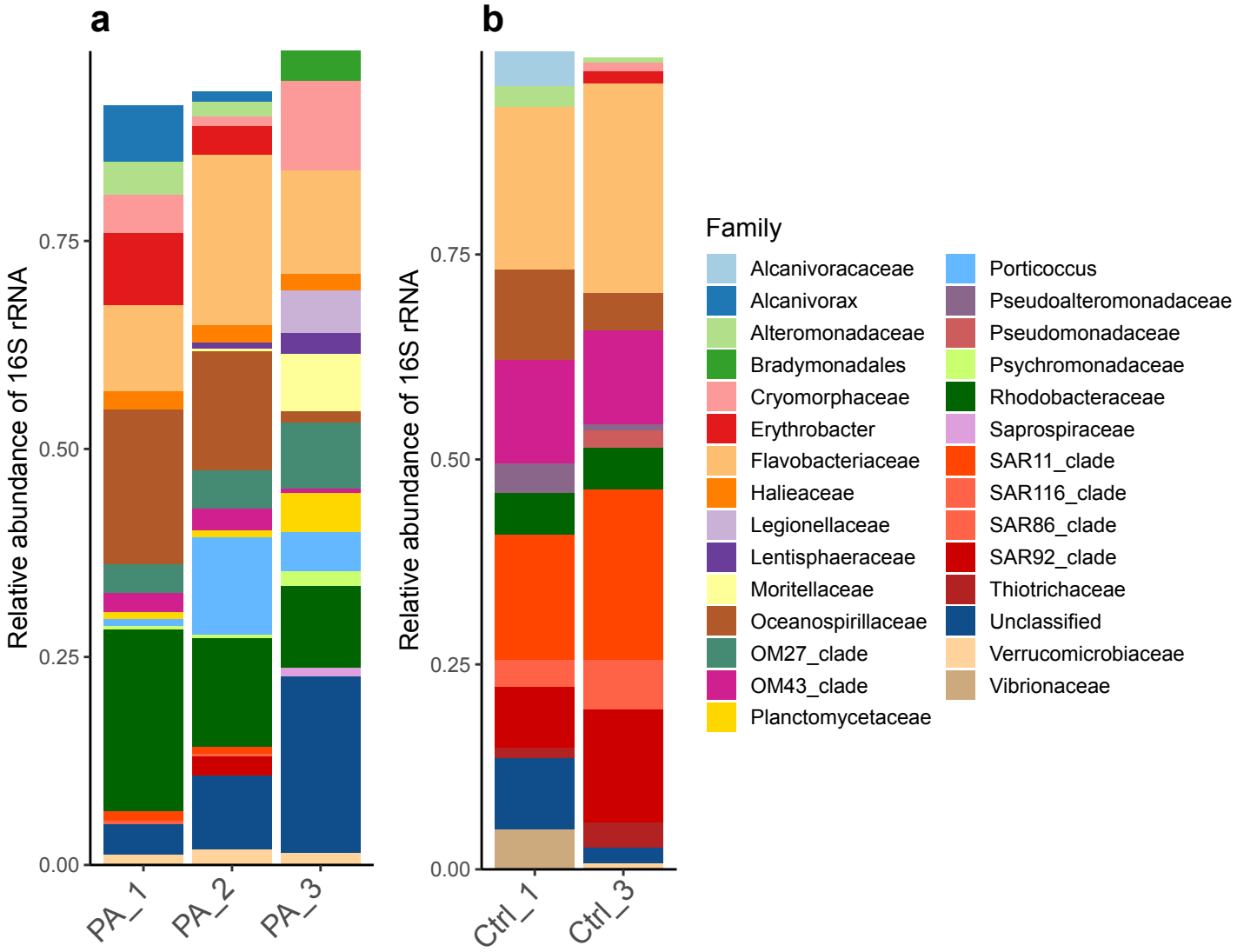
a
b
Relative abundance of 16S rRNA
0.00
0.25
0.50
0.75
PA_1
PA_2
PA_3
Ctrl_1
Ctrl_3
Family
Alcanivoracaceae
Alcanivorax
Alteromonadaceae
Bradymonadales
Cryomorphaceae
Erythrobacter
Flavobacteriaceae
Halieaceae
Legionellaceae
Lentisphaeraceae
Moritellaceae
Oceanospirillaceae
OM27_clade
OM43_clade
Planctomycetaceae
Porticoccus
Pseudoalteromonadaceae
Pseudomonadaceae
Psychromonadaceae
Rhodobacteraceae
Saprospiraceae
SAR11_clade
SAR116_clade
SAR86_clade
SAR92_clade
Thiotrichaceae
Unclassified
Verrucomicrobiaceae
Vibrionaceae

Fig. S6

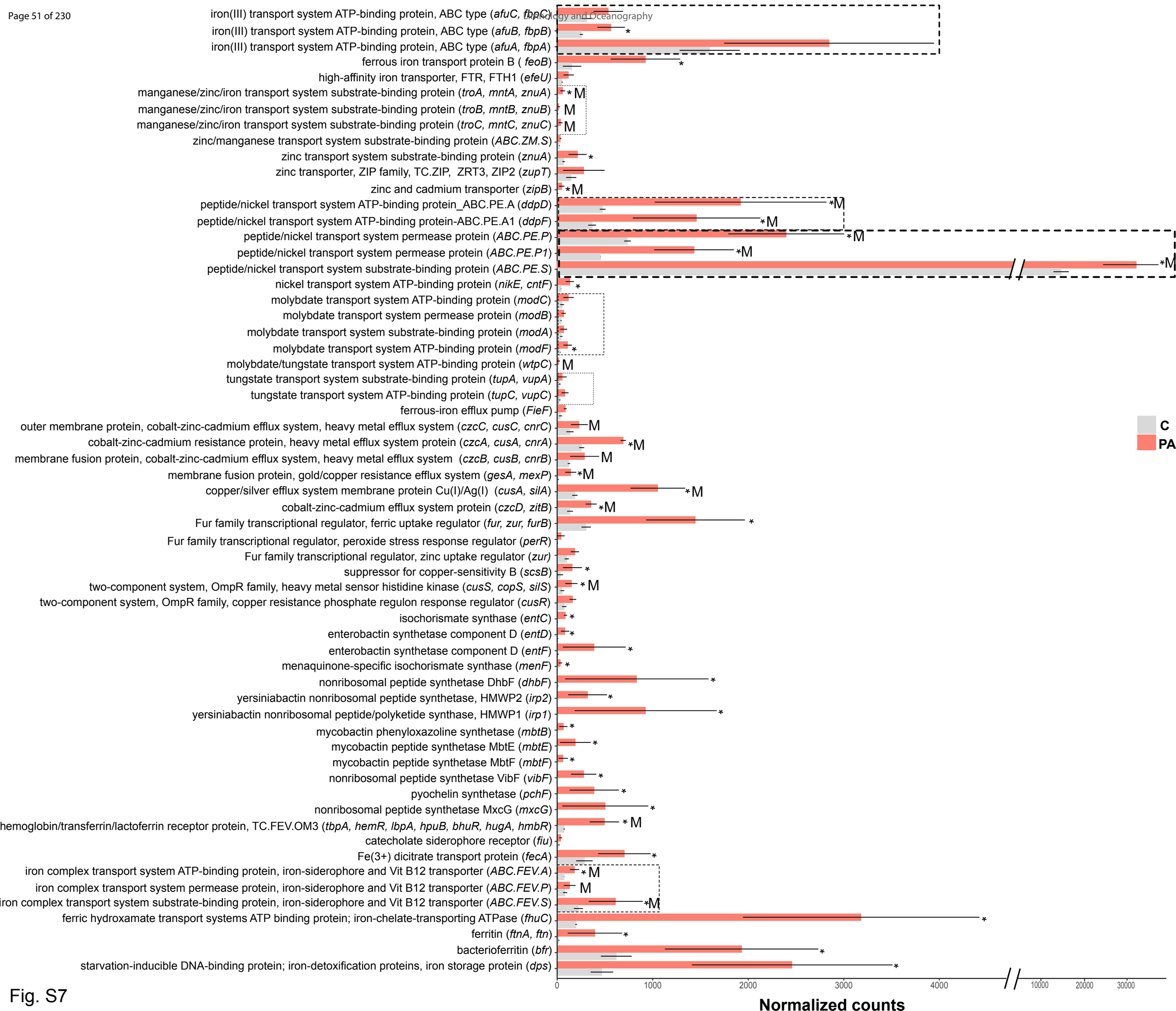
iron(III) transport system ATP-binding protein, ABC type (afuC, fbpC)
iron(III) transport system ATP-binding protein, ABC type (afuB, fbpB)
iron(III) transport system ATP-binding protein, ABC type (afuA, fbpA)
ferrous iron transport protein B (feoB)
high-affinity iron transporter, FTR, FTH1 (efeU)
manganese/zinc/iron transport system substrate-binding protein (troA, mntA, znuA)
manganese/zinc/iron transport system substrate-binding protein (troB, mntB, znuB)
manganese/zinc/iron transport system substrate-binding protein (troC, mntC, znuC)
zinc/manganese transport system substrate-binding protein (ABC.ZM.S)
zinc transport system substrate-binding protein (znuA)
zinc transporter, ZIP family, TC.ZIP, ZRT3, ZIP2 (zupT)
zinc and cadmium transporter (zipB)
peptide/nickel transport system ATP-binding protein_ABC.PE.A (ddpD)
peptide/nickel transport system ATP-binding protein-ABC.PE.A1 (ddpF)
peptide/nickel transport system permease protein (ABC.PE.P)
peptide/nickel transport system permease protein (ABC.PE.P1)
peptide/nickel transport system substrate-binding protein (ABC.PE.S)
nickel transport system ATP-binding protein (nikE, cntF)
molybdate transport system ATP-binding protein (modC)
molybdate transport system permease protein (modB)
molybdate transport system substrate-binding protein (modA)
molybdate transport system ATP-binding protein (modF)
molybdate/tungstate transport system ATP-binding protein (wtpC)
tungstate transport system substrate-binding protein (tupA, vupA)
tungstate transport system ATP-binding protein (tupC, vupC)
ferrous-iron efflux pump (FieF)
outer membrane protein, cobalt-zinc-cadmium efflux system, heavy metal efflux system (czcC, cusC, cnrC)
cobalt-zinc-cadmium resistance protein, heavy metal efflux system protein (czcA, cusA, cnrA)
membrane fusion protein, cobalt-zinc-cadmium efflux system, heavy metal efflux system (czcB, cusB, cnrB)
membrane fusion protein, gold/copper resistance efflux system (gesA, mexP)
copper/silver efflux system membrane protein Cu(I)/Ag(I) (cusA, silA)
cobalt-zinc-cadmium efflux system protein (czcD, zitB)
Fur family transcriptional regulator, ferric uptake regulator (fur, zur, furB)
Fur family transcriptional regulator, peroxide stress response regulator (perR)
Fur family transcriptional regulator, zinc uptake regulator (zur)
suppressor for copper-sensitivity B (scsB)
two-component system, OmpR family, heavy metal sensor histidine kinase (cusS, copS, silS)
two-component system, OmpR family, copper resistance phosphate regulon response regulator (cusR)
isochorismate synthase (entC)
enterobactin synthetase component D (entD)
enterobactin synthetase component D (entF)
menaquinone-specific isochorismate synthase (menF)
nonribosomal peptide synthetase DhbF (dhbF)
yersiniabactin nonribosomal peptide synthetase, HMWP2 (irp2)
yersiniabactin nonribosomal peptide/polyketide synthase, HMWP1 (irp1)
mycobactin phenyloxazoline synthetase (mbtB)
mycobactin peptide synthetase MbtE (mbtE)
mycobactin peptide synthetase MbtF (mbtF)
nonribosomal peptide synthetase VibF (vibF)
pyochelin synthetase (pchF)
nonribosomal peptide synthetase MxcG (mxcG)
hemoglobin/transferrin/lactoferrin receptor protein, TC.FEV.OM3 (tbpA, hemR, lbpA, hpuB, bhuR, hugA, hmbR)
catecholate siderophore receptor (fiu)
Fe(3+) dicitrate transport protein (fecA)
iron complex transport system ATP-binding protein, iron-siderophore and Vit B12 transporter (ABC.FEV.A)
iron complex transport system permease protein, iron-siderophore and Vit B12 transporter (ABC.FEV.P)
iron complex transport system substrate-binding protein, iron-siderophore and Vit B12 transporter (ABC.FEV.S)
ferric hydroxamate transport systems ATP binding protein; iron-chelate-transporting ATPase (fhuC)
ferritin (ftnA, ftn)
bacterioferritin (bfr)
starvation-inducible DNA-binding protein; iron-detoxification proteins, iron storage protein (dps)
C
PA
0
1000
2000
3000
4000
10000
20000
30000
Normalized counts

Fig. S7

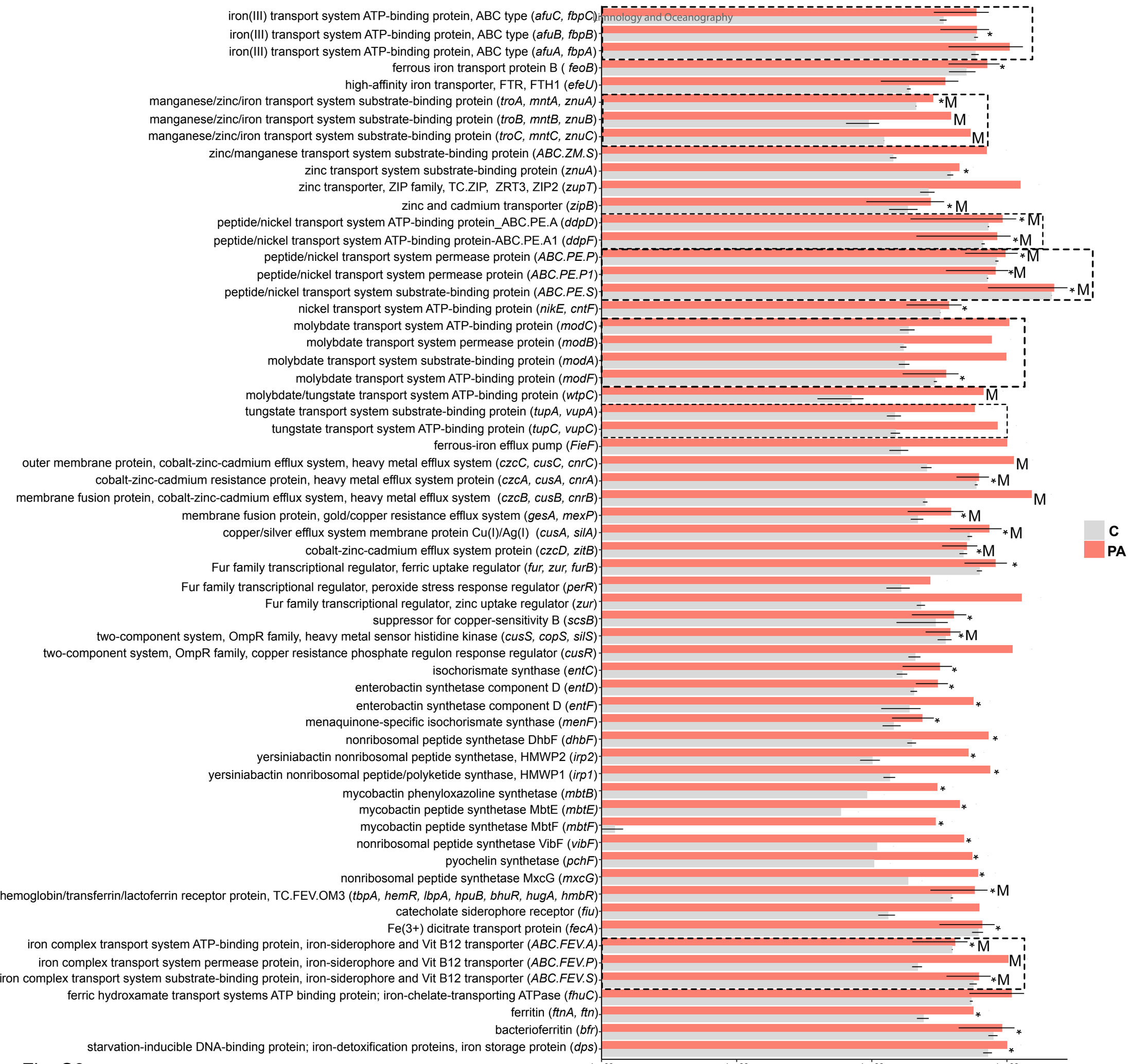
iron(III) transport system ATP-binding protein, ABC type (afuC, fbpC)
iron(III) transport system ATP-binding protein, ABC type (afuB, fbpB)
iron(III) transport system ATP-binding protein, ABC type (afuA, fbpA)
ferrous iron transport protein B (feoB)
high-affinity iron transporter, FTR, FTH1 (efeU)
manganese/zinc/iron transport system substrate-binding protein (troA, mntA, znuA)
manganese/zinc/iron transport system substrate-binding protein (troB, mntB, znuB)
manganese/zinc/iron transport system substrate-binding protein (troC, mntC, znuC)
zinc/manganese transport system substrate-binding protein (ABC.ZM.S)
zinc transport system substrate-binding protein (znuA)
zinc transporter, ZIP family, TC.ZIP, ZRT3, ZIP2 (zupT)
zinc and cadmium transporter (zipB)
peptide/nickel transport system ATP-binding protein_ABC.PE.A (ddpD)
peptide/nickel transport system ATP-binding protein-ABC.PE.A1 (ddpF)
peptide/nickel transport system permease protein (ABC.PE.P)
peptide/nickel transport system permease protein (ABC.PE.P1)
peptide/nickel transport system substrate-binding protein (ABC.PE.S)
nickel transport system ATP-binding protein (nikE, cntF)
molybdate transport system ATP-binding protein (modC)
molybdate transport system permease protein (modB)
molybdate transport system substrate-binding protein (modA)
molybdate transport system ATP-binding protein (modF)
molybdate/tungstate transport system ATP-binding protein (wtpC)
tungstate transport system substrate-binding protein (tupA, vupA)
tungstate transport system ATP-binding protein (tupC, vupC)
ferrous-iron efflux pump (FieF)
outer membrane protein, cobalt-zinc-cadmium efflux system, heavy metal efflux system (czcC, cusC, cnrC)
cobalt-zinc-cadmium resistance protein, heavy metal efflux system protein (czcA, cusA, cnrA)
membrane fusion protein, cobalt-zinc-cadmium efflux system, heavy metal efflux system (czcB, cusB, cnrB)
membrane fusion protein, gold/copper resistance efflux system (gesA, mexP)
copper/silver efflux system membrane protein Cu(I)/Ag(I) (cusA, silA)
cobalt-zinc-cadmium efflux system protein (czcD, zitB)
Fur family transcriptional regulator, ferric uptake regulator (fur, zur, furB)
Fur family transcriptional regulator, peroxide stress response regulator (perR)
Fur family transcriptional regulator, zinc uptake regulator (zur)
suppressor for copper-sensitivity B (scsB)
two-component system, OmpR family, heavy metal sensor histidine kinase (cusS, copS, silS)
two-component system, OmpR family, copper resistance phosphate regulon response regulator (cusR)
isochorismate synthase (entC)
enterobactin synthetase component D (entD)
enterobactin synthetase component D (entF)
menaquinone-specific isochorismate synthase (menF)
nonribosomal peptide synthetase DhbF (dhbF)
yersiniabactin nonribosomal peptide synthetase, HMWP2 (irp2)
yersiniabactin nonribosomal peptide/polyketide synthase, HMWP1 (irp1)
mycobactin phenyloxazoline synthetase (mbtB)
mycobactin peptide synthetase MbtE (mbtE)
mycobactin peptide synthetase MbtF (mbtF)
nonribosomal peptide synthetase VibF (vibF)
pyochelin synthetase (pchF)
nonribosomal peptide synthetase MxcG (mxcG)
hemoglobin/transferrin/lactoferrin receptor protein, TC.FEV.OM3 (tbpA, hemR, lbpA, hpuB, bhuR, hugA, hmbR)
catecholate siderophore receptor (fiu)
Fe(3+) dicitrate transport protein (fecA)
iron complex transport system ATP-binding protein, iron-siderophore and Vit B12 transporter (ABC.FEV.A)
iron complex transport system permease protein, iron-siderophore and Vit B12 transporter (ABC.FEV.P)
iron complex transport system substrate-binding protein, iron-siderophore and Vit B12 transporter (ABC.FEV.S)
ferric hydroxamate transport systems ATP binding protein; iron-chelate-transporting ATPase (fhuC)
ferritin (ftnA, ftn)
bacterioferritin (bfr)
starvation-inducible DNA-binding protein; iron-detoxification proteins, iron storage protein (dps)
C
PA
1e+00
1e+03
1e+06
1e+09
Transcripts per Liter

Fig. S8

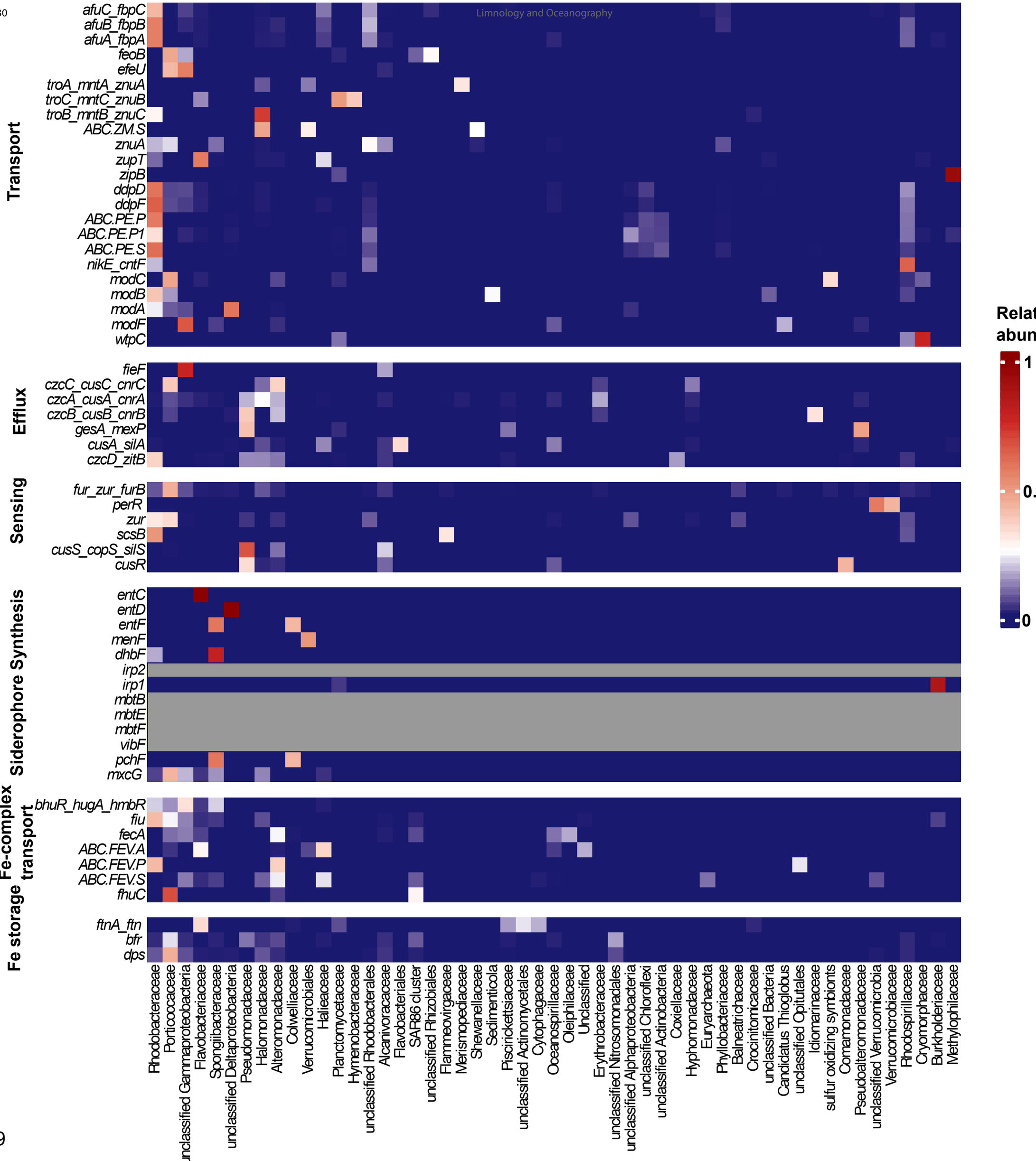
Transport
afuC_fbpC
afuB_fbpB
afuA_fbpA
feoB
efeU
troA_mntA_znuA
troC_mntC_znuB
troB_mntB_znuC
ABC.ZM.S
znuA
zupT
zipB
ddpD
ddpF
ABC.PE.P
ABC.PE.P1
ABC.PE.S
nikE_cntF
modC
modB
modA
modF
wtpC
Efflux
fieF
czcC_cusC_cnrC
czcA_cusA_cnrA
czcB_cusB_cnrB
gesA_mexP
cusA_silA
czcD_zitB
Sensing
fur_zur_furB
perR
zur
scsB
cusS_copS_silS
cusR
Siderophore Synthesis
entC
entD
entF
menF
dhbF
irp2
irp1
mbtB
mbtE
mbtF
vibF
pchF
mxcG
Fe-complex transport
Fe storage
bhuR_hugA_hmbR
fiu
fecA
ABC.FEV.A
ABC.FEV.P
ABC.FEV.S
fhuC
ftnA_ftn
bfr
dps
Rhodobacteraceae
Porticoccaceae
unclassified Gammaproteobacteria
Flavobacteriaceae
Spongiibacteraceae
unclassified Deltaproteobacteria
Pseudomonadaceae
Halomonadaceae
Alteromonadaceae
Colwelliaceae
Verrucomicrobiales
Halieaceae
Planctomycetaceae
Hymenobacteraceae
unclassified Rhodobacterales
Alcanivoracaceae
Flavobacteriales
SAR86 cluster
unclassified Rhizobiales
Flammeovirgaceae
Merismopediaceae
Shewanellaceae
Sedimenticola
Piscirickettsiaceae
unclassified Actinomycetales
Cytophagaceae
Oceanospirillaceae
Oleiphilaceae
Unclassified
Erythrobacteraceae
unclassified Nitrosomonadales
unclassified Alphaproteobacteria
unclassified Chloroflexi
unclassified Actinobacteria
Coxiellaceae
Hyphomonadaceae
Euryarchaeota
Phyllobacteriaceae
Balneatrichaceae
Crocinitomicaceae
unclassified Bacteria
Candidatus Thioglobus
unclassified Opitutales
Idiomarinaceae
sulfur oxidizing symbionts
Comamonadaceae
Pseudoalteromonadaceae
unclassified Verrucomicrobia
Verrucomicrobiaceae
Rhodospirillaceae
Cryomorphaceae
Burkholderiaceae
Methylophilaceae
Relative trancscript abundance
1
0.5
0

Fig. S9

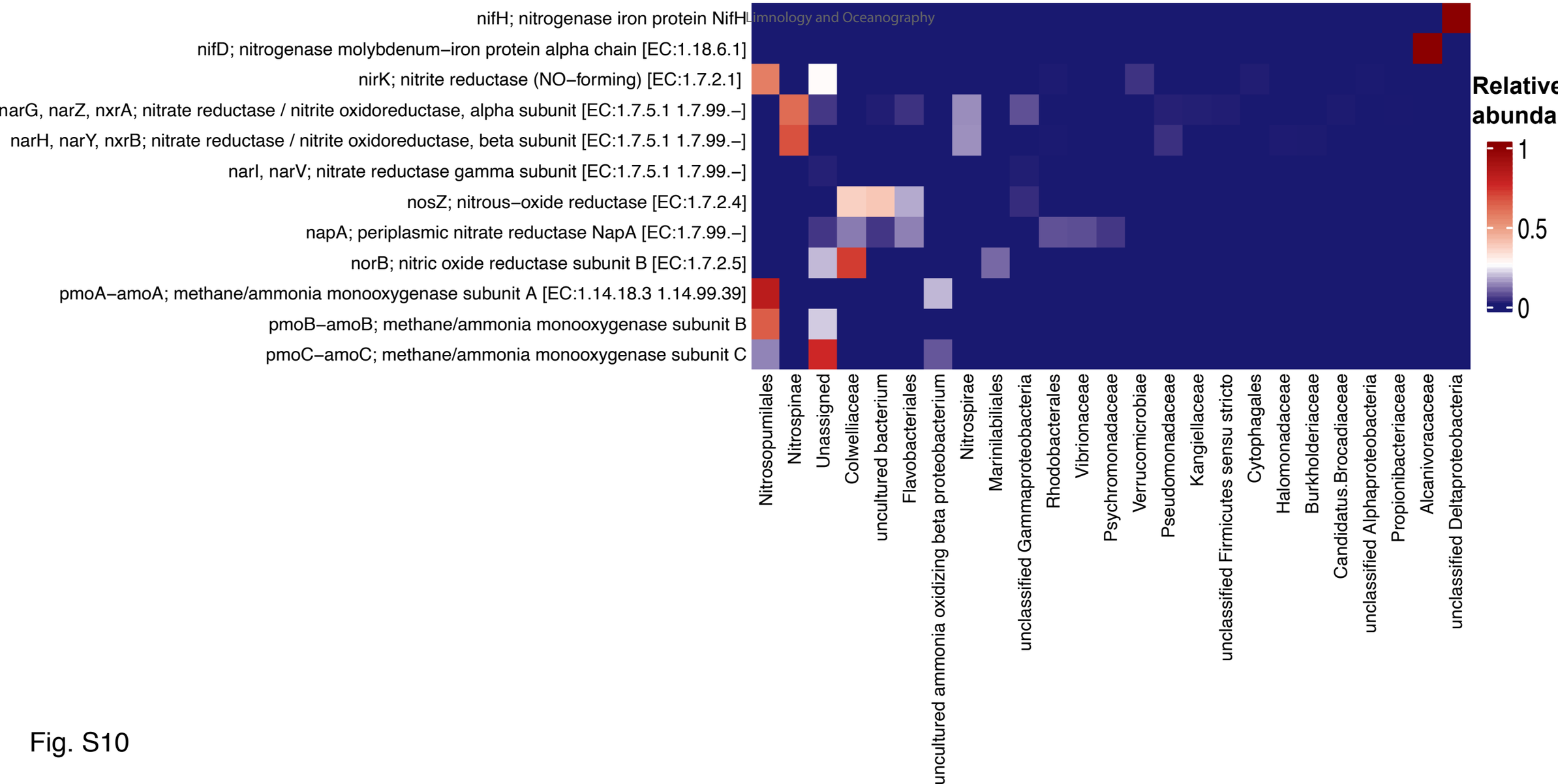
nifH; nitrogenase iron protein NifH
nifD; nitrogenase molybdenum–iron protein alpha chain [EC:1.18.6.1]
nirK; nitrite reductase (NO–forming) [EC:1.7.2.1]
narG, narZ, nxrA; nitrate reductase / nitrite oxidoreductase, alpha subunit [EC:1.7.5.1 1.7.99.–]
narH, narY, nxrB; nitrate reductase / nitrite oxidoreductase, beta subunit [EC:1.7.5.1 1.7.99.–]
narI, narV; nitrate reductase gamma subunit [EC:1.7.5.1 1.7.99.–]
nosZ; nitrous–oxide reductase [EC:1.7.2.4]
napA; periplasmic nitrate reductase NapA [EC:1.7.99.–]
norB; nitric oxide reductase subunit B [EC:1.7.2.5]
pmoA–amoA; methane/ammonia monooxygenase subunit A [EC:1.14.18.3 1.14.99.39]
pmoB–amoB; methane/ammonia monooxygenase subunit B
pmoC–amoC; methane/ammonia monooxygenase subunit C
Nitrosopumilales
Nitrospinae
Unassigned
Colwelliaceae
uncultured bacterium
Flavobacteriales
uncultured ammonia oxidizing beta proteobacterium
Nitrospirae
Marinilabiliales
unclassified Gammaproteobacteria
Rhodobacterales
Vibrionaceae
Psychromonadaceae
Verrucomicrobiae
Pseudomonadaceae
Kangiellaceae
unclassified Firmicutes sensu stricto
Cytophagales
Halomonadaceae
Burkholderiaceae
Candidatus.Brocadiaceae
unclassified Alphaproteobacteria
Propionibacteriaceae
Alcanivoracaceae
unclassified Deltaproteobacteria
Relative transcript abundance
1
0.5
0

Fig. S10

Supplementary Tables.

Table S1.

List of retrieved trace-metal related KEGG orthologous (KO) genes obtained from ExPASy

Table S2.

Fold changes of normalized transcript counts of trace metal related KEGG orthologous (KO) genes in prokaryotic communities attached to particles as compared to those in particle-free incubations. Significant results are marked with an asterisk (adapted p-value <0.05).

Table S3.

Fold changes of normalized transcript counts of KEGG orthologous (KO) genes involved in the nitrogen cycle in prokaryotic communities attached to particles as compared to those in particle-free incubations.

Table S3. Fold changes of normalized transcript counts of KEGG orthologous (KO) genes involved in the nitrogen cycle in prokaryotic communities attached to particles as compared to those in particle-free incubations.

	KEGG	baseMean	log2FoldChange	lfcSE	stat	pvalue	padj	Name
1	K00260	37,60712386	10,46838693	1,759704149	5,948947121	2,69872800178 75E-09	2,247322059042 47E-08	gudB, rocG; glutamate dehydrogenase [EC:1.4.1.2]
2	K00261	885,3507075	2,259970209	0,576191273	3,922256924	8,77233763334644E-05	0,000279917	GLUD1_2, gdhA; glutamate dehydrogenase (NAD(P)+) [EC:1.4.1.3]
3	K00262	1798,80668982927	2,169761914	0,492264601	4,40771469	1,04467031274805E-05	4,027330181534 95E-05	E1.4.1.4, gdhA; glutamate dehydrogenase (NADP+) [EC:1.4.1.4]
4	K00264	12,56429315	-0,775263572	1,584654967	-0,489231781	0,624677612	0,699006265	GLT1; glutamate synthase (NADH) [EC:1.4.1.14]
5	K00265	5501,70601338099	0,928711583	0,515449313	1,80175152	0,071584508	0,11062626	gltB; glutamate synthase (NADPH) large chain [EC:1.4.1.13]
6	K00266	2057,78031961726	1,355237387	0,574708734	2,358129098	0,018367304	0,033076864	gltD; glutamate synthase (NADPH) small chain [EC:1.4.1.13]
7	K00284	475,1062948	2,422812882	0,534200088	4,535403374	5,74934957947598E-06	2,345329387922 71E-05	GLU, gltS; glutamate synthase (ferredoxin) [EC:1.4.7.1]
8	K00362	394,5524098	1,791092946	0,578386761	3,096704606	0,001956848	0,004527838	nirB; nitrite reductase (NADH) large subunit [EC:1.7.1.15]
9	K00363	28,50845654	1,882298968	0,903189598	2,084057403	0,037154946	0,061835874	nirD; nitrite reductase (NADH) small subunit [EC:1.7.1.15]
10	K00367	101,27214989769	4,267322923	0,64581233	6,607682641	3,90382421914 11E-11	4,832809126904 62E-10	narB; ferredoxin-nitrate reductase [EC:1.7.7.2]
11	K00368	1033,74047812124	2,901392166	0,580609198	4,99715157	5,81833366456801E-07	2,902897076179 94E-06	nirK; nitrite reductase (NO-forming) [EC:1.7.2.1]
12	K00370	1750,37032733636	1,913454345	0,5046342	3,791765092	0,00014958	0,000453838	narG, narZ, nxrA; nitrate reductase / nitrite oxidoreductase, alpha subunit [EC:1.7.5.1 1.7.99.-]
13	K00371	782,9366268	1,995276243	0,568159402	3,511824739	0,000445041	0,001213511	narH, narY, nxrB; nitrate reductase / nitrite oxidoreductase, beta subunit [EC:1.7.5.1 1.7.99.-]
14	K00372	184,5299892	3,27949725	0,559256844	5,864027026	4,51773896939091E-09	3,527340881666 09E-08	nasA; assimilatory nitrate reductase catalytic subunit [EC:1.7.99.-]
15	K00374	86,05242788	2,053981317	0,813426527	2,525097535	0,011566618	0,02192118	narI, narV; nitrate reductase gamma subunit [EC:1.7.5.1 1.7.99.-]
16	K00376	97,74528118	6,237931615	0,748419386	8,334807637	7,76242905534476E-17	2,722730797442 9E-15	nosZ; nitrous-oxide reductase [EC:1.7.2.4]
17	K00459	982,7290438	0,24985122	0,510774572	0,48916143	0,624727414	0,699006265	ncd2, npd; nitronate monooxygenase [EC:1.13.12.16]
18	K00926	19,13751038	2,688283632	1,138431023	2,361393511	0,0182064	0,032812624	arcC; carbamate kinase [EC:2.7.2.2]
19	K01455	476,6796209	2,585805518	0,472640794	5,47097405	4,47568834774778E-08	2,755643224743 65E-07	E3.5.1.49; formamidase [EC:3.5.1.49]
20	K01501	12,15982604	1,34285333	1,359316468	0,987888665	0,323207178	0,409873797	E3.5.5.1; nitrilase [EC:3.5.5.1]
21	K01673	1333,38751951476	2,915826879	0,512297094	5,691671714	1,25801553102846E-08	8,798507414896 93E-08	cynT, can; carbonic anhydrase [EC:4.2.1.1]
22	K01674	287,4910239	4,66910174	0,628459387	7,429440681	1,09057841083461E-13	2,326902323577 99E-12	cah; carbonic anhydrase [EC:4.2.1.1]
23	K01915	9338,25414370086	1,872282078	0,504826767	3,708761502	0,000208275	0,000608401	glnA, GLUL; glutamine synthetase [EC:6.3.1.2]
24	K02567	252,8240175	5,433978036	0,601294873	9,037126839	1,60843696204102E-19	8,659375737499 93E-18	napA; periplasmic nitrate reductase NapA [EC:1.7.99.-]
25	K02575	331,4838189	1,938076299	0,775168712	2,500199338	0,012412344	0,023304604	NRT, narK, nrtP, nasA; MFS transporter, NNP family, nitrate/nitrite transporter
26	K02586	19,0672798	3,596096441	1,101459459	3,264846845	0,001095233	0,002691575	nifD; nitrogenase molybdenum-iron protein alpha chain [EC:1.18.6.1]
27	K02588	46,23827903	9,285180536	1,627628548	5,704729467	1,16528015410576E-08	8,237018493907 88E-08	nifH; nitrogenase iron protein NifH
28	K03385	41,95619655	10,61773328	1,67195532	6,350488646	2,14632052863595E-10	2,248295033390 15E-09	nrfA; nitrite reductase (cytochrome c-552) [EC:1.7.2.2]
29	K04561	110,7657737	5,223594224	0,910648264	5,736127139	9,68659586584602E-09	6,985816021630 38E-08	norB; nitric oxide reductase subunit B [EC:1.7.2.5]
30	K05601	47,13447267	10,78944903	1,651305808	6,533889105	6,40834027091527E-11	7,588392699319 11E-10	hcp; hydroxylamine reductase [EC:1.7.99.1]
31	K10535	56,97980093	0,527451314	0,779626905	0,676543243	0,498695801	0,585882151	hao; hydroxylamine dehydrogenase [EC:1.7.2.6]
32	K10944	351,8454379	2,987307403	0,608067191	4,912791623	8,97886895540917E-07	4,321430692676 14E-06	pmoA-amoA; methane/ammonia monooxygenase subunit A [EC:1.14.18.3 1.14.99.39]
33	K10945	511,4777025	1,162652781	0,593922366	1,957583763	0,050278874	0,080886444	pmoB-amoB; methane/ammonia monooxygenase subunit B
34	K10946	719,8034764	1,842517918	0,562160122	3,277567804	0,001047056	0,002591057	pmoC-amoC; methane/ammonia monooxygenase subunit C
35	K15371	2284,84773320443	2,513679024	0,534363179	4,70406481	2,55032231044917E-06	1,117123206942 26E-05	GDH2; glutamate dehydrogenase [EC:1.4.1.2]
36	K15576	51,46598835	2,503065765	0,748067739	3,346041588	0,000819741	0,002086532	nrtA, nasF, cynA; nitrate/nitrite transport system substrate-binding protein
37	K15577	19,80497687	3,635468986	1,384832513	2,625204819	0,008659686	0,016938887	nrtB, nasE, cynB; nitrate/nitrite transport system permease protein
38	K15578	10,54776424	3,059319906	1,822525667	1,67861554	0,093226996	0,139870704	nrtC, nasD; nitrate/nitrite transport system ATP-binding protein [EC:3.6.3.-]
39	K15864	90,7251984	0,88487197	0,74149845	1,193356465	0,232729797	0,311067829	nirS; nitrite reductase (NO-forming) / hydroxylamine reductase [EC:1.7.2.1 1.7.99.1]

Supplementary Methods

Internal standard addition

Prior to the lysis step of the extraction, known copy numbers of two artificial internal mRNA (MTST5 = 3.70 x 10^8 molecules; MTST6 = 3.72 x 10^8 molecules) standards ~ 1000 nt in length were added to each sample individually (*1*) (dx.doi.org/10.17504/protocols.io.ffwbipe). Standards were synthesized using custom templates that were transcribed in vitro to RNA according to the protocol.

Nucleic acid extraction

In order to enhance efficiency prior to DNA extraction, each filter (PC, 47 mm, Nuclepore) was cut into smaller pieces of several millimetres on a sterile petri dish with a sterile razor blade. The pieces were transferred back to the Eppendorf tube (2 ml) where lysis buffer (ZYMO research) was added immediately. DNA from all experiment samples was extracted using a ZR Fungal/Bacterial DNA MiniPrepTM Kit (ZYMO research) following the manufacturer's guidelines with the addition of a 45 min lysozyme digestion at 37°C and a 1 h Proteinase K digestion (20 mg ml^{-1} final concentration) at 55°C.

Amplicon sequencing

DNA was amplified and pooled as described previously *(2)* with a modification to the PCR amplification step. Briefly, the V4 - V5 region of the 16S rRNA gene from DNA samples was amplified with the primer sets 515F-Y (5' - GTGYCAGCMGCCGCGGTAA) and 926R (5' - CCGYCAATTYMTTTRAGTTT). Triplicate 10 µl reaction mixtures contained 2 µg DNA, 5 µl KAPA2G Fast HotStart ReadyMix, 0.2 µM forward primer and 0.2 µM reverse primer. Cycling reaction started with a 3 min heating step at 95 °C followed by 22 cycles of 95 °C for 45 s, 50 °C for 45 s, 68 °C for 90 s, and a final extension of 68 °C for 5 min. The quality of amplification products was examined on a 1 % agarose gel electrophoresis and when bands were visible, triplicate reactions

were pooled. Unique paired barcodes were added to each sample. The Master 25 µl mixtures contained 1 µl PCR product, 12.5 µl KAPA2G Fast HotStart ReadyMix (Kapa Biosystems, USA), 0.5 µl barcode 1 and 0.5 µl barcode 2. The cycling program included a 30 s initial denaturation at 98°C followed by 8 cycles of 98 °C for 10 s, 60 °C for 20 s, 72 °C for 30 s, and a final extension of 72 °C for 2 min. 3 µl PCR products were used to check for amplification on 1% agarose gel electrophoresis. The remaining 22 µl barcoded amplicon product was cleaned to remove unwanted dNTPs and primers by Exonuclease I and Shrimp Alkaline Phosphatase at 37 °C, 30 min for treatment and at 85 °C, 15 min to inactivate. The concentration of double-stranded DNA was quantified by PicoGreen fluorescence assay (Life Technologies). After calculating the PCR product concentration of each sample, they were pooled at equal nanogram manually. The pooled PCR amplicons were concentrated using Wizard SV gel and PCR clean-up system (Promega, USA) according to the manufacturer's protocol. Amplicons were sequenced with MiSeq Illumina 2 × 300 bp chemistry by Fasteris SA sequencing service (Switzerland) in a batch of 300 samples on one lane. Mock community DNA (LGC standards, UK) was used as a standard for subsequent analyses and considered as a DNA control for all treatments. All samples from the platform were demultiplexed and barcodes were trimmed off. A total of 764,658 raw sequences were obtained for 14 samples and sequences were deposited in the Sequence Read Archive under BioProject number PRJNA636955.

Amplicon analysis

The analysis of the raw sequences was done by following the standard pipeline of the DADA2 package *(3)* (https://benjineb.github.io/dada2/index.html, version 1.6) in 'R' (R Core Team (2019), https://www.R-project.org/) with the following parameters: trimLeft = c(19, 20), maxN = 0, maxEE = c(2, 5), truncQ = 2. Briefly, the package includes the following steps: filtering, dereplication, sample inference, chimera identification, and merging of paired-end reads. DADA2 infers exact amplicon sequence variants (ASVs) from sequencing data, instead of building operational taxonomic units from sequence similarity. We obtained an average of 21,500 reads per sample. The sequence data were normalized by dividing counts by sample size. The taxonomy assignments were done with the SILVA

v.128 database (https://www.arb-silva.de/documentation/release-128/) and the "assignTaxonomy" function in DADA2 that implements the RDP naiveBayesian classifier method *(4)*. Visualization of results was performed in the ggplot2*(5)* package in R and were enhanced using the open source tool inkscape (https://inkscape.org/).

1. Satinsky, B. M., S. M. Gifford, B. C. Crump, and M. A. Moran. 2013. Use of Internal Standards for Quantitative Metatranscriptome and Metagenome Analysis. Microbial Metagenomics, Metatranscriptomics, and Metaproteomics **531**: 237–250. doi:10.1016/B978-0-12-407863-5.00012-5
2. Parada, A. E., Needham, D. M. & Fuhrman, J. A. Every base matters: Assessing small subunit rRNA primers for marine microbiomes with mock communities, time series and global field samples. *Environmental Microbiology* **18**, 1403–1414 (2016).
3. Callahan, B. J. *et al.* DADA2: High-resolution sample inference from Illumina amplicon data. *Nature Methods* **13**, 581–583 (2016).
4. Wang, Q., Garrity, G. M., Tiedje, J. M. & Cole, J. R. Naïve Bayesian Classifier for Rapid Assignment of rRNA Sequences into the New Bacterial Taxonomy. *Appl. Environ. Microbiol.* **73**, 5261–5267 (2007).
5. Wickham, H. *ggplot2: Elegant Graphics for Data Analysis* (Springer-Verlag, 2009). doi:10.1007/978-0-387-98141-3.

Supplementary Table 1. List of all retrieved trace-met

KO Number	Metal co-factor
K21342	Co2+
K00099	Cobalt_cation
K03416	Cobalt_cation
K17489	Cobalt_cation
K17490	Cobalt_cation
K00918	Cobalt_cation
K06124	Cobalt_cation
K08722	Cobalt_cation
K21510	Cobalt_cation
K03684	Cobalt_cation
K01262	Cobalt_cation
K14208	Cobalt_cation
K01263	Cobalt_cation
K01264	Cobalt_cation
K01265	Cobalt_cation
K06016	Cobalt_cation
K05526	Cobalt_cation
K19669	Cobalt_cation
K02510	Cobalt_cation
K03335	Cobalt_cation
K01735	Cobalt_cation
K13829	Cobalt_cation
K13830	Cobalt_cation
K13546	Cobalt_cation
K00863	Cobalt_cation
K18910	Cobalt_cation
K15633	Cobalt_cation
K15634	Cobalt_cation
K15635	Cobalt_cation
K11942	Cobalt_cation
K00548	Cob(II)alamin
K01699	Cob(II)alamin
K13919	Cob(II)alamin
K13920	Cob(II)alamin
K06120	Cob(II)alamin
K06121	Cob(II)alamin
K06122	Cob(II)alamin
K04835	Cob(II)alamin
K03735	Cob(II)alamin
K03736	Cob(II)alamin
K01844	Cob(II)alamin

K18011	Cob(II)alamin
K17898	Cob(II)alamin
K17899	Cob(II)alamin
K01846	Cob(II)alamin
K19268	Cob(II)alamin
K01847	Cob(II)alamin
K01848	Cob(II)alamin
K01849	Cob(II)alamin
K20450	Cob(II)alamin
K21840	Cu_cation
K04618	Cu_cation
K03518	Cu_cation
K03519	Cu_cation
K03520	Cu_cation
K16877	Cu_cation
K16878	Cu_cation
K16879	Cu_cation
K00368	Cu_cation
K15864	Cu_cation
K00376	Cu_cation
K13444	Cu_cation
K00404	Cu_cation
K02256	Cu_cation
K02274	Cu_cation
K02275	Cu_cation
K02276	Cu_cation
K02277	Cu_cation
K15408	Cu_cation
K15862	Cu_cation
K00422	Cu_cation
K05909	Cu_cation
K00423	Cu_cation
K20204	Cu_cation
K20219	Cu_cation
K20204	Cu_cation
K07155	Cu_cation
K00503	Cu_cation
K00504	Cu_cation
K00505	Cu_cation
K10944	Cu_cation
K10944	Cu_cation
K03594	Cu_cation
K13624	Cu_cation

K14735	Cu_cation
K19054	Cu_cation
K22336	Cu_cation
K22552	Cu_cation
K13079	Cu_cation
K02297	Cu_cation
K02298	Cu_cation
K02826	Cu_cation
K02827	Cu_cation
K02828	Cu_cation
K02829	Cu_cation
K00193	Cu2+
K14138	Cu2+
K22171	Fe-S
K22172	Fe-S
K22173	Fe-S
K22174	Fe-S
K22175	Fe-S
K22176	Fe-S
K22177	Fe-S
K22178	Fe-S
K22179	Fe-S
K22180	Fe-S
K22181	Fe-S
K13549	Fe-S
K18355	Fe-S
K18356	Fe-S
K18357	Fe-S
K18358	Fe-S
K18359	Fe-S
K05891	Fe-S
K00157	Fe-S
K03518	Fe-S
K03519	Fe-S
K03520	Fe-S
K00169	Fe-S
K00170	Fe-S
K00171	Fe-S
K00172	Fe-S
K03737	Fe-S
K00174	Fe-S
K00175	Fe-S
K00176	Fe-S

K00177	Fe-S
K03738	Fe-S
K11389	Fe-S
K00186	Fe-S
K00187	Fe-S
K00188	Fe-S
K00189	Fe-S
K00179	Fe-S
K00180	Fe-S
K04090	Fe-S
K19070	Fe-S
K19071	Fe-S
K19072	Fe-S
K00174	Fe-S
K00175	Fe-S
K07469	Fe-S
K18020	Fe-S
K18021	Fe-S
K18022	Fe-S
K17722	Fe-S
K17723	Fe-S
K17828	Fe-S
K10797	Fe-S
K22430	Fe-S
K22431	Fe-S
K22432	Fe-S
K00234	Fe-S
K00235	Fe-S
K00239	Fe-S
K00240	Fe-S
K04037	Fe-S
K04038	Fe-S
K04039	Fe-S
K04112	Fe-S
K04113	Fe-S
K04114	Fe-S
K04115	Fe-S
K04107	Fe-S
K04108	Fe-S
K04109	Fe-S
K11333	Fe-S
K11334	Fe-S
K11335	Fe-S

K11333	Fe-S
K11334	Fe-S
K11335	Fe-S
K02495	Fe-S
K00265	Fe-S
K00266	Fe-S
K00285	Fe-S
K00284	Fe-S
K00311	Fe-S
K22162	Fe-S
K00317	Fe-S
K00317	Fe-S
K18853	Fe-S
K00356	Fe-S
K03885	Fe-S
K03934	Fe-S
K03935	Fe-S
K03936	Fe-S
K03940	Fe-S
K03941	Fe-S
K03942	Fe-S
K03943	Fe-S
K10534	Fe-S
K17877	Fe-S
K00362	Fe-S
K00363	Fe-S
K00370	Fe-S
K00371	Fe-S
K00374	Fe-S
K00366	Fe-S
K00367	Fe-S
K00380	Fe-S
K00381	Fe-S
K20202	Fe-S
K20203	Fe-S
K16964	Fe-S
K07306	Fe-S
K08352	Fe-S
K21307	Fe-S
K17892	Fe-S
K08264	Fe-S
K08265	Fe-S
K00436	Fe-S

K18005	Fe-S
K18006	Fe-S
K18007	Fe-S
K17992	Fe-S
K17993	Fe-S
K17994	Fe-S
K18330	Fe-S
K18331	Fe-S
K18332	Fe-S
K17993	Fe-S
K17994	Fe-S
K00437	Fe-S
K18008	Fe-S
K05922	Fe-S
K05927	Fe-S
K00532	Fe-S
K00533	Fe-S
K00534	Fe-S
K06441	Fe-S
K18016	Fe-S
K18017	Fe-S
K18023	Fe-S
K14068	Fe-S
K14069	Fe-S
K14070	Fe-S
K17995	Fe-S
K17996	Fe-S
K06281	Fe-S
K06282	Fe-S
K03268	Fe-S
K16268	Fe-S
K18068	Fe-S
K15751	Fe-S
K02229	Fe-S
K16968	Fe-S
K16969	Fe-S
K15511	Fe-S
K15512	Fe-S
K21317	Fe-S
K21318	Fe-S
K21319	Fe-S
K00499	Fe-S
K15982	Fe-S

K15983	Fe-S
K08080	Fe-S
K22553	Fe-S
K00087	Fe-S
K00106	Fe-S
K11177	Fe-S
K11178	Fe-S
K13479	Fe-S
K13481	Fe-S
K13482	Fe-S
K00122	Fe-S
K00123	Fe-S
K00126	Fe-S
K22515	Fe-S
K18029	Fe-S
K18030	Fe-S
K00106	Fe-S
K18361	Fe-S
K08348	Fe-S
K03526	Fe-S
K18010	Fe-S
K03527	Fe-S
K21312	Fe-S
K10700	Fe-S
K14581	Fe-S
K00531	Fe-S
K02586	Fe-S
K02591	Fe-S
K00536	Fe-S
K08355	Fe-S
K08356	Fe-S
K11784	Fe-S
K04034	Fe-S
K21647	Fe-S
K04068	Fe-S
K04069	Fe-S
K04070	Fe-S
K07309	Fe-S
K07310	Fe-S
K12527	Fe-S
K17050	Fe-S
K17051	Fe-S
K17052	Fe-S

K06941	Fe-S
K15632	Fe-S
K12902	Fe-S
K12914	Fe-S
K13602	Fe-S
K13601	Fe-S
K00193	Fe-S
K14138	Fe-S
K03517	Fe-S
K07561	Fe-S
K11779	Fe-S
K11781	Fe-S
K01012	Fe-S
K03644	Fe-S
K06168	Fe-S
K14441	Fe-S
K15865	Fe-S
K18707	Fe-S
K07464	Fe-S
K15449	Fe-S
K03716	Fe-S
K03147	Fe-S
K03150	Fe-S
K03639	Fe-S
K20967	Fe-S
K01681	Fe-S
K01682	Fe-S
K01702	Fe-S
K01703	Fe-S
K01704	Fe-S
K21359	Fe-S
K01705	Fe-S
K20625	Fe-S
K16792	Fe-S
K16793	Fe-S
K20455	Fe-S
K14534	Fe-S
K23121	Fe-S
K20505	Fe-S
K20505	Fe-S
K01752	Fe-S
K17989	Fe-S
K01754	Fe-S

K17989	Fe-S
K13309	Fe-S
K10026	Fe-S
K06163	Fe-S
K01843	Fe-S
K19814	Fe-S
K15822	Fe-S
K00329	Fe-S
K00330	Fe-S
K00331	Fe-S
K00332	Fe-S
K00333	Fe-S
K00334	Fe-S
K00335	Fe-S
K00336	Fe-S
K00337	Fe-S
K00338	Fe-S
K00339	Fe-S
K00340	Fe-S
K00341	Fe-S
K00342	Fe-S
K00343	Fe-S
K03878	Fe-S
K03879	Fe-S
K03880	Fe-S
K03881	Fe-S
K03882	Fe-S
K03883	Fe-S
K03884	Fe-S
K03934	Fe-S
K03935	Fe-S
K03936	Fe-S
K03940	Fe-S
K03941	Fe-S
K03942	Fe-S
K03943	Fe-S
K05572	Fe-S
K05573	Fe-S
K05574	Fe-S
K05575	Fe-S
K05576	Fe-S
K05577	Fe-S
K05578	Fe-S

K05579	Fe-S
K05580	Fe-S
K05581	Fe-S
K05582	Fe-S
K05583	Fe-S
K05584	Fe-S
K05585	Fe-S
K05586	Fe-S
K05587	Fe-S
K05588	Fe-S
K13378	Fe-S
K13380	Fe-S
K15863	Fe-S
K00346	Fe-S
K00347	Fe-S
K00348	Fe-S
K00349	Fe-S
K00350	Fe-S
K00351	Fe-S
K03614	Fe-S
K03615	Fe-S
K03616	Fe-S
K10765	Fe3+
K10767	Fe3+
K19469	Fe3+
K00524	Fe3+
K00525	Fe3+
K00526	Fe3+
K10807	Fe3+
K10808	Fe3+
K12970	Fe3+
K19448	Fe3+
K20579	Fe3+
K00001	Fe_cation
K00121	Fe_cation
K04072	Fe_cation
K11440	Fe_cation
K13951	Fe_cation
K13952	Fe_cation
K13953	Fe_cation
K13954	Fe_cation
K13980	Fe_cation
K18857	Fe_cation

K00190	Fe_cation
K00192	Fe_cation
K00198	Fe_cation
K11174	Fe_cation
K00228	Fe_cation
K19817	Fe_cation
K17877	Fe_cation
K00368	Fe_cation
K15864	Fe_cation
K04561	Fe_cation
K00392	Fe_cation
K00394	Fe_cation
K00395	Fe_cation
K17893	Fe_cation
K12903	Fe_cation
K22392	Fe_cation
K17992	Fe_cation
K17993	Fe_cation
K17994	Fe_cation
K18330	Fe_cation
K18331	Fe_cation
K18332	Fe_cation
K00440	Fe_cation
K00441	Fe_cation
K00443	Fe_cation
K03381	Fe_cation
K00448	Fe_cation
K00449	Fe_cation
K00450	Fe_cation
K00451	Fe_cation
K00452	Fe_cation
K04100	Fe_cation
K04101	Fe_cation
K18028	Fe_cation
K00454	Fe_cation
K00455	Fe_cation
K05713	Fe_cation
K17725	Fe_cation
K10712	Fe_cation
K07155	Fe_cation
K16049	Fe_cation
K00457	Fe_cation
K00458	Fe_cation

K00460	Fe_cation
K08022	Fe_cation
K19246	Fe_cation
K00461	Fe_cation
K04098	Fe_cation
K11948	Fe_cation
K00462	Fe_cation
K16421	Fe_cation
K09162	Fe_cation
K20148	Fe_cation
K09840	Fe_cation
K16952	Fe_cation
K14583	Fe_cation
K04099	Fe_cation
K15718	Fe_cation
K00515	Fe_cation
K21817	Fe_cation
K15240	Fe_cation
K17912	Fe_cation
K17913	Fe_cation
K10252	Fe_cation
K12905	Fe_cation
K00469	Fe_cation
K12675	Fe_cation
K03919	Fe_cation
K10859	Fe_cation
K05599	Fe_cation
K05600	Fe_cation
K16319	Fe_cation
K16320	Fe_cation
K03268	Fe_cation
K16268	Fe_cation
K18068	Fe_cation
K14579	Fe_cation
K14580	Fe_cation
K08686	Fe_cation
K20808	Fe_cation
K08689	Fe_cation
K15750	Fe_cation
K05708	Fe_cation
K05709	Fe_cation
K15751	Fe_cation
K22353	Fe_cation

K22354	Fe_cation
K22357	Fe_cation
K22358	Fe_cation
K22359	Fe_cation
K04035	Fe_cation
K13600	Fe_cation
K21724	Fe_cation
K21722	Fe_cation
K21723	Fe_cation
K15511	Fe_cation
K15512	Fe_cation
K21731	Fe_cation
K15746	Fe_cation
K22492	Fe_cation
K23037	Fe_cation
K15982	Fe_cation
K15983	Fe_cation
K00500	Fe_cation
K00501	Fe_cation
K00502	Fe_cation
K05933	Fe_cation
K08080	Fe_cation
K00507	Fe_cation
K00508	Fe_cation
K10226	Fe_cation
K10223	Fe_cation
K10944	Fe_cation
K00518	Fe_cation
K04564	Fe_cation
K04565	Fe_cation
K16627	Fe_cation
K05919	Fe_cation
K20445	Fe_cation
K20446	Fe_cation
K20447	Fe_cation
K20448	Fe_cation
K05299	Fe_cation
K15022	Fe_cation
K05297	Fe_cation
K21738	Fe_cation
K22567	Fe_cation
K19885	Fe_cation
K03418	Fe_cation

K15358	Fe_cation
K14331	Fe_cation
K15404	Fe_cation
K03779	Fe_cation
K03780	Fe_cation
K01703	Fe_cation
K01704	Fe_cation
K22209	Fe_cation
K20452	Fe_cation
K20453	Fe_cation
K00491	Ferriheme_b
K18076	Fe2+
K00446	Fe2+
K07104	Fe2+
K00456	Fe2+
K08967	Fe2+
K15059	Fe2+
K00464	Fe2+
K15059	Fe2+
K21196	Fe2+
K12708	Fe2+
K00471	Fe2+
K00472	Fe2+
K00473	Fe2+
K13645	Fe2+
K13646	Fe2+
K13647	Fe2+
K21236	Fe2+
K22406	Fe2+
K22407	Fe2+
K08134	Fe2+
K22459	Fe2+
K22460	Fe2+
K00474	Fe2+
K00475	Fe2+
K12692	Fe2+
K05282	Fe2+
K04125	Fe2+
K04124	Fe2+
K00476	Fe2+
K03119	Fe2+
K00477	Fe2+
K12697	Fe2+

K18054	Fe2+
K18054	Fe2+
K12745	Fe2+
K10276	Fe2+
K10277	Fe2+
K16914	Fe2+
K19415	Fe2+
K20149	Fe2+
K09592	Fe2+
K18055	Fe2+
K14976	Fe2+
K14975	Fe2+
K18056	Fe2+
K18057	Fe2+
K20574	Fe2+
K17825	Fe2+
K18058	Fe2+
K20157	Fe2+
K20612	Fe2+
K18066	Fe2+
K21728	Fe2+
K21729	Fe2+
K21195	Fe2+
K21036	Fe2+
K10860	Fe2+
K10674	Fe2+
K21614	Fe2+
K21615	Fe2+
K05549	Fe2+
K05550	Fe2+
K14579	Fe2+
K14580	Fe2+
K21323	Fe2+
K21317	Fe2+
K21318	Fe2+
K21319	Fe2+
K15760	Fe2+
K15761	Fe2+
K15763	Fe2+
K15764	Fe2+
K21323	Fe2+
K18315	Fe2+
K05277	Fe2+

K13077	Fe2+
K05278	Fe2+
K18912	Fe2+
K20246	Fe2+
K17487	Fe2+
K01462	Fe2+
K17488	Fe2+
K21593	Fe2+
K18684	Fe2+
K07173	Fe2+
K16845	Fe2+
K16846	Fe2+
K18684	Fe2+
K03711	fur,zur,furB
K22297	furA
K09823	zur
K02076	zurR, zur
K09825	perR
K09826	irr
K07722	nikR
K18507	ryhB
K03666	hfq
K02217	ftnA, ftn
K03594	bfr
K04047	dps
K11328	nrsS, rppB
K11330	nrsR, rppA
K10824	nikE, cntF
K15584	nikA, cntA
K15585	nikB, cntB
K15586	nikC, cntC
K15587	nikD, cntD
K02006	cbiO
K02007	cbiM
K02008	cbiQ
K02009	cbiN
K10094	cbiK
K16915	cbiL
K02006	cbiO
K02007	cbiM
K02008	cbiQ
K02009	cbiN
K02031	ABC.PE.A

K02032	ABC.PE.A1
K02033	ABC.PE.P
K02034	ABC.PE.P1
K02035	ABC.PE.S
K07043	uncharacterized protein | (GenBank)
K01517	manganese-dependent ADP-ribose/C
K14950	manganese-transporting P-type ATPa
K02258	cytochrome c oxidase assembly prote
K02260	cytochrome c oxidase assembly prote
K11182	diamine oxidase [EC:1.4.3.22]AOC1, A
K22557	COMM domain containing 1,COMMD
K07213	copper chaperone,ATOX1, ATX1, HAH
K00276	primary-amine oxidase [EC:1.4.3.21]A
K04569	copper chaperone for superoxide dis
K06201	copper homeostasis protein,CUTC, C
K17686	P-type Cu+ transporter [EC:7.2.2.8],A
K14686	solute carrier family 31 (copper trans
K14687	solute carrier family 31 (copper trans
K14687	solute carrier family 31 (copper trans
K17686	P-type Cu+ transporter [EC:7.2.2.8],A
K09841	Mo cation
K04107	Mo cation
K04108	Mo cation
K04109	Mo cation
K00157	Mo cation
K11817	Mo cation
K22417	Mo cation
K00200	Mo cation
K00201	Mo cation
K00202	Mo cation
K00203	Mo cation
K11261	Mo cation
K10534	Mo cation
K00367	Mo cation
K00087	Mo cation
K00106	Mo cation
K11177	Mo cation
K11178	Mo cation
K13479	Mo cation
K13481	Mo cation
K13482	Mo cation
K00122	Mo cation
K00123	Mo cation

K00126	Mo cation
K22515	Mo cation
K00531	Mo cation
K02586	Mo cation
K02591	Mo cation
K02017	Mo cation
K00537	Mo cation
K18065	Mo cation
K22547	Mo cation
K08355	Mo cation
K08356	Mo cation
K07309	Mo cation
K07310	Mo cation
K12527	Mo cation
K17050	Mo cation
K17051	Mo cation
K02018	Mo cation
K02020	Mo cation
K05776	Mo cation
K15497	Mo cation
K17052	Mo cation
K00031	Mn2+
K07246	Mn2+
K00099	Mn2+
K17753	Mn2+
K04112	Mn2+
K04113	Mn2+
K04114	Mn2+
K04115	Mn2+
K20204	Mn2+
K20219	Mn2+
K03781	Mn2+
K19885	Mn2+
K00462	Mn2+
K00518	Mn2+
K04564	Mn2+
K04565	Mn2+
K16627	Mn2+
K00524	Mn2+
K00525	Mn2+
K00526	Mn2+
K10807	Mn2+
K10808	Mn2+

K12970	Mn2+
K19448	Mn2+
K08247	Mn2+
K00696	Mn2+
K00710	Mn2+
K00719	Mn2+
K00733	Mn2+
K00734	Mn2+
K00735	Mn2+
K10157	Mn2+
K10158	Mn2+
K10812	Mn2+
K00750	Mn2+
K00753	Mn2+
K05528	Mn2+
K05529	Mn2+
K13058	Mn2+
K16870	Mn2+
K18788	Mn2+
K21364	Mn2+
K06984	Mn2+
K17251	Mn2+
K21306	Mn2+
K00801	Mn2+
K02291	Mn2+
K17841	Mn2+
K12503	Mn2+
K10208	Mn2+
K18430	Mn2+
K00861	Mn2+
K11753	Mn2+
K20884	Mn2+
K00919	Mn2+
K00991	Mn2+
K12506	Mn2+
K12447	Mn2+
K02488	Mn2+
K11444	Mn2+
K13069	Mn2+
K13590	Mn2+
K18967	Mn2+
K18968	Mn2+
K20954	Mn2+

K20955	Mn2+
K20956	Mn2+
K20957	Mn2+
K20958	Mn2+
K20959	Mn2+
K20960	Mn2+
K20961	Mn2+
K21019	Mn2+
K21020	Mn2+
K21021	Mn2+
K21022	Mn2+
K21023	Mn2+
K21084	Mn2+
K21085	Mn2+
K21088	Mn2+
K03638	Mn2+
K03831	Mn2+
K15376	Mn2+
K07141	Mn2+
K01004	Mn2+
K18706	Mn2+
K19665	Mn2+
K17884	Mn2+
K01007	Mn2+
K06124	Mn2+
K07181	Mn2+
K13243	Mn2+
K13244	Mn2+
K13245	Mn2+
K13246	Mn2+
K14051	Mn2+
K20962	Mn2+
K20963	Mn2+
K20964	Mn2+
K20965	Mn2+
K20966	Mn2+
K21024	Mn2+
K21086	Mn2+
K21090	Mn2+
K06167	Mn2+
K17224	Mn2+
K20979	Mn2+
K03684	Mn2+

K01259	Mn2+
K11142	Mn2+
K01262	Mn2+
K14208	Mn2+
K01271	Mn2+
K14213	Mn2+
K06016	Mn2+
K01475	Mn2+
K01476	Mn2+
K12255	Mn2+
K02083	Mn2+
K18459	Mn2+
K12676	Mn2+
K14977	Mn2+
K01517	Mn2+
K20758	Mn2+
K19669	Mn2+
K01569	Mn2+
K22212	Mn2+
K08093	Mn2+
K13812	Mn2+
K13831	Mn2+
K02510	Mn2+
K01666	Mn2+
K18365	Mn2+
K18365	Mn2+
K18314	Mn2+
K17835	Mn2+
K03335	Mn2+
K02549	Mn2+
K14759	Mn2+
K09483	Mn2+
K15652	Mn2+
K14180	Mn2+
K12467	Mn2+
K21925	Mn2+
K15088	Mn2+
K21925	Mn2+
K21926	Mn2+
K15096	Mn2+
K14178	Mn2+
K15086	Mn2+
K22049	Mn2+

K15087	Mn2+
K12742	Mn2+
K22053	Mn2+
K15794	Mn2+
K14186	Mn2+
K22057	Mn2+
K21980	Mn2+
K07385	Mn2+
K21930	Mn2+
K20519	Mn2+
K01770	Mn2+
K12506	Mn2+
K00863	Mn2+
K18910	Mn2+
K01818	Mn2+
K01818	Mn2+
K01823	Mn2+
K15633	Mn2+
K15634	Mn2+
K15635	Mn2+
K01856	Mn2+
K01860	Mn2+
K13559	Mn2+
K22115	Mn2+
K13037	Mn2+
K06914	Mn2+
K01958	Mn2+
K01959	Mn2+
K01960	Mn2+
K14415	Mn2+
K00096	Ni2+
K00192	Ni2+
K00198	Ni2+
K00436	Ni2+
K18005	Ni2+
K18006	Ni2+
K18007	Ni2+
K17992	Ni2+
K17993	Ni2+
K17994	Ni2+
K18330	Ni2+
K18331	Ni2+
K18332	Ni2+

K17993	Ni2+
K17994	Ni2+
K00437	Ni2+
K18008	Ni2+
K05922	Ni2+
K05927	Ni2+
K00532	Ni2+
K00533	Ni2+
K00534	Ni2+
K06441	Ni2+
K18016	Ni2+
K18017	Ni2+
K18023	Ni2+
K00440	Ni2+
K00441	Ni2+
K00443	Ni2+
K14068	Ni2+
K14069	Ni2+
K14070	Ni2+
K06281	Ni2+
K06282	Ni2+
K08967	Ni2+
K00193	Ni2+
K14138	Ni2+
K01427	Ni2+
K01428	Ni2+
K01429	Ni2+
K01430	Ni2+
K14048	Ni2+
K06016	Ni2+
K00001	Zn2+
K00121	Zn2+
K04072	Zn2+
K11440	Zn2+
K13951	Zn2+
K13952	Zn2+
K13953	Zn2+
K13954	Zn2+
K13980	Zn2+
K18857	Zn2+
K00002	Zn2+
K00094	Zn2+
K00098	Zn2+

K00153	Zn2+
K23232	Zn2+
K19649	Zn2+
K13548	Zn2+
K18124	Zn2+
K05352	Zn2+
K21681	Zn2+
K21836	Zn2+
K00119	Zn2+
K17067	Zn2+
K00192	Zn2+
K00198	Zn2+
K17067	Zn2+
K17068	Zn2+
K14469	Zn2+
K15020	Zn2+
K00344	Zn2+
K00359	Zn2+
K07305	Zn2+
K12267	Zn2+
K08071	Zn2+
K00544	Zn2+
K08247	Zn2+
K00548	Zn2+
K00549	Zn2+
K14082	Zn2+
K18013	Zn2+
K05954	Zn2+
K05955	Zn2+
K05955	Zn2+
K11713	Zn2+
K00861	Zn2+
K11753	Zn2+
K20884	Zn2+
K03148	Zn2+
K22837	Zn2+
K01011	Zn2+
K21947	Zn2+
K03750	Zn2+
K15376	Zn2+
K07560	Zn2+
K09716	Zn2+
K01077	Zn2+

K01113	Zn2+
K01114	Zn2+
K16619	Zn2+
K13985	Zn2+
K06167	Zn2+
K17487	Zn2+
K01254	Zn2+
K01255	Zn2+
K11142	Zn2+
K01256	Zn2+
K11140	Zn2+
K01257	Zn2+
K01258	Zn2+
K01260	Zn2+
K19701	Zn2+
K01261	Zn2+
K11141	Zn2+
K05994	Zn2+
K19701	Zn2+
K01263	Zn2+
K19702	Zn2+
K08660	Zn2+
K01273	Zn2+
K08641	Zn2+
K18866	Zn2+
K01283	Zn2+
K01284	Zn2+
K08779	Zn2+
K08780	Zn2+
K08781	Zn2+
K08782	Zn2+
K01291	Zn2+
K01292	Zn2+
K01294	Zn2+
K01295	Zn2+
K01296	Zn2+
K07260	Zn2+
K08640	Zn2+
K18866	Zn2+
K01298	Zn2+
K05996	Zn2+
K01299	Zn2+
K01300	Zn2+

K01301	Zn2+
K14592	Zn2+
K07752	Zn2+
K01306	Zn2+
K20110	Zn2+
K01387	Zn2+
K01389	Zn2+
K08635	Zn2+
K19957	Zn2+
K01390	Zn2+
K08618	Zn2+
K01392	Zn2+
K08604	Zn2+
K01399	Zn2+
K08603	Zn2+
K01400	Zn2+
K01401	Zn2+
K08605	Zn2+
K20744	Zn2+
K01410	Zn2+
K01412	Zn2+
K17732	Zn2+
K01414	Zn2+
K07763	Zn2+
K06704	Zn2+
K07764	Zn2+
K14677	Zn2+
K06015	Zn2+
K01461	Zn2+
K20817	Zn2+
K07047	Zn2+
K15525	Zn2+
K02535	Zn2+
K16363	Zn2+
K18458	Zn2+
K19794	Zn2+
K01467	Zn2+
K17836	Zn2+
K17837	Zn2+
K17838	Zn2+
K18698	Zn2+
K18699	Zn2+
K18766	Zn2+

K18767	Zn2+
K18768	Zn2+
K18780	Zn2+
K18781	Zn2+
K18782	Zn2+
K18790	Zn2+
K18791	Zn2+
K18792	Zn2+
K18793	Zn2+
K18794	Zn2+
K18795	Zn2+
K18796	Zn2+
K18797	Zn2+
K18970	Zn2+
K18971	Zn2+
K18972	Zn2+
K18973	Zn2+
K18976	Zn2+
K19095	Zn2+
K19096	Zn2+
K19097	Zn2+
K19098	Zn2+
K19099	Zn2+
K19100	Zn2+
K19101	Zn2+
K19209	Zn2+
K19210	Zn2+
K19211	Zn2+
K19212	Zn2+
K19213	Zn2+
K19214	Zn2+
K19215	Zn2+
K19216	Zn2+
K19217	Zn2+
K19218	Zn2+
K19316	Zn2+
K19317	Zn2+
K19318	Zn2+
K19319	Zn2+
K19320	Zn2+
K19321	Zn2+
K19322	Zn2+
K20319	Zn2+

K20320	Zn2+
K21266	Zn2+
K21276	Zn2+
K21277	Zn2+
K22331	Zn2+
K22332	Zn2+
K22333	Zn2+
K22334	Zn2+
K22335	Zn2+
K22346	Zn2+
K22351	Zn2+
K22352	Zn2+
K15358	Zn2+
K01489	Zn2+
K18456	Zn2+
K11991	Zn2+
K08710	Zn2+
K03382	Zn2+
K21589	Zn2+
K19670	Zn2+
K20499	Zn2+
K21140	Zn2+
K20941	Zn2+
K01622	Zn2+
K01623	Zn2+
K01624	Zn2+
K11645	Zn2+
K16305	Zn2+
K16306	Zn2+
K14577	Zn2+
K01737	Zn2+
K01672	Zn2+
K01673	Zn2+
K01674	Zn2+
K01743	Zn2+
K18245	Zn2+
K18246	Zn2+
K01698	Zn2+
K07385	Zn2+
K21342	Zn2+
K22363	Zn2+
K01809	Zn2+
K15916	Zn2+

K16011	Zn2+
K01827	Zn2+
K22203	Zn2+
K01958	Zn2+
K01959	Zn2+
K01960	Zn2+
K06857	W
K05772	W
K05773	W
K15497	W
K16267	Cd
K15726	Cd
K15725	Cd
K15727	Cd
K16264	Cd

Supplementary Table 2. Fold changes of normalized transcript counts of trace metal rela

KO	baseMean	log2FoldChange	lfcSE	stat	pvalue
K06120	170.0435071	-2.69115573	0.801730189	-3.356685038	0.000788829
K00544	428.8079767	-2.617797947	0.718182083	-3.64503377	0.000267357
K01699	397.9601603	-1.675433165	0.623603026	-2.686698261	0.007216211
K14581	158.9130404	-1.52129548	0.791238736	-1.922675687	0.054520792
K07104	19.88498557	-1.509876512	0.896638524	-1.683930002	0.092195197
K01283	1264.696752	-1.265763372	0.596251232	-2.122869194	0.033764815
K07469	53.35999698	-1.209393345	0.722522177	-1.673849446	0.094160192
K18788	65.57317013	-1.18319208	0.868147378	-1.36289311	0.172916201
K01848	29.73254624	-0.975973226	0.791471899	-1.233111658	0.217534108
K16846	627.9024622	-0.916247538	0.577980623	-1.585256496	0.112908069
K17723	6975.65971	-0.848817301	0.457357729	-1.855915506	0.063465602
K11779	727.5601048	-0.691075025	0.624720142	-1.106215373	0.26863331
K03614	215.0788311	-0.686731922	0.645270053	-1.064255064	0.287213168
K00462	97.13098999	-0.655788256	0.690053509	-0.950344064	0.341937456
K00462	97.13098999	-0.655788256	0.690053509	-0.950344064	0.341937456
K10797	125.3264799	-0.584382515	0.721798373	-0.809620161	0.418158517
K05526	178.5462818	-0.576067681	0.714732116	-0.805991039	0.420248016
K00394	1831.795699	-0.56986308	0.611252367	-0.932287727	0.351187848
K04101	66.13439053	-0.519021405	0.700754897	-0.740660404	0.458899373
K00153	160.7019072	-0.497109614	0.676127299	-0.735230799	0.462198945
K00179	106.1107196	-0.461259565	0.562776966	-0.819613439	0.41243651
K14534	57.45002534	-0.460433675	0.602449572	-0.764269238	0.444706813
K13953	682.637367	-0.452975895	0.526205336	-0.860834858	0.389329004
K13953	682.637367	-0.452975895	0.526205336	-0.860834858	0.389329004
K06282	13.64422029	-0.452381313	1.045128758	-0.432847446	0.665125602
K06282	13.64422029	-0.452381313	1.045128758	-0.432847446	0.665125602
K16319	440.1791771	-0.443411643	0.533709337	-0.830811104	0.406080349
K03119	1547.66649	-0.399563503	0.575254933	-0.694585096	0.487315355
K00477	165.2306835	-0.389015689	0.620739029	-0.626697647	0.530857447
K06015	1307.614748	-0.382801882	0.484899845	-0.789445255	0.429851814
K16049	315.8497609	-0.367256794	0.532395482	-0.689819517	0.490307694
K01428	144.443314	-0.359921732	0.602880295	-0.597003642	0.550504949
K06016	826.139223	-0.336905312	0.516671863	-0.65206824	0.514357151
K06016	826.139223	-0.336905312	0.516671863	-0.65206824	0.514357151
K06016	826.139223	-0.336905312	0.516671863	-0.65206824	0.514357151
K01461	575.004188	-0.325038241	0.532284927	-0.610647089	0.541433242
K17828	400.5991444	-0.317349452	0.596284524	-0.532211451	0.594579553
K07141	313.144932	-0.307542681	0.566889963	-0.542508602	0.587468184
K01475	60.74484774	-0.183972404	0.706149502	-0.260528973	0.79445577
K02826	3.440838398	-0.166320246	1.986943957	-0.083706561	0.93328974
K09826	121.1476345	-0.098279829	0.64124133	-0.153264964	0.878189329
K08093	5476.323839	-0.054241556	0.59578976	-0.091041437	0.927459666
K23121	2.858555795	-0.043419648	2.018158538	-0.021514488	0.982835246
K18459	316.4432136	-0.038509722	0.67128595	-0.057367091	0.954252778
K12506	262.0954191	-0.034929689	1.148417084	-0.030415508	0.975735677
K00331	2003.30086	-0.029018631	0.617369652	-0.047003656	0.962510314
K07173	5.359448043	-0.020672273	1.136727368	-0.018185779	0.985490648

K19702	729.1610229	-0.018668937	0.516305739	-0.036158686	0.971155828
K07260	43.91379182	-0.013753518	0.861109509	-0.015971858	0.987256843
K00471	493.8354788	-0.005678682	0.608323091	-0.009334977	0.992551874
K00180	10.97732614	0.017257568	1.07578885	0.01604178	0.98720106
K03919	17.03934038	0.029332933	0.961272259	0.030514698	0.975656571
K01295	203.3315047	0.065182896	0.544193094	0.119778984	0.904658231
K18456	30.31396179	0.071440402	0.86198526	0.082878914	0.933947821
K15587	139.6283864	0.081152259	1.166568067	0.069564959	0.944539928
K00395	304.2905411	0.102323633	0.582564711	0.175643376	0.860574123
K14583	216.2520828	0.126235959	0.599370121	0.210614367	0.8331882
K01754	3319.284007	0.127244	0.53138344	0.23945797	0.810750484
K03779	23.58401357	0.140710216	1.005581173	0.139929247	0.888715893
K04565	214.9315097	0.161408776	0.513387177	0.314399702	0.753217482
K04565	214.9315097	0.161408776	0.513387177	0.314399702	0.753217482
K00172	82.9554235	0.166401336	0.791853716	0.21014151	0.833557228
K04108	1301.264472	0.194328164	0.517609911	0.375433623	0.707338003
K01698	2159.345339	0.196139266	0.496780325	0.394820922	0.692975053
K17893	220.515833	0.212599801	0.609903038	0.348579672	0.727404891
K03615	376.1147536	0.22820401	0.590494696	0.386462422	0.699154228
K22297	38.33631214	0.234583173	0.636754156	0.368404621	0.712571553
K02510	561.41464	0.260306243	0.553111717	0.47062146	0.63791108
K02510	561.41464	0.260306243	0.553111717	0.47062146	0.63791108
K00087	214.0376052	0.277247287	0.492203004	0.563278332	0.57324537
K04090	3680.123541	0.290553066	0.428676213	0.677791436	0.497903942
K15358	259.7273518	0.294428331	0.630426582	0.467030325	0.640478182
K15358	259.7273518	0.294428331	0.630426582	0.467030325	0.640478182
K21817	180.0844499	0.308179371	0.642679783	0.479522429	0.631567016
K00122	805.7606938	0.331744767	0.611495356	0.542513961	0.587464493
K21947	5.995127211	0.333556857	1.318303027	0.253019867	0.800252861
K00472	223.2125592	0.337073501	0.558886066	0.603116667	0.54643108
K03526	1748.029595	0.379744465	0.531661919	0.714259291	0.47506686
K10674	300.5410276	0.398668644	0.499958124	0.797404072	0.425216395
K15511	151.6002249	0.406930384	0.540842377	0.75240107	0.451809903
K15511	151.6002249	0.406930384	0.540842377	0.75240107	0.451809903
K00338	520.5555381	0.413708585	0.663240333	0.623768738	0.532779473
K03148	393.1576253	0.413811201	0.626461394	0.660553395	0.508898765
K00330	1349.736467	0.415138868	0.532596951	0.779461594	0.435707853
K03518	1230.900853	0.448771173	0.545527724	0.822636784	0.410714574
K03518	1230.900853	0.448771173	0.545527724	0.822636784	0.410714574
K01273	1481.718898	0.496931316	0.536754043	0.92580824	0.354545644
K02298	77.70322818	0.497780336	0.601619532	0.827400557	0.408010065
K03519	2150.469059	0.500238267	0.530687188	0.9426236	0.345873464
K03519	2150.469059	0.500238267	0.530687188	0.9426236	0.345873464
K03638	501.455799	0.504492406	0.563903099	0.894643789	0.370977536
K21019	84.56121234	0.528983387	0.575224432	0.919612168	0.357775466
K00317	340.034407	0.572437004	0.589488681	0.971073785	0.331511537
K01429	15.42756788	0.6358331	0.9351645	0.679915779	0.49655779
K03616	326.2710238	0.635993998	0.564224561	1.127200128	0.259657876
K21307	585.8684813	0.645687208	0.584761231	1.104189495	0.269510946

K00121	2398.16108	0.655745717	0.515101959	1.273040619	0.203003629
K00121	2398.16108	0.655745717	0.515101959	1.273040619	0.203003629
K00096	24.02008254	0.65575701	0.758573437	0.864460812	0.387334799
K06281	20.89213657	0.655917162	0.88082006	0.744666466	0.456473376
K06281	20.89213657	0.655917162	0.88082006	0.744666466	0.456473376
K16870	114.0551744	0.68423824	0.79098078	0.865050399	0.387011127
K17722	977.9442377	0.68499252	0.443982418	1.542837042	0.12287032
K00098	155.4738297	0.689144937	0.629946425	1.093973884	0.273966432
K08352	242.9251761	0.694361223	0.53021447	1.309585577	0.19033607
K00863	73.40262046	0.71880504	0.551286037	1.303869484	0.192278087
K00863	73.40262046	0.71880504	0.551286037	1.303869484	0.192278087
K11177	851.8394701	0.72976353	0.60921403	1.197877091	0.23096487
K00381	7915.792445	0.735571969	0.677840471	1.085169742	0.277846483
K00285	880.1082914	0.77265133	0.545326203	1.41686082	0.156523624
K00423	185.0759668	0.773910705	0.550171805	1.406670967	0.159524979
K17067	645.3330119	0.777208904	0.523254138	1.48533733	0.137454488
K03527	1436.613775	0.783700595	0.535368372	1.463852994	0.143234119
K00342	1570.346551	0.801914395	0.584131771	1.372831329	0.169804789
K01301	284.8240446	0.804744706	0.560439236	1.435917857	0.151025717
K05549	46.23574199	0.806080521	0.69156287	1.165592537	0.243779227
K07246	139.2167852	0.8261407	0.641636644	1.287552242	0.197901873
K00549	797.8110855	0.849793872	0.586225627	1.449602052	0.147169524
K17837	119.5902578	0.858235405	0.605340783	1.417772319	0.156257248
K22515	333.5186714	0.863545178	0.548377651	1.574727154	0.115319437
K09823	364.3677904	0.868792594	0.511344586	1.699035479	0.089312499
K00499	1327.312648	0.883655097	0.516996456	1.709209194	0.087412206
K15864	239.0899966	0.884759486	0.716157487	1.235425869	0.21667205
K15864	239.0899966	0.884759486	0.716157487	1.235425869	0.21667205
K01704	1212.13358	0.890867173	0.537301358	1.658040054	0.097309382
K01704	1212.13358	0.890867173	0.537301358	1.658040054	0.097309382
K13482	1350.554072	0.900826202	0.52643732	1.711174659	0.087048875
K00334	814.1643169	0.912049525	0.551760475	1.652980897	0.098334752
K00265	11545.25142	0.928726507	0.520560413	1.78408977	0.074409079
K00333	768.7991497	0.93576478	0.590277136	1.585297351	0.112898791
K07047	3038.63441	0.946407701	0.515596034	1.835560475	0.066422687
K00336	4123.854848	0.953859752	0.667999734	1.427934329	0.153310762
K13378	1833.418754	0.962860035	0.712442571	1.351491438	0.176538061
K15982	566.295023	0.966996429	0.574433513	1.683391389	0.092299349
K15982	566.295023	0.966996429	0.574433513	1.683391389	0.092299349
K04039	8.911474051	0.969251383	1.006261206	0.96322046	0.335436899
K13646	206.1877158	0.972445049	0.591674603	1.643547051	0.100269799
K13920	9.38337298	0.978599409	1.185987697	0.825134537	0.409295214
K00329	908.1461171	1.000801788	0.705534946	1.418500662	0.156044645
K02083	23.97492416	1.012022457	0.799570739	1.26570722	0.205617923
K00335	2531.020117	1.016086684	0.596892545	1.702294145	0.088700242
K00344	5001.082436	1.03198046	0.553286037	1.865184354	0.062155568
K13954	517.8501742	1.033248049	0.491897439	2.100535534	0.035681758
K13954	517.8501742	1.033248049	0.491897439	2.100535534	0.035681758
K01004	258.0544867	1.047665435	0.717074191	1.461027949	0.144007772

K22209	47.91815541	1.062363447	0.68796253	1.544217019	0.122535767
K00464	255.7752227	1.106572805	0.580802367	1.905248442	0.056747784
K17224	196.0226693	1.118579284	0.725766375	1.541238782	0.123258682
K12255	124.6886567	1.122253286	0.577240838	1.944168209	0.05187517
K19670	221.4777936	1.124036049	0.535118853	2.100535317	0.035681777
K03520	3973.147341	1.151997456	0.502186791	2.29396208	0.021792677
K03520	3973.147341	1.151997456	0.502186791	2.29396208	0.021792677
K00099	847.933107	1.166115435	0.488931235	2.385029533	0.01707775
K00099	847.933107	1.166115435	0.488931235	2.385029533	0.01707775
K00548	4738.125412	1.172629703	0.561629588	2.087905851	0.036806328
K00548	4738.125412	1.172629703	0.561629588	2.087905851	0.036806328
K02549	231.2983425	1.184803151	0.583020114	2.032182293	0.042135205
K11178	442.0397072	1.185548774	0.560103708	2.116659391	0.034288766
K18068	25.4567311	1.188472023	0.764246593	1.555089725	0.119924702
K18068	25.4567311	1.188472023	0.764246593	1.555089725	0.119924702
K01077	1840.856464	1.192956421	0.542823296	2.197688327	0.027971324
K02297	62.95167418	1.196360408	0.815436816	1.467140537	0.142337829
K02035	50063.86974	1.20239692	0.509600064	2.359491304	0.01830001
K01271	1188.860448	1.203206857	0.525029271	2.291694813	0.02192326
K00123	11067.59547	1.223567756	0.514955724	2.376063996	0.017498428
K03517	1716.433619	1.240404155	0.502924616	2.466381869	0.013648574
K01703	3890.381009	1.243324172	0.540567556	2.300034765	0.021446251
K01703	3890.381009	1.243324172	0.540567556	2.300034765	0.021446251
K01847	2085.571109	1.247807332	0.534024087	2.336612454	0.019459344
K00525	22690.95686	1.266232206	0.534539432	2.368828436	0.017844529
K00525	22690.95686	1.266232206	0.534539432	2.368828436	0.017844529
K00356	569.8511301	1.267187579	0.676081524	1.874311802	0.060887462
K13069	239.1127642	1.269056738	0.560972677	2.262243404	0.023682369
K00341	1828.23413	1.281480311	0.620956	2.063721601	0.03904412
K00001	3440.744787	1.291845005	0.496897298	2.599822961	0.009327187
K00001	3440.744787	1.291845005	0.496897298	2.599822961	0.009327187
K03750	849.5400006	1.316816909	0.524551932	2.510365186	0.012060636
K01856	2.913687494	1.351199885	1.391038414	0.971360583	0.33136875
K00266	3945.329073	1.355401208	0.607024038	2.232862495	0.025558014
K01011	4997.937268	1.38153433	0.717460014	1.925590698	0.054155501
K18030	1253.201626	1.39287585	0.479715095	2.903548097	0.003689603
K00696	65.17203971	1.398776608	0.715086871	1.956093261	0.050454169
K01255	4179.620319	1.42786044	0.527917378	2.704704373	0.00683652
K18910	81.20319082	1.436155143	0.585621006	2.452362755	0.014192151
K18910	81.20319082	1.436155143	0.585621006	2.452362755	0.014192151
K00228	1028.339244	1.436928407	0.562047319	2.556596855	0.010570164
K00340	232.7444584	1.441345721	0.67675659	2.129784538	0.033189406
K15760	231.8461381	1.44739101	0.603546237	2.398144368	0.016478369
K01958	1083.222509	1.453399017	0.626965022	2.318150083	0.020441166
K01958	1083.222509	1.453399017	0.626965022	2.318150083	0.020441166
K01012	838.7587363	1.478431022	0.519880904	2.843787894	0.004458071
K00332	420.5276203	1.495498952	0.528816239	2.828012535	0.004683797
K16877	31.93403199	1.508147199	0.756492813	1.993604132	0.046195333
K00170	105.2084377	1.541984054	0.63720892	2.419903435	0.015524629

K05994	1045.561653	1.554091969	0.525771536	2.955831312	0.003118276
K08689	38.36409166	1.554349487	0.758334979	2.049687184	0.040394966
K01262	2945.85872	1.563457884	0.533740138	2.929249224	0.003397819
K01262	2945.85872	1.563457884	0.533740138	2.929249224	0.003397819
K01259	1660.59379	1.604869002	0.513438678	3.125726731	0.001773663
K10026	742.3336395	1.608098621	0.572139168	2.810677386	0.004943733
K00919	716.859744	1.608396027	0.487856783	3.296861056	0.000977719
K00441	144.8509437	1.613646057	0.642211789	2.512638487	0.011983206
K00441	144.8509437	1.613646057	0.642211789	2.512638487	0.011983206
K03594	2655.986763	1.638041112	0.531504579	3.081894639	0.002056876
K03594	2655.986763	1.638041112	0.531504579	3.081894639	0.002056876
K01284	1386.218554	1.644064196	0.53436493	3.076669337	0.002093274
K02034	2241.453376	1.649135636	0.485484476	3.396886443	0.000681572
K05708	25.83829636	1.664884156	0.845350397	1.96946043	0.048900242
K01623	1300.06031	1.671020228	0.586854032	2.847420546	0.004407509
K10824	189.3509828	1.679978146	0.556129907	3.020837623	0.002520765
K01489	195.9244022	1.695103291	0.57810317	2.932181274	0.003365902
K07560	242.0359726	1.698545569	0.573498681	2.961725327	0.003059206
K02033	3582.29738	1.702153147	0.477189067	3.567041375	0.000361034
K02258	1428.082134	1.710188452	0.547528516	3.123469191	0.001787326
K01681	6190.678187	1.721866825	0.570854267	3.016298422	0.002558813
K11444	52.7887936	1.73194015	0.803722572	2.154897985	0.031169818
K01809	315.7625207	1.73577522	0.661690011	2.623245311	0.008709654
K18430	654.6633201	1.737502976	0.569235341	3.052345578	0.002270605
K00343	1552.242799	1.748467186	0.582207057	3.00317072	0.002671825
K00450	85.09792969	1.787254368	0.571465411	3.127493514	0.001763037
K00362	560.0379641	1.791454632	0.598618951	2.99264604	0.002765703
K16968	633.0343949	1.797064908	0.466819489	3.849592726	0.000118314
K03639	1398.294697	1.797905379	0.525773905	3.419540911	0.000627269
K01735	1680.444378	1.798901102	0.547641304	3.284816336	0.001020489
K01430	12.03564454	1.817441233	0.892190079	2.037056089	0.041644422
K00475	5.668572964	1.830530318	1.297014506	1.411341438	NA
K04124	5.668572964	1.830530318	1.297014506	1.411341438	NA
K04125	5.668572964	1.830530318	1.297014506	1.411341438	NA
K05277	5.668572964	1.830530318	1.297014506	1.411341438	NA
K05278	5.668572964	1.830530318	1.297014506	1.411341438	NA
K05282	5.668572964	1.830530318	1.297014506	1.411341438	NA
K05933	5.668572964	1.830530318	1.297014506	1.411341438	NA
K00337	1208.357208	1.852402021	0.620436444	2.985643477	0.002829824
K00002	167.0254188	1.857195628	0.69104302	2.68752534	0.007198364
K03644	2418.358342	1.857464437	0.490095247	3.790007041	0.000150643
K01467	79.90219191	1.860212571	0.81059991	2.294859089	0.021741201
K00339	673.190413	1.883389201	0.58167631	3.237864716	0.001204279
K00392	323.1374613	1.892820174	0.635767107	2.977222561	0.002908728
K00363	33.54795348	1.898384668	0.657412574	2.887661026	0.003881179
K00311	5105.389466	1.902816281	0.563771977	3.375152291	0.000737749
K07305	1522.476446	1.905283518	0.532708966	3.576593676	0.000348101
K00370	3685.177416	1.913434796	0.50077358	3.820957955	0.000132934
K06941	2730.15101	1.917306463	0.5450114	3.517919926	0.000434944

K01959	334.430016	1.929239016	0.50696434	3.805472821	0.000141534
K01959	334.430016	1.929239016	0.50696434	3.805472821	0.000141534
K11753	1183.493546	1.955026165	0.51841039	3.771194026	0.000162468
K11753	1183.493546	1.955026165	0.51841039	3.771194026	0.000162468
K15633	1442.644676	1.955505478	0.590612603	3.31097824	0.000929704
K15633	1442.644676	1.955505478	0.590612603	3.31097824	0.000929704
K00174	2397.587442	1.962573155	0.648799935	3.024928101	0.002486922
K01256	3937.959635	1.988089852	0.524589263	3.789802786	0.000150767
K02032	2121.645707	1.992527267	0.544783503	3.657466231	0.000254721
K03335	323.8659806	1.99445512	0.627003085	3.180933505	0.001468013
K03335	323.8659806	1.99445512	0.627003085	3.180933505	0.001468013
K00371	1395.149321	1.995312206	0.570822838	3.495501709	0.000473171
K00239	7898.541162	1.997228782	0.533611848	3.742849395	0.000181945
K00175	1064.25007	1.997337216	0.607943858	3.285397475	0.001018386
K02031	2555.420203	2.008106319	0.538307091	3.730410306	0.000191168
K01770	322.7379208	2.011754148	0.596088595	3.374924741	0.000738359
K01624	2517.039044	2.015426702	0.526210522	3.830076777	0.000128103
K02495	604.6910746	2.020352981	0.554989197	3.640346499	0.000272271
K00169	138.2088995	2.048539197	0.559644883	3.660426924	0.000251795
K00374	214.3725991	2.050384493	0.719097839	2.851328959	0.00435369
K20455	768.991302	2.052497998	0.523174053	3.923164741	8.74E-05
K00240	2894.620522	2.054768595	0.526039543	3.906110525	9.38E-05
K03781	1056.313648	2.059192185	0.586280093	3.512301046	0.000444244
K01414	975.28054	2.063046781	0.498394857	4.139382165	3.48E-05
K17686	1607.924471	2.070576176	0.463855526	4.463838548	8.05E-06
K17686	1607.924471	2.070576176	0.463855526	4.463838548	8.05E-06
K16011	688.4539016	2.101783848	0.535858079	3.922277053	8.77E-05
K08967	45.40179624	2.111888782	0.624727097	3.380498127	0.000723546
K08967	45.40179624	2.111888782	0.624727097	3.380498127	0.000723546
K00991	349.988644	2.152493194	0.580533687	3.707783444	0.000209081
K01823	454.6975919	2.16956395	0.557360365	3.892569486	9.92E-05
K03666	251.0798543	2.190953488	0.575190649	3.809090936	0.000139479
K02276	6680.789618	2.215318822	0.562285747	3.93984524	8.15E-05
K00031	10252.96198	2.217285123	0.542988387	4.083485353	4.44E-05
K03711	1734.81632	2.250704891	0.5153714	4.367151319	1.26E-05
K09162	87.31092193	2.276865298	0.707391245	3.218678934	0.001287826
K01960	412.0618554	2.29656268	0.504106251	4.555711574	5.22E-06
K01960	412.0618554	2.29656268	0.504106251	4.555711574	5.22E-06
K13481	1656.224579	2.322088105	0.655171124	3.544246715	0.000393737
K03684	1405.746848	2.333642376	0.552169197	4.226317567	2.38E-05
K03684	1405.746848	2.333642376	0.552169197	4.226317567	2.38E-05
K00524	6.170515385	2.344759511	1.789823102	1.310050981	0.19017859
K00524	6.170515385	2.344759511	1.789823102	1.310050981	0.19017859
K01476	213.6281947	2.358977499	0.568450443	4.14983844	3.33E-05
K13444	274.1713825	2.366723334	0.525525255	4.50353872	6.68E-06
K01299	292.902149	2.376968342	0.57185552	4.156588965	3.23E-05
K12527	538.6492235	2.388691537	1.088962305	2.193548414	0.02826789
K04047	1662.032743	2.390425074	0.516839188	4.625084805	3.74E-06
K06167	248.853373	2.409382783	0.583438671	4.129624765	3.63E-05

K06167	248.853373	2.409382783	0.583438671	4.129624765	3.63E-05
K01113	1009.84648	2.42172694	0.49881817	4.85492928	1.20E-06
K00284	640.0791031	2.423496062	0.575176462	4.213482682	2.51E-05
K01265	2013.50147	2.424364613	0.53331019	4.54588091	5.47E-06
K02535	4960.534558	2.428274609	0.536106839	4.529460236	5.91E-06
K02275	7981.408145	2.466508438	0.556812835	4.42969034	9.44E-06
K15764	31.5322	2.468500799	0.814201756	3.031804808	0.002430963
K07043	146.0734684	2.47693259	0.661932853	3.741969564	0.000182584
K00449	80.121979	2.48050218	0.602885314	4.114384815	3.88E-05
K18912	338.1231604	2.521982427	0.518947679	4.859800958	1.18E-06
K03418	828.3215291	2.53009993	0.494897875	5.11236774	3.18E-07
K01114	136.4321717	2.543000201	0.6408776	3.967996699	7.25E-05
K01682	11159.3488	2.574190337	0.517176612	4.977391236	6.44E-07
K18028	17.9160762	2.583770355	0.930975597	2.775336286	0.005514466
K03268	12.44604624	2.598029368	0.94465499	2.750241513	0.005955135
K03268	12.44604624	2.598029368	0.94465499	2.750241513	0.005955135
K14579	12.44604624	2.598029368	0.94465499	2.750241513	0.005955135
K14579	12.44604624	2.598029368	0.94465499	2.750241513	0.005955135
K07306	469.0919084	2.599989382	0.470804159	5.522443528	3.34E-08
K17050	459.5034232	2.601837318	0.471096628	5.522937681	3.33E-08
K14441	1062.146023	2.606379591	0.544366442	4.787913787	1.69E-06
K02274	15217.5384	2.607882173	0.520828078	5.007184292	5.52E-07
K06168	2937.201766	2.615266472	0.509905878	5.128920031	2.91E-07
K14977	232.3030722	2.621942102	0.669868723	3.914113336	9.07E-05
K03147	1515.502941	2.630896094	0.526403575	4.997868975	5.80E-07
K00526	5159.590293	2.631746176	0.502998834	5.232111882	1.68E-07
K00526	5159.590293	2.631746176	0.502998834	5.232111882	1.68E-07
K04069	89.54936729	2.644643948	1.103800222	2.395944389	0.016577605
K15634	388.639724	2.657519744	0.562375909	4.725522023	2.30E-06
K15634	388.639724	2.657519744	0.562375909	4.725522023	2.30E-06
K17825	156.8789337	2.664733123	0.631716226	4.218243907	2.46E-05
K01462	1552.219073	2.694870694	0.564032267	4.777866182	1.77E-06
K05297	245.4287593	2.740340789	0.527813088	5.191877298	2.08E-07
K00348	2034.023343	2.740431963	0.515832506	5.312639143	1.08E-07
K07464	100.1663117	2.750808463	0.553469476	4.970117739	6.69E-07
K04564	5483.289578	2.760529959	0.521644762	5.291972928	1.21E-07
K04564	5483.289578	2.760529959	0.521644762	5.291972928	1.21E-07
K13590	579.3630475	2.762130979	0.573666737	4.814870378	1.47E-06
K01258	246.3201893	2.766033696	0.535741638	5.162999287	2.43E-07
K00457	1625.020874	2.78446192	0.502359149	5.542771389	2.98E-08
K00380	1731.846399	2.803835239	0.634911048	4.416107184	1.00E-05
K09825	9.362665486	2.825844989	1.131446384	2.497550949	0.012505449
K18029	13.06395876	2.82890973	0.983935187	2.875097635	0.004039026
K14051	3.893605796	2.83494866	1.284355378	2.207293019	0.027293595
K02291	820.2559073	2.853273231	0.533910147	5.344107518	9.09E-08
K00455	29.26219252	2.861551351	0.841775522	3.399423334	0.000675281
K00351	4047.765419	2.878643921	0.501839822	5.736180737	9.68E-09
K16969	15.34040513	2.883170967	0.86379152	3.337808835	0.000844418
K00446	160.646658	2.89311717	0.660070346	4.383043697	1.17E-05

K00368	1427.429492	2.901168536	0.560499277	5.176043315	2.27E-07
K00368	1427.429492	2.901168536	0.560499277	5.176043315	2.27E-07
K04098	72.23958927	2.901865717	0.549405104	5.281832474	1.28E-07
K01673	1704.469009	2.915778736	0.495061819	5.889726539	3.87E-09
K16845	12.6170553	2.919070183	1.137214667	2.566859422	NA
K15512	547.7390745	2.939356862	0.477653172	6.153747189	7.57E-10
K15512	547.7390745	2.939356862	0.477653172	6.153747189	7.57E-10
K00366	3.341917426	2.95001601	1.543505453	1.911244307	0.055973192
K18054	3.389174574	2.951822382	1.522888071	1.938305538	NA
K01007	2408.120594	2.964377116	0.501933307	5.905918322	3.51E-09
K08641	70.5126412	2.968231664	0.642056709	4.623005451	3.78E-06
K00504	896.9885551	2.970114041	0.520789406	5.703099964	1.18E-08
K03885	629.9065776	2.978915891	0.558494472	5.333832364	9.62E-08
K17489	80.58909098	2.98247722	0.704984642	4.230556304	2.33E-05
K10944	645.593722	2.986434966	0.578056028	5.166341708	2.39E-07
K10944	645.593722	2.986434966	0.578056028	5.166341708	2.39E-07
K00801	26.52731864	3.011487361	0.946401693	3.182039279	0.00146242
K00500	493.7304774	3.048429764	0.497966279	6.121759428	9.25E-10
K12267	296.4860238	3.077859761	0.581844029	5.28983646	1.22E-07
K12503	4.472232033	3.116800764	1.370090272	2.274887157	0.0229127
K01737	644.998779	3.130729297	0.553913897	5.652014352	1.59E-08
K03150	51.33921656	3.137792475	0.622664617	5.039297866	4.67E-07
K18707	499.631112	3.164697824	0.562356904	5.627561073	1.83E-08
K18967	200.7711764	3.172246168	0.637378258	4.977022873	6.46E-07
K02488	199.8079097	3.183615832	0.502616947	6.334079758	2.39E-10
K00349	1521.149945	3.191620932	0.547246498	5.832145006	5.47E-09
K00350	1424.527389	3.225195909	0.511665865	6.303324351	2.91E-10
K03738	579.4294089	3.248641115	0.535550165	6.065988448	1.31E-09
K05550	19.9355981	3.249844418	0.945796669	3.436092054	0.00059017
K01752	604.5383749	3.268382648	0.566157124	5.772925058	7.79E-09
K01843	124.3188307	3.27873724	0.596890507	5.493029625	3.95E-08
K00508	1624.725033	3.285753159	0.516835523	6.357444507	2.05E-10
K00451	1112.878794	3.308215215	0.548402218	6.032461403	1.61E-09
K00404	980.971375	3.335000828	0.504919404	6.605016164	3.97E-11
K00507	1139.08489	3.358077256	0.440300964	7.626776974	2.41E-14
K00347	3718.576883	3.373119118	0.510164228	6.611829942	3.80E-11
K00346	5264.635461	3.411764949	0.523234529	6.520527149	7.01E-11
K15983	39.84267444	3.439893307	0.773794816	4.445485077	8.77E-06
K15983	39.84267444	3.439893307	0.773794816	4.445485077	8.77E-06
K05587	96.72077459	3.454685336	0.627676819	5.503923722	3.71E-08
K18331	96.72077459	3.454685336	0.627676819	5.503923722	3.71E-08
K18331	96.72077459	3.454685336	0.627676819	5.503923722	3.71E-08
K18331	96.72077459	3.454685336	0.627676819	5.503923722	3.71E-08
K00469	2.347371225	3.457613563	1.769707765	1.953776568	0.050727647
K11942	1220.148232	3.496981054	0.522017356	6.698974692	2.10E-11
K04072	74.79039617	3.553081931	0.636333235	5.583681217	2.35E-08
K04072	74.79039617	3.553081931	0.636333235	5.583681217	2.35E-08
K18365	73.50004775	3.559903193	0.735018734	4.843282258	1.28E-06
K14048	1.884040605	3.573591962	1.877389197	1.903490213	0.05697661

K02586	26.82414937	3.614470533	0.884892276	4.084644687	4.41E-05
K08660	6.805942675	3.643394921	1.27288891	2.862303924	0.004205734
K03735	6.141527502	3.646067431	1.309959523	2.783343581	0.00538018
K03780	1.822683151	3.65246608	1.99299281	1.832653917	0.066854055
K16363	1290.829058	3.671999077	0.504300386	7.281372731	3.30E-13
K00518	1165.647293	3.717967858	0.57913308	6.419885145	1.36E-10
K00518	1165.647293	3.717967858	0.57913308	6.419885145	1.36E-10
K00505	219.4809873	3.727998828	0.599817257	6.215224358	5.13E-10
K06201	130.0929079	3.729642257	0.756369177	4.930981284	8.18E-07
K00491	5.372050013	3.745866103	1.169569583	3.202773188	0.001361111
K05299	89.06488552	3.781322503	0.631122895	5.991420269	2.08E-09
K07213	6.512083576	3.819972707	1.238166185	3.085185779	0.00203425
K19701	135.7780323	3.860779277	0.592341162	6.517830472	7.13E-11
K04100	1.588502641	3.894121042	1.927593117	2.020198665	NA
K00452	121.1640057	3.900249498	0.606005842	6.435993231	1.23E-10
K01666	387.2040386	3.914031131	0.584644168	6.694723634	2.16E-11
K03381	210.7963442	3.918990081	0.579690918	6.760482108	1.38E-11
K03831	99.66753594	3.965699966	0.663333003	5.978445141	2.25E-09
K17838	33.84602109	3.990384144	0.899811961	4.434686707	9.22E-06
K00030	282.8308453	4.003102234	0.544883802	7.346708084	2.03E-13
K00456	97.52919445	4.016124404	0.693392326	5.791994308	6.96E-09
K00476	30.4090934	4.070108551	1.0502136	3.875505468	0.000106404
K00461	1.106476872	4.087162374	2.32032324	1.7614625	0.078160155
K18793	29.97256143	4.145163118	0.935108166	4.432816725	9.30E-06
K18794	29.97256143	4.145163118	0.935108166	4.432816725	9.30E-06
K18973	29.97256143	4.145163118	0.935108166	4.432816725	9.30E-06
K18976	29.97256143	4.145163118	0.935108166	4.432816725	9.30E-06
K19212	29.97256143	4.145163118	0.935108166	4.432816725	9.30E-06
K19318	29.97256143	4.145163118	0.935108166	4.432816725	9.30E-06
K19321	29.97256143	4.145163118	0.935108166	4.432816725	9.30E-06
K15916	109.9230108	4.147225626	0.589198827	7.038754044	1.94E-12
K11645	444.1069603	4.162479395	0.574453915	7.245976198	4.29E-13
K00367	85.3133103	4.266691254	0.620330048	6.878098633	6.07E-12
K11991	789.6178752	4.273890649	0.511550625	8.354775537	6.56E-17
K05577	0.579689492	4.278758511	2.977045271	1.437250066	0.150646952
K15746	155.1462916	4.290208544	0.612394039	7.005634073	2.46E-12
K07181	146.2111204	4.341939557	0.757386992	5.732788657	9.88E-09
K19215	13.14104607	4.409803479	1.084282742	4.067023581	4.76E-05
K13831	2.512747982	4.417805938	1.728854669	2.555336789	0.01060851
K02217	232.5503236	4.486155833	0.617002023	7.270893227	3.57E-13
K13624	5.639115585	4.592761396	1.423530721	3.226317021	0.001253944
K02277	226.3479639	4.616556641	0.557873276	8.275278349	1.28E-16
K15635	19.55879104	4.651192059	0.828206229	5.615982943	1.95E-08
K15635	19.55879104	4.651192059	0.828206229	5.615982943	1.95E-08
K01674	214.3993168	4.669573833	0.594576712	7.853610369	4.04E-15
K10208	1.419401839	4.677554454	2.163829357	2.161702095	0.030641146
K00474	4.818447051	4.759487147	1.383961817	3.439030679	0.000583801
K01399	1536.773456	4.762074714	0.570550557	8.346455287	7.03E-17
K21020	0.093826708	4.928149265	4.330439088	1.138025305	0.255109916

K08604	1753.73656	5.000284409	0.552359551	9.052589744	1.40E-19
K01401	1305.26982	5.092227446	0.496278231	10.26083178	1.06E-24
K08603	1305.26982	5.092227446	0.496278231	10.26083178	1.06E-24
K14415	228.7328108	5.094406573	0.533482162	9.549347546	1.31E-21
K03737	46.2700746	5.095979737	0.78363107	6.503034312	7.87E-11
K07752	4.722893799	5.106399397	1.453038579	3.51429031	0.000440931
K08605	1140.12605	5.166282524	0.53028686	9.742429833	1.99E-22
K04561	51.15349749	5.225208164	0.893291553	5.849387185	4.93E-09
K17836	49.79416082	5.322151467	0.696624487	7.63991443	2.17E-14
K01400	1707.514306	5.398124267	0.494633182	10.91338888	9.95E-28
K21024	0.231696978	5.420406618	4.255151835	1.273845641	0.202718126
K01387	265.4062657	5.592179215	1.040874836	5.372576051	7.76E-08
K05996	256.7980049	5.799498928	0.571599242	10.14609276	3.45E-24
K01818	1.450641477	5.831920829	2.202705963	2.64761658	0.008106141
K15059	24.57313726	5.952989326	1.030605063	5.776208114	7.64E-09
K04034	976.6187572	6.003734329	0.55433694	10.83047853	2.47E-27
K15750	1.170999076	6.191816894	2.512427748	2.464475604	0.01372139
K16268	1.170999076	6.191816894	2.512427748	2.464475604	0.01372139
K16268	1.170999076	6.191816894	2.512427748	2.464475604	0.01372139
K13243	2.755642053	6.206189463	1.639434319	3.785567613	0.000153358
K00376	45.39932075	6.233077167	0.704755793	8.844307816	9.21E-19
K01517	4.473811366	6.336354304	1.666819372	3.80146428	0.000143843
K01517	4.473811366	6.336354304	1.666819372	3.80146428	0.000143843
K11784	59.67747431	6.355969802	0.846869989	7.505248603	6.13E-14
K00448	1.547613262	6.583456635	2.218233967	2.967881988	0.002998594
K04114	4.060107384	6.757431989	1.756023203	3.848145047	0.000119016
K04114	4.060107384	6.757431989	1.756023203	3.848145047	0.000119016
K04115	4.060107384	6.757431989	1.756023203	3.848145047	0.000119016
K04115	4.060107384	6.757431989	1.756023203	3.848145047	0.000119016
K00473	4.367314946	6.795124279	1.501035456	4.526957876	5.98E-06
K01569	16.69261228	6.881706036	1.062793668	6.47511012	9.47E-11
K13647	3.222848096	6.944159827	1.612537375	4.306355893	NA
K04035	1066.119523	7.084298763	0.648166462	10.92975213	8.31E-28
K14735	13.6437197	7.360697969	1.316228874	5.592262951	2.24E-08
K15862	45.08657072	8.286255296	0.970573497	8.537483585	1.37E-17
K01264	86.0031771	8.612639822	0.886342592	9.71705512	2.55E-22

ated KEGG orthologous (KO) genes in prokaryotic commun

padj	Metal Co-Factor
0.002053697	Cob(II)alamin
0.000790085	Zn2+
0.014310849	Cob(II)alamin
0.083581642	Fe-S
0.132503795	Fe2+
0.054984599	Zn2+
0.135013918	Fe-S
0.22894957	Mn2+
0.280221113	Cob(II)alamin
0.158359572	Fe2+
0.095459063	Fe-S
0.337154467	Fe-S
0.357228152	Fe-S
0.414811908	Mn2+
0.414811908	Fe_cation
0.491179783	Fe-S
0.493399713	Cobalt_cation
0.423481152	Fe_cation
0.53009977	Fe_cation
0.533281583	Zn2+
0.485150156	Fe-S
0.517203125	Fe-S
0.4624802	Zn2+
0.4624802	Fe_cation
0.719446997	Ni2+
0.719446997	Fe-S
0.479384251	Fe_cation
0.557318324	Fe2+
0.59784948	Fe2+
0.502764933	Zn2+
0.559704742	Fe_cation
0.614655932	Ni2+
0.581918022	Cobalt_cation
0.581918022	Mn2+
0.581918022	Ni2+
0.606994546	Zn2+
0.656014575	Fe-S
0.649472876	Mn2+
0.83374853	Mn2+
0.948834974	Cu_cation
0.902466855	irr
0.944267007	Mn2+
0.987228252	Fe-S
0.964790538	Mn2+
0.982292239	Mn2+
0.971946689	Fe-S
0.989493453	Fe2+

0.979276854 Zn2+
0.990261277 Zn2+
0.994361999 Fe2+
0.990261277 Fe-S
0.982292239 Fe_cation
0.925906076 Zn2+
0.949308804 Zn2+
0.957123469 nikD, cntD
0.889913922 Fe_cation
0.866487687 Fe_cation
0.847789846 Fe-S
0.911957529 Fe_cation
0.798950275 Mn2+
0.798950275 Fe_cation
0.866689156 Fe-S
0.758750073 Fe-S
0.745607979 Zn2+
0.776065987 Fe_cation
0.750785948 Fe-S
0.763370261 furA
0.696363961 Cobalt_cation
0.696363961 Mn2+
0.636595937 Fe-S
0.566805685 Fe-S
0.698087331 Zn2+
0.698087331 Fe_cation
0.690353156 Fe_cation
0.649472876 Fe-S
0.838053409 Zn2+
0.611349911 Fe2+
 0.54558201 Fe-S
0.498522613 Fe2+
0.523862139 Fe_cation
0.523862139 Fe-S
0.599195113 Fe-S
0.576930864 Zn2+
0.508651624 Fe-S
0.483469728 Fe-S
0.483469728 Cu_cation
0.426905422 Zn2+
0.481317529 Cu_cation
0.418911908 Fe-S
0.418911908 Cu_cation
0.443987639 Mn2+
 0.43041693 Mn2+
 0.40429034 Fe-S
0.565663989 Ni2+
0.327403351 Fe-S
0.338016772 Fe-S

0.26349434 Zn2+
0.26349434 Fe_cation
0.46056262 Ni2+
0.528401867 Fe-S
0.528401867 Ni2+
0.460390523 Mn2+
0.170542072 Fe-S
0.342908871 Zn2+
0.248809671 Fe-S
0.251088975 Cobalt_cation
0.251088975 Mn2+
0.295291005 Fe-S
0.347237869 Fe-S
0.210228958 Fe-S
0.213621748 Cu_cation
0.188143685 Zn2+
0.194989896 Fe-S
0.225494192 Fe-S
0.203927996 Zn2+
0.309911159 Fe2+
0.257590937 Mn2+
0.199562843 Zn2+
0.21004237 Zn2+
0.161375403 Fe-S
0.129073661 zur
0.126734882 Fe-S
0.279183376 Cu_cation
0.279183376 Fe_cation
0.138804843 Fe_cation
0.138804843 Fe-S
0.126393433 Fe-S
0.140025061 Fe-S
0.109814474 Fe-S
0.158359572 Fe-S
0.099332658 Zn2+
0.206699865 Fe-S
0.232949325 Fe-S
0.132614932 Fe_cation
0.132614932 Fe-S
0.408557818 Fe-S
0.142493212 Fe2+
0.482373191 Cob(II)alamin
0.209870709 Fe-S
0.266398063 Mn2+
0.128376462 Fe-S
0.093716721 Zn2+
0.057801673 Fe_cation
0.057801673 Zn2+
0.195651119 Mn2+

0.17012548 Fe_cation
0.086566197 Fe2+
0.170976621 Mn2+
0.079972199 Mn2+
0.057801673 Zn2+
0.037659208 Fe-S
0.037659208 Cu_cation
0.030426089 Mn2+
0.030426089 Cobalt_cation
0.059370469 Cob(II)alamin
0.059370469 Zn2+
0.066853804 Mn2+
0.055746023 Fe-S
0.16692222 Fe-S
0.16692222 Fe_cation
0.04664682 Zn2+
0.19391519 Cu_cation
0.032278005 ABC.PE.S
0.037845181 Mn2+
0.031027289 Fe-S
0.024982803 Fe-S
0.037229727 Fe-S
0.037229727 Fe_cation
0.034152289 Cob(II)alamin
0.031553416 Mn2+
0.031553416 Fe3+
0.091965422 Fe-S
0.040360439 Mn2+
0.06259213 Fe-S
0.017873381 Fe_cation
0.017873381 Zn2+
0.022340872 Zn2+
0.404215914 Mn2+
0.04321437 Fe-S
0.083098944 Zn2+
0.007972639 Fe-S
0.07824511 Mn2+
0.013656467 Zn2+
0.02585335 Mn2+
0.02585335 Cobalt_cation
0.019953758 Fe_cation
0.054203106 Fe-S
0.029464397 Fe2+
0.035735899 Zn2+
0.035735899 Mn2+
0.009407044 Fe-S
0.009799701 Fe-S
0.072573794 Cu_cation
0.027971489 Fe-S

0.006851891	Zn2+
0.064465047	Fe_cation
0.007424267	Mn2+
0.007424267	Cobalt_cation
0.004161836	Mn2+
0.010258238	Fe-S
0.002480164	Mn2+
0.022214088	Fe_cation
0.022214088	Ni2+
0.004749741	Cu_cation
0.004749741	bfr
0.004822528	Zn2+
0.001806807	ABC.PE.P1
0.076097827	Fe_cation
0.009320242	Zn2+
0.005690713	nikE, cntF
0.007363283	Zn2+
0.006737854	Zn2+
0.00103296	ABC.PE.P
0.004189919	cytochrome c oxidase assembly protein su
0.005761068	Fe-S
0.051316544	Mn2+
0.016827092	Zn2+
0.005194758	Mn2+
0.005979857	Fe-S
0.004140834	Fe_cation
0.006156522	Fe-S
0.000383069	Fe-S
0.001676334	Fe-S
0.002572818	Cobalt_cation
0.066160032	Ni2+
NA	Fe2+
NA	Fe2+
NA	Fe2+
NA	Fe2+
NA	Fe2+
NA	Fe2+
NA	Fe_cation
0.006282284	Fe-S
0.014290964	Zn2+
0.000473778	Fe-S
0.037609691	Zn2+
0.002978467	Fe-S
0.006445876	Fe_cation
0.008339221	Fe-S
0.001933949	Fe-S
0.001002919	Zn2+
0.000424565	Fe-S
0.001216956	Fe-S

0.00044884 Zn2+
0.00044884 Mn2+
0.00050806 Zn2+
0.00050806 Mn2+
0.002369609 Cobalt_cation
0.002369609 Mn2+
0.005624586 Fe-S
0.000473866 Zn2+
0.00075636 ABC.PE.A1
0.003538692 Cobalt_cation
0.003538692 Mn2+
0.001307635 Fe-S
0.000561159 Fe-S
0.002568827 Fe-S
0.000586676 ABC.PE.A
0.001934524 Mn2+
0.000410995 Zn2+
0.000804128 Fe-S
0.000749925 Fe-S
0.009222213 Fe-S
0.000294127 Fe-S
0.000312477 Fe-S
0.001240172 Mn2+
0.00012744 Zn2+
3.41E-05 P-type Cu+ transporter [EC:7.2.2.8],ATP7B
3.41E-05 P-type Cu+ transporter [EC:7.2.2.8],ATP7B,
0.000294812 Zn2+
0.00190176 Fe2+
0.00190176 Ni2+
0.000637298 Mn2+
0.000328237 Mn2+
0.000443176 hfq
0.00027591 Cu_cation
0.000159405 Mn2+
5.10E-05 fur,zur,furB
0.003162947 Fe_cation
2.32E-05 Zn2+
2.32E-05 Mn2+
0.001116897 Fe-S
9.05E-05 Mn2+
9.05E-05 Cobalt_cation
0.248723482 Mn2+
0.248723482 Fe3+
0.000122117 Mn2+
2.88E-05 Cu_cation
0.000118742 Zn2+
0.04702287 Fe-S
1.73E-05 dps
0.000132383 Mn2+

0.000132383 Zn2+
6.30E-06 Zn2+
9.50E-05 Fe-S
2.41E-05 Cobalt_cation
2.58E-05 Zn2+
3.92E-05 Cu_cation
0.005520755 Fe2+
0.000562426 uncharacterized protein | (GenBank) Cons
0.00014092 Fe_cation
6.18E-06 Fe2+
1.86E-06 Fe_cation
0.000247813 Zn2+
3.56E-06 Fe-S
0.011293918 Fe_cation
0.012096216 Fe_cation
0.012096216 Fe-S
0.012096216 Fe_cation
0.012096216 Fe2+
2.38E-07 Fe-S
2.38E-07 Fe-S
8.51E-06 Fe-S
3.09E-06 Cu_cation
1.74E-06 Fe-S
0.000303111 Mn2+
3.22E-06 Fe-S
1.04E-06 Mn2+
1.04E-06 Fe3+
0.029620412 Fe-S
1.12E-05 Cobalt_cation
1.12E-05 Mn2+
9.33E-05 Fe2+
8.87E-06 Fe2+
1.27E-06 Fe_cation
6.98E-07 Fe-S
3.68E-06 Fe-S
7.76E-07 Fe_cation
7.76E-07 Mn2+
7.55E-06 Mn2+
1.46E-06 Zn2+
2.16E-07 Fe_cation
4.15E-05 Fe-S
0.023061149 perR
0.008644564 Fe-S
0.045695744 Mn2+
5.95E-07 Mn2+
0.001793013 Fe_cation
7.91E-08 Fe-S
0.002178916 Fe-S
4.78E-05 Fe2+

1.37E-06	Cu_cation
1.37E-06	Fe_cation
8.17E-07	Fe_cation
3.49E-08	Zn2+
NA	Fe2+
7.89E-09	Fe-S
7.89E-09	Fe_cation
0.085516521	Fe-S
NA	Fe2+
3.19E-08	Mn2+
1.74E-05	Zn2+
9.43E-08	Cu_cation
6.27E-07	Fe-S
8.90E-05	Cobalt_cation
1.44E-06	Cu_cation
1.44E-06	Fe_cation
0.003530373	Mn2+
9.49E-09	Fe_cation
7.84E-07	Zn2+
0.039337686	Mn2+
1.23E-07	Zn2+
2.65E-06	Fe-S
1.41E-07	Fe-S
3.56E-06	Mn2+
2.76E-09	Mn2+
4.77E-08	Fe-S
3.33E-09	Fe-S
1.30E-08	Fe-S
0.001585762	Fe2+
6.46E-08	Fe-S
2.76E-07	Fe-S
2.41E-09	Fe_cation
1.58E-08	Fe_cation
5.44E-10	Cu_cation
6.04E-13	Fe_cation
5.22E-10	Fe-S
9.20E-10	Fe-S
3.70E-05	Fe-S
3.70E-05	Fe_cation
2.61E-07	Fe-S
2.61E-07	Ni2+
2.61E-07	Fe_cation
2.61E-07	Fe-S
0.078546033	Fe_cation
3.07E-10	Cobalt_cation
1.76E-07	Zn2+
1.76E-07	Fe_cation
6.65E-06	Mn2+
0.086834882	Ni2+

0.000158842	Fe-S
0.008952199	Zn2+
0.011055532	Cob(II)alamin
0.099917305	Fe_cation
6.78E-12	Zn2+
1.66E-09	Fe_cation
1.66E-09	Mn2+
5.58E-09	Cu_cation
4.44E-06	copper homeostasis protein,CUTC, CGI-32
0.003306798	Ferriheme_b
1.97E-08	Fe_cation
0.004706286	copper chaperone,ATOX1, ATX1, HAH1
9.33E-10	Zn2+
NA	Fe_cation
1.51E-09	Fe_cation
3.14E-10	Mn2+
2.10E-10	Fe_cation
2.11E-08	Mn2+
3.86E-05	Zn2+
4.39E-12	Mn2+
5.87E-08	Fe2+
0.000349077	Fe2+
0.114597807	Fe_cation
3.87E-05	Zn2+
3.87E-05	Zn2+
3.87E-05	Zn2+
3.87E-05	Zn2+
3.87E-05	Zn2+
3.87E-05	Zn2+
3.87E-05	Zn2+
3.44E-11	Zn2+
8.49E-12	Zn2+
9.83E-11	Fe-S
2.24E-15	Zn2+
0.203552481	Fe-S
4.30E-11	Fe_cation
8.05E-08	Mn2+
0.000170102	Zn2+
0.020003231	Mn2+
7.21E-12	ftnA, ftn
0.003090478	Cu_cation
4.11E-15	Cu_cation
1.49E-07	Mn2+
1.49E-07	Cobalt_cation
1.12E-13	Zn2+
0.050564027	Mn2+
0.001570355	Fe2+
2.38E-15	Zn2+
0.322491287	Mn2+

7.67E-18	Zn2+
1.34E-22	Zn2+
1.34E-22	Zn2+
9.49E-20	Mn2+
1.02E-09	Fe-S
0.001232313	Zn2+
1.69E-20	Zn2+
4.34E-08	Fe_cation
5.51E-13	Zn2+
2.14E-25	Zn2+
0.263261995	Mn2+
5.16E-07	Zn2+
3.97E-22	Zn2+
0.015840616	Mn2+
6.35E-08	Fe2+
5.09E-25	Fe-S
0.02506968	Fe_cation
0.02506968	Fe-S
0.02506968	Fe_cation
0.000481093	Mn2+
4.38E-17	Cu_cation
0.000454998	manganese-dependent ADP-ribose/CDP-al
0.000454998	Mn2+
1.42E-12	Fe-S
0.006621282	Fe_cation
0.000384332	Fe-S
0.000384332	Mn2+
0.000384332	Fe-S
0.000384332	Mn2+
2.61E-05	Fe2+
1.20E-09	Mn2+
NA	Fe2+
1.87E-25	Fe_cation
1.69E-07	Cu_cation
5.30E-16	Cu_cation
2.07E-20	Cobalt_cation

ıities attached to particles as compared to those in particle-free incubations. Significant results (<0.05)
KO Name
ko:K06120_dhaB; glycerol dehydratase large subunit [EC:4.2.1.30]
ko:K00544_BHMT; betaine-homocysteine S-methyltransferase [EC:2.1.1.5]
ko:K01699_pduC; propanediol dehydratase large subunit [EC:4.2.1.28]
ko:K14581_nahAa, nagAa, ndoR, nbzAa, dntAa; naphthalene 1,2-dioxygenase ferredoxin reductase co
ko:K07104_catE; catechol 2,3-dioxygenase [EC:1.13.11.2]
ko:K01283_ACE, CD143; peptidyl-dipeptidase A [EC:3.4.15.1]
ko:K07469_mop; aldehyde oxidoreductase [EC:1.2.99.7]
ko:K18788_wbbD; UDP-Gal:alpha-D-GlcNAc-diphosphoundecaprenol beta-1,3-galactosyltransferase [
ko:K01848_E5.4.99.2A, mcmA1; methylmalonyl-CoA mutase, N-terminal domain [EC:5.4.99.2]
ko:K16846_suyB; (2R)-sulfolactate sulfo-lyase subunit beta [EC:4.4.1.24]
ko:K17723_preA; dihydropyrimidine dehydrogenase (NAD+) subunit PreA [EC:1.3.1.1]
ko:K11779_fbiC; FO synthase [EC:2.5.1.147 4.3.1.32]
ko:K03614_rnfD; Na+-translocating ferredoxin:NAD+ oxidoreductase subunit D [EC:7.2.1.2]
ko:K00462_bphC; biphenyl-2,3-diol 1,2-dioxygenase [EC:1.13.11.39]
ko:K00462_bphC; biphenyl-2,3-diol 1,2-dioxygenase [EC:1.13.11.39]
ko:K10797_enr; 2-enoate reductase [EC:1.3.1.31]
ko:K05526_astE; succinylglutamate desuccinylase [EC:3.5.1.96]
ko:K00394_aprA; adenylylsulfate reductase, subunit A [EC:1.8.99.2]
ko:K04101_ligB; protocatechuate 4,5-dioxygenase, beta chain [EC:1.13.11.8]
ko:K00153_E1.1.1.306; S-(hydroxymethyl)mycothiol dehydrogenase [EC:1.1.1.306]
ko:K00179_iorA; indolepyruvate ferredoxin oxidoreductase, alpha subunit [EC:1.2.7.8]
ko:K14534_abfD; 4-hydroxybutyryl-CoA dehydratase / vinylacetyl-CoA-Delta-isomerase [EC:4.2.1.120
ko:K13953_adhP; alcohol dehydrogenase, propanol-preferring [EC:1.1.1.1]
ko:K13953_adhP; alcohol dehydrogenase, propanol-preferring [EC:1.1.1.1]
ko:K06282_hyaA, hybO; hydrogenase small subunit [EC:1.12.99.6]
ko:K06282_hyaA, hybO; hydrogenase small subunit [EC:1.12.99.6]
ko:K16319_andAc; anthranilate 1,2-dioxygenase large subunit [EC:1.14.12.1]
ko:K03119_tauD; taurine dioxygenase [EC:1.14.11.17]
ko:K00477_PHYH; phytanoyl-CoA hydroxylase [EC:1.14.11.18]
ko:K06015_E3.5.1.81; N-acyl-D-amino-acid deacylase [EC:3.5.1.81]
ko:K16049_hsaC; 3,4-dihydroxy-9,10-secoandrosta-1,3,5(10)-triene-9,17-dione 4,5-dioxygenase [EC:1
ko:K01428_ureC; urease subunit alpha [EC:3.5.1.5]
ko:K06016_pydC; beta-ureidopropionase / N-carbamoyl-L-amino-acid hydrolase [EC:3.5.1.6 3.5.1.87]
ko:K06016_pydC; beta-ureidopropionase / N-carbamoyl-L-amino-acid hydrolase [EC:3.5.1.6 3.5.1.87]
ko:K06016_pydC; beta-ureidopropionase / N-carbamoyl-L-amino-acid hydrolase [EC:3.5.1.6 3.5.1.87]
ko:K01461_E3.5.1.82; N-acyl-D-glutamate deacylase [EC:3.5.1.82]
ko:K17828_pyrDI; dihydroorotate dehydrogenase (NAD+) catalytic subunit [EC:1.3.1.14]
ko:K07141_mocA; molybdenum cofactor cytidylyltransferase [EC:2.7.7.76]
ko:K01475_E3.5.2.20; isatin hydrolase [EC:3.5.2.20]
ko:K02826_qoxA; cytochrome aa3-600 menaquinol oxidase subunit II [EC:7.1.1.5]
ko:K09826_irr; Fur family transcriptional regulator, iron response regulator
ko:K08093_hxlA; 3-hexulose-6-phosphate synthase [EC:4.1.2.43]
ko:K23121_pflD; trans-4-hydroxy-L-proline dehydratase [EC:4.2.1.172]
ko:K18459_gpuA; guanidinopropionase [EC:3.5.3.17]
ko:K12506_ispDF; 2-C-methyl-D-erythritol 4-phosphate cytidylyltransferase / 2-C-methyl-D-erythritol
ko:K00331_nuoB; NADH-quinone oxidoreductase subunit B [EC:7.1.1.2]
ko:K07173_luxS; S-ribosylhomocysteine lyase [EC:4.4.1.21]

ko:K19702_E3.4.11.24; aminopeptidase S [EC:3.4.11.24]
ko:K07260_vanY; zinc D-Ala-D-Ala carboxypeptidase [EC:3.4.17.14]
ko:K00471_E1.14.11.1; gamma-butyrobetaine dioxygenase [EC:1.14.11.1]
ko:K00180_iorB; indolepyruvate ferredoxin oxidoreductase, beta subunit [EC:1.2.7.8]
ko:K03919_alkB; DNA oxidative demethylase [EC:1.14.11.33]
ko:K01295_cpg; glutamate carboxypeptidase [EC:3.4.17.11]
ko:K18456_E3.5.4.32; 8-oxoguanine deaminase [EC:3.5.4.32]
ko:K15587_nikD, cntD; nickel transport system ATP-binding protein [EC:3.6.3.24]
ko:K00395_aprB; adenylylsulfate reductase, subunit B [EC:1.8.99.2]
ko:K14583_nahC; 1,2-dihydroxynaphthalene dioxygenase [EC:1.13.11.56]
ko:K01754_E4.3.1.19, ilvA, tdcB; threonine dehydratase [EC:4.3.1.19]
ko:K03779_ttdA; L(+)-tartrate dehydratase alpha subunit [EC:4.2.1.32]
ko:K04565_SOD1; superoxide dismutase, Cu-Zn family [EC:1.15.1.1]
ko:K04565_SOD1; superoxide dismutase, Cu-Zn family [EC:1.15.1.1]
ko:K00172_porG; pyruvate ferredoxin oxidoreductase gamma subunit [EC:1.2.7.1]
ko:K04108_hcrA, hbaC; 4-hydroxybenzoyl-CoA reductase subunit alpha [EC:1.3.7.9]
ko:K01698_hemB, ALAD; porphobilinogen synthase [EC:4.2.1.24]
ko:K17893_AOX1, AOX2; ubiquinol oxidase [EC:1.10.3.11]
ko:K03615_rnfC; Na+-translocating ferredoxin:NAD+ oxidoreductase subunit C [EC:7.2.1.2]
ko:K22297_furA; Fur family transcriptional regulator, stress-responsive regulator
ko:K02510_hpaI, hpcH; 4-hydroxy-2-oxoheptanedioate aldolase [EC:4.1.2.52]
ko:K02510_hpaI, hpcH; 4-hydroxy-2-oxoheptanedioate aldolase [EC:4.1.2.52]
ko:K00087_ygeS, xdhA; xanthine dehydrogenase molybdenum-binding subunit [EC:1.17.1.4]
ko:K04090_E1.2.7.8; indolepyruvate ferredoxin oxidoreductase [EC:1.2.7.8]
ko:K15358_ena; enamidase [EC:3.5.2.18]
ko:K15358_ena; enamidase [EC:3.5.2.18]
ko:K21817_blh; beta-carotene 15,15'-dioxygenase [EC:1.13.11.63]
ko:K00122_FDH; formate dehydrogenase [EC:1.17.1.9]
ko:K21947_ttuA; tRNA-5-methyluridine54 2-sulfurtransferase [EC:2.8.1.15]
ko:K00472_P4HA; prolyl 4-hydroxylase [EC:1.14.11.2]
ko:K03526_gcpE, ispG; (E)-4-hydroxy-3-methylbut-2-enyl-diphosphate synthase [EC:1.17.7.1 1.17.7.3]
ko:K10674_ectD; ectoine hydroxylase [EC:1.14.11.55]
ko:K15511_boxA; benzoyl-CoA 2,3-epoxidase subunit A [EC:1.14.13.208]
ko:K15511_boxA; benzoyl-CoA 2,3-epoxidase subunit A [EC:1.14.13.208]
ko:K00338_nuoI; NADH-quinone oxidoreductase subunit I [EC:7.1.1.2]
ko:K03148_thiF; sulfur carrier protein ThiS adenylyltransferase [EC:2.7.7.73]
ko:K00330_nuoA; NADH-quinone oxidoreductase subunit A [EC:7.1.1.2]
ko:K03518_coxS; aerobic carbon-monoxide dehydrogenase small subunit [EC:1.2.5.3]
ko:K03518_coxS; aerobic carbon-monoxide dehydrogenase small subunit [EC:1.2.5.3]
ko:K01273_DPEP; membrane dipeptidase [EC:3.4.13.19]
ko:K02298_cyoB; cytochrome o ubiquinol oxidase subunit I [EC:7.1.1.3]
ko:K03519_coxM, cutM; aerobic carbon-monoxide dehydrogenase medium subunit [EC:1.2.5.3]
ko:K03519_coxM, cutM; aerobic carbon-monoxide dehydrogenase medium subunit [EC:1.2.5.3]
ko:K03638_moaB; molybdopterin adenylyltransferase [EC:2.7.7.75]
ko:K21019_sadC; diguanylate cyclase [EC:2.7.7.65]
ko:K00317_dmd-tmd; dimethylamine/trimethylamine dehydrogenase [EC:1.5.8.1 1.5.8.2]
ko:K01429_ureB; urease subunit beta [EC:3.5.1.5]
ko:K03616_rnfB; Na+-translocating ferredoxin:NAD+ oxidoreductase subunit B [EC:7.2.1.2]
ko:K21307_soeA; sulfite dehydrogenase (quinone) subunit SoeA [EC:1.8.5.6]

ko:K00121_frmA, ADH5, adhC; S-(hydroxymethyl)glutathione dehydrogenase / alcohol dehydrogenas
ko:K00121_frmA, ADH5, adhC; S-(hydroxymethyl)glutathione dehydrogenase / alcohol dehydrogenas
ko:K00096_araM, egsA; glycerol-1-phosphate dehydrogenase [NAD(P)+] [EC:1.1.1.261]
ko:K06281_hyaB, hybC; hydrogenase large subunit [EC:1.12.99.6]
ko:K06281_hyaB, hybC; hydrogenase large subunit [EC:1.12.99.6]
ko:K16870_wbbL; N-acetylglucosaminyl-diphospho-decaprenol L-rhamnosyltransferase [EC:2.4.1.289
ko:K17722_preT; dihydropyrimidine dehydrogenase (NAD+) subunit PreT [EC:1.3.1.1]
ko:K00098_idnD; L-idonate 5-dehydrogenase [EC:1.1.1.264]
ko:K08352_phsA, psrA; thiosulfate reductase / polysulfide reductase chain A [EC:1.8.5.5]
ko:K00863_DAK, TKFC; triose/dihydroxyacetone kinase / FAD-AMP lyase (cyclizing) [EC:2.7.1.28 2.7.1.
ko:K00863_DAK, TKFC; triose/dihydroxyacetone kinase / FAD-AMP lyase (cyclizing) [EC:2.7.1.28 2.7.1.
ko:K11177_yagR; xanthine dehydrogenase YagR molybdenum-binding subunit [EC:1.17.1.4]
ko:K00381_cysI; sulfite reductase (NADPH) hemoprotein beta-component [EC:1.8.1.2]
ko:K00285_dadA; D-amino-acid dehydrogenase [EC:1.4.5.1]
ko:K00423_E1.10.3.3; L-ascorbate oxidase [EC:1.10.3.3]
ko:K17067_mdo; formaldehyde dismutase / methanol dehydrogenase [EC:1.2.98.1 1.1.99.37]
ko:K03527_ispH, lytB; 4-hydroxy-3-methylbut-2-en-1-yl diphosphate reductase [EC:1.17.7.4]
ko:K00342_nuoM; NADH-quinone oxidoreductase subunit M [EC:7.1.1.2]
ko:K01301_NAALAD; N-acetylated-alpha-linked acidic dipeptidase [EC:3.4.17.21]
ko:K05549_benA-xylX; benzoate/toluate 1,2-dioxygenase subunit alpha [EC:1.14.12.10 1.14.12.-]
ko:K07246_ttuC, dmlA; tartrate dehydrogenase/decarboxylase / D-malate dehydrogenase [EC:1.1.1.9
ko:K00549_metE; 5-methyltetrahydropteroyltriglutamate--homocysteine methyltransferase [EC:2.1.1
ko:K17837_bla2, blm, ccrA, blaB; metallo-beta-lactamase class B [EC:3.5.2.6]
ko:K22515_fdwB; formate dehydrogenase beta subunit [EC:1.17.1.9]
ko:K09823_zur; Fur family transcriptional regulator, zinc uptake regulator
ko:K00499_CMO; choline monooxygenase [EC:1.14.15.7]
ko:K15864_nirS; nitrite reductase (NO-forming) / hydroxylamine reductase [EC:1.7.2.1 1.7.99.1]
ko:K15864_nirS; nitrite reductase (NO-forming) / hydroxylamine reductase [EC:1.7.2.1 1.7.99.1]
ko:K01704_leuD, IPMI-S; 3-isopropylmalate/(R)-2-methylmalate dehydratase small subunit [EC:4.2.1.
ko:K01704_leuD, IPMI-S; 3-isopropylmalate/(R)-2-methylmalate dehydratase small subunit [EC:4.2.1.
ko:K13482_xdhB; xanthine dehydrogenase large subunit [EC:1.17.1.4]
ko:K00334_nuoE; NADH-quinone oxidoreductase subunit E [EC:7.1.1.2]
ko:K00265_gltB; glutamate synthase (NADPH) large chain [EC:1.4.1.13]
ko:K00333_nuoD; NADH-quinone oxidoreductase subunit D [EC:7.1.1.2]
ko:K07047_nfdA; N-substituted formamide deformylase [EC:3.5.1.91]
ko:K00336_nuoG; NADH-quinone oxidoreductase subunit G [EC:7.1.1.2]
ko:K13378_nuoCD; NADH-quinone oxidoreductase subunit C/D [EC:7.1.1.2]
ko:K15982_kshA; 3-ketosteroid 9alpha-monooxygenase subunit A [EC:1.14.15.30]
ko:K15982_kshA; 3-ketosteroid 9alpha-monooxygenase subunit A [EC:1.14.15.30]
ko:K04039_chlB; light-independent protochlorophyllide reductase subunit B [EC:1.3.7.7]
ko:K13646_PLOD3; lysyl hydroxylase/galactosyltransferase/glucosyltransferase [EC:1.14.11.4 2.4.1.50
ko:K13920_pduE; propanediol dehydratase small subunit [EC:4.2.1.28]
ko:K00329_E7.1.1.2; NADH dehydrogenase [EC:7.1.1.2]
ko:K02083_allC; allantoate deiminase [EC:3.5.3.9]
ko:K00335_nuoF; NADH-quinone oxidoreductase subunit F [EC:7.1.1.2]
ko:K00344_qor, CRYZ; NADPH2:quinone reductase [EC:1.6.5.5]
ko:K13954_yiaY; alcohol dehydrogenase [EC:1.1.1.1]
ko:K13954_yiaY; alcohol dehydrogenase [EC:1.1.1.1]
ko:K01004_pcs; phosphatidylcholine synthase [EC:2.7.8.24]

ko:K22209_tarD; D(-)-tartrate dehydratase [EC:4.2.1.81]
ko:K00464_diox1; all-trans-8'-apo-beta-carotenal 15,15'-oxygenase [EC:1.13.11.75]
ko:K17224_soxB; S-sulfosulfanyl-L-cysteine sulfohydrolase [EC:3.1.6.20]
ko:K12255_gbuA; guanidinobutyrase [EC:3.5.3.7]
ko:K19670_phnA; phosphonoacetate hydrolase [EC:3.11.1.2]
ko:K03520_coxL, cutL; aerobic carbon-monoxide dehydrogenase large subunit [EC:1.2.5.3]
ko:K03520_coxL, cutL; aerobic carbon-monoxide dehydrogenase large subunit [EC:1.2.5.3]
ko:K00099_dxr; 1-deoxy-D-xylulose-5-phosphate reductoisomerase [EC:1.1.1.267]
ko:K00099_dxr; 1-deoxy-D-xylulose-5-phosphate reductoisomerase [EC:1.1.1.267]
ko:K00548_metH, MTR; 5-methyltetrahydrofolate--homocysteine methyltransferase [EC:2.1.1.13]
ko:K00548_metH, MTR; 5-methyltetrahydrofolate--homocysteine methyltransferase [EC:2.1.1.13]
ko:K02549_menC; O-succinylbenzoate synthase [EC:4.2.1.113]
ko:K11178_yagS; xanthine dehydrogenase YagS FAD-binding subunit [EC:1.17.1.4]
ko:K18068_pht3; phthalate 4,5-dioxygenase [EC:1.14.12.7]
ko:K18068_pht3; phthalate 4,5-dioxygenase [EC:1.14.12.7]
ko:K01077_E3.1.3.1, phoA, phoB; alkaline phosphatase [EC:3.1.3.1]
ko:K02297_cyoA; cytochrome o ubiquinol oxidase subunit II [EC:7.1.1.3]
ko:K02035_ABC.PE.S; peptide/nickel transport system substrate-binding protein
ko:K01271_pepQ; Xaa-Pro dipeptidase [EC:3.4.13.9]
ko:K00123_fdoG, fdhF, fdwA; formate dehydrogenase major subunit [EC:1.17.1.9]
ko:K03517_nadA; quinolinate synthase [EC:2.5.1.72]
ko:K01703_leuC, IPMI-L; 3-isopropylmalate/(R)-2-methylmalate dehydratase large subunit [EC:4.2.1.3
ko:K01703_leuC, IPMI-L; 3-isopropylmalate/(R)-2-methylmalate dehydratase large subunit [EC:4.2.1.3
ko:K01847_MUT; methylmalonyl-CoA mutase [EC:5.4.99.2]
ko:K00525_E1.17.4.1A, nrdA, nrdE; ribonucleoside-diphosphate reductase alpha chain [EC:1.17.4.1]
ko:K00525_E1.17.4.1A, nrdA, nrdE; ribonucleoside-diphosphate reductase alpha chain [EC:1.17.4.1]
ko:K00356_E1.6.99.3; NADH dehydrogenase [EC:1.6.99.3]
ko:K13069_E2.7.7.65; diguanylate cyclase [EC:2.7.7.65]
ko:K00341_nuoL; NADH-quinone oxidoreductase subunit L [EC:7.1.1.2]
ko:K00001_E1.1.1.1, adh; alcohol dehydrogenase [EC:1.1.1.1]
ko:K00001_E1.1.1.1, adh; alcohol dehydrogenase [EC:1.1.1.1]
ko:K03750_moeA; molybdopterin molybdotransferase [EC:2.10.1.1]
ko:K01856_catB; muconate cycloisomerase [EC:5.5.1.1]
ko:K00266_gltD; glutamate synthase (NADPH) small chain [EC:1.4.1.13]
ko:K01011_TST, MPST, sseA; thiosulfate/3-mercaptopyruvate sulfurtransferase [EC:2.8.1.1 2.8.1.2]
ko:K18030_nicB; nicotinate dehydrogenase subunit B [EC:1.17.2.1]
ko:K00696_E2.4.1.14; sucrose-phosphate synthase [EC:2.4.1.14]
ko:K01255_CARP, pepA; leucyl aminopeptidase [EC:3.4.11.1]
ko:K18910_dpe, lre; D-psicose/D-tagatose/L-ribulose 3-epimerase [EC:5.1.3.30 5.1.3.31]
ko:K18910_dpe, lre; D-psicose/D-tagatose/L-ribulose 3-epimerase [EC:5.1.3.30 5.1.3.31]
ko:K00228_CPOX, hemF; coproporphyrinogen III oxidase [EC:1.3.3.3]
ko:K00340_nuoK; NADH-quinone oxidoreductase subunit K [EC:7.1.1.2]
ko:K15760_tmoA, tbuA1, touA; toluene monooxygenase system protein A [EC:1.14.13.236 1.14.13.-]
ko:K01958_PC, pyc; pyruvate carboxylase [EC:6.4.1.1]
ko:K01958_PC, pyc; pyruvate carboxylase [EC:6.4.1.1]
ko:K01012_bioB; biotin synthase [EC:2.8.1.6]
ko:K00332_nuoC; NADH-quinone oxidoreductase subunit C [EC:7.1.1.2]
ko:K16877_hmfA; 2-furoyl-CoA dehydrogenase large subunit [EC:1.3.99.8]
ko:K00170_porB; pyruvate ferredoxin oxidoreductase beta subunit [EC:1.2.7.1]

ko:K05994_E3.4.11.10; bacterial leucyl aminopeptidase [EC:3.4.11.10]
ko:K08689_bphAa, bphA1, bphA; biphenyl 2,3-dioxygenase subunit alpha [EC:1.14.12.18]
ko:K01262_pepP; Xaa-Pro aminopeptidase [EC:3.4.11.9]
ko:K01262_pepP; Xaa-Pro aminopeptidase [EC:3.4.11.9]
ko:K01259_pip; proline iminopeptidase [EC:3.4.11.5]
ko:K10026_queE; 7-carboxy-7-deazaguanine synthase [EC:4.3.99.3]
ko:K00919_ispE; 4-diphosphocytidyl-2-C-methyl-D-erythritol kinase [EC:2.7.1.148]
ko:K00441_frhB; coenzyme F420 hydrogenase subunit beta [EC:1.12.98.1]
ko:K00441_frhB; coenzyme F420 hydrogenase subunit beta [EC:1.12.98.1]
ko:K03594_bfr; bacterioferritin [EC:1.16.3.1]
ko:K03594_bfr; bacterioferritin [EC:1.16.3.1]
ko:K01284_dcp; peptidyl-dipeptidase Dcp [EC:3.4.15.5]
ko:K02034_ABC.PE.P1; peptide/nickel transport system permease protein
ko:K05708_hcaE, hcaA1; 3-phenylpropionate/trans-cinnamate dioxygenase subunit alpha [EC:1.14.12
ko:K01623_ALDO; fructose-bisphosphate aldolase, class I [EC:4.1.2.13]
ko:K10824_nikE, cntF; nickel transport system ATP-binding protein [EC:3.6.3.24]
ko:K01489_cdd, CDA; cytidine deaminase [EC:3.5.4.5]
ko:K07560_dtd, DTD; D-aminoacyl-tRNA deacylase [EC:3.1.1.96]
ko:K02033_ABC.PE.P; peptide/nickel transport system permease protein
ko:K02258_COX11, ctaG; cytochrome c oxidase assembly protein subunit 11
ko:K01681_ACO, acnA; aconitate hydratase [EC:4.2.1.3]
ko:K11444_wspR; two-component system, chemotaxis family, response regulator WspR [EC:2.7.7.65]
ko:K01809_manA, MPI; mannose-6-phosphate isomerase [EC:5.3.1.8]
ko:K18430_legI, neuB2; N,N'-diacetyllegionaminate synthase [EC:2.5.1.101]
ko:K00343_nuoN; NADH-quinone oxidoreductase subunit N [EC:7.1.1.2]
ko:K00450_E1.13.11.4; gentisate 1,2-dioxygenase [EC:1.13.11.4]
ko:K00362_nirB; nitrite reductase (NADH) large subunit [EC:1.7.1.15]
ko:K16968_msmA; methanesulfonate monooxygenase subunit alpha [EC:1.14.13.111]
ko:K03639_moaA, CNX2; GTP 3',8-cyclase [EC:4.1.99.22]
ko:K01735_aroB; 3-dehydroquinate synthase [EC:4.2.3.4]
ko:K01430_ureA; urease subunit gamma [EC:3.5.1.5]
ko:K00475_F3H; naringenin 3-dioxygenase [EC:1.14.11.9]
ko:K04124_E1.14.11.15; gibberellin 3beta-dioxygenase [EC:1.14.11.15]
ko:K04125_E1.14.11.13; gibberellin 2beta-dioxygenase [EC:1.14.11.13]
ko:K05277_ANS; anthocyanidin synthase [EC:1.14.20.4]
ko:K05278_FLS; flavonol synthase [EC:1.14.20.6]
ko:K05282_E1.14.11.12; gibberellin-44 dioxygenase [EC:1.14.11.12]
ko:K05933_E1.14.17.4; aminocyclopropanecarboxylate oxidase [EC:1.14.17.4]
ko:K00337_nuoH; NADH-quinone oxidoreductase subunit H [EC:7.1.1.2]
ko:K00002_AKR1A1, adh; alcohol dehydrogenase (NADP+) [EC:1.1.1.2]
ko:K03644_lipA; lipoyl synthase [EC:2.8.1.8]
ko:K01467_ampC; beta-lactamase class C [EC:3.5.2.6]
ko:K00339_nuoJ; NADH-quinone oxidoreductase subunit J [EC:7.1.1.2]
ko:K00392_sir; sulfite reductase (ferredoxin) [EC:1.8.7.1]
ko:K00363_nirD; nitrite reductase (NADH) small subunit [EC:1.7.1.15]
ko:K00311_ETFDH; electron-transferring-flavoprotein dehydrogenase [EC:1.5.5.1]
ko:K07305_msrB; peptide-methionine (R)-S-oxide reductase [EC:1.8.4.12]
ko:K00370_narG, narZ, nxrA; nitrate reductase / nitrite oxidoreductase, alpha subunit [EC:1.7.5.1 1.7.
ko:K06941_rlmN; 23S rRNA (adenine2503-C2)-methyltransferase [EC:2.1.1.192]

ko:K01959_pycA; pyruvate carboxylase subunit A [EC:6.4.1.1]
ko:K01959_pycA; pyruvate carboxylase subunit A [EC:6.4.1.1]
ko:K11753_ribF; riboflavin kinase / FMN adenylyltransferase [EC:2.7.1.26 2.7.7.2]
ko:K11753_ribF; riboflavin kinase / FMN adenylyltransferase [EC:2.7.1.26 2.7.7.2]
ko:K15633_gpmI; 2,3-bisphosphoglycerate-independent phosphoglycerate mutase [EC:5.4.2.12]
ko:K15633_gpmI; 2,3-bisphosphoglycerate-independent phosphoglycerate mutase [EC:5.4.2.12]
ko:K00174_korA, oorA, oforA; 2-oxoglutarate/2-oxoacid ferredoxin oxidoreductase subunit alpha [EC
ko:K01256_pepN; aminopeptidase N [EC:3.4.11.2]
ko:K02032_ABC.PE.A1; peptide/nickel transport system ATP-binding protein
ko:K03335_iolE; inosose dehydratase [EC:4.2.1.44]
ko:K03335_iolE; inosose dehydratase [EC:4.2.1.44]
ko:K00371_narH, narY, nxrB; nitrate reductase / nitrite oxidoreductase, beta subunit [EC:1.7.5.1 1.7.9
ko:K00239_sdhA, frdA; succinate dehydrogenase / fumarate reductase, flavoprotein subunit [EC:1.3.5
ko:K00175_korB, oorB, oforB; 2-oxoglutarate/2-oxoacid ferredoxin oxidoreductase subunit beta [EC:1
ko:K02031_ABC.PE.A; peptide/nickel transport system ATP-binding protein
ko:K01770_ispF; 2-C-methyl-D-erythritol 2,4-cyclodiphosphate synthase [EC:4.6.1.12]
ko:K01624_FBA, fbaA; fructose-bisphosphate aldolase, class II [EC:4.1.2.13]
ko:K02495_hemN, hemZ; oxygen-independent coproporphyrinogen III oxidase [EC:1.3.98.3]
ko:K00169_porA; pyruvate ferredoxin oxidoreductase alpha subunit [EC:1.2.7.1]
ko:K00374_narI, narV; nitrate reductase gamma subunit [EC:1.7.5.1 1.7.99.-]
ko:K20455_acnD; 2-methylcitrate dehydratase (2-methyl-trans-aconitate forming) [EC:4.2.1.117]
ko:K00240_sdhB, frdB; succinate dehydrogenase / fumarate reductase, iron-sulfur subunit [EC:1.3.5.1
ko:K03781_katE, CAT, catB, srpA; catalase [EC:1.11.1.6]
ko:K01414_prlC; oligopeptidase A [EC:3.4.24.70]
ko:K17686_copA, ATP7; Cu+-exporting ATPase [EC:3.6.3.54]
ko:K17686_copA, ATP7; Cu+-exporting ATPase [EC:3.6.3.54]
ko:K16011_algA, xanB, rfbA, wbpW, pslB; mannose-1-phosphate guanylyltransferase / mannose-6-ph
ko:K08967_mtnD, mtnZ, ADI1; 1,2-dihydroxy-3-keto-5-methylthiopentene dioxygenase [EC:1.13.11.53
ko:K08967_mtnD, mtnZ, ADI1; 1,2-dihydroxy-3-keto-5-methylthiopentene dioxygenase [EC:1.13.11.53
ko:K00991_ispD; 2-C-methyl-D-erythritol 4-phosphate cytidylyltransferase [EC:2.7.7.60]
ko:K01823_idi, IDI; isopentenyl-diphosphate Delta-isomerase [EC:5.3.3.2]
ko:K03666_hfq; host factor-I protein
ko:K02276_coxC, ctaE; cytochrome c oxidase subunit III [EC:1.9.3.1]
ko:K00031_IDH1, IDH2, icd; isocitrate dehydrogenase [EC:1.1.1.42]
ko:K03711_fur, zur, furB; Fur family transcriptional regulator, ferric uptake regulator
ko:K09162_cld; chlorite dismutase [EC:1.13.11.49]
ko:K01960_pycB; pyruvate carboxylase subunit B [EC:6.4.1.1]
ko:K01960_pycB; pyruvate carboxylase subunit B [EC:6.4.1.1]
ko:K13481_xdhA; xanthine dehydrogenase small subunit [EC:1.17.1.4]
ko:K03684_rnd; ribonuclease D [EC:3.1.13.5]
ko:K03684_rnd; ribonuclease D [EC:3.1.13.5]
ko:K00524_nrdJ; ribonucleotide reductase, class II [EC:1.17.4.1]
ko:K00524_nrdJ; ribonucleotide reductase, class II [EC:1.17.4.1]
ko:K01476_E3.5.3.1, rocF, arg; arginase [EC:3.5.3.1]
ko:K13444_SUMF1, FGE; formylglycine-generating enzyme [EC:1.8.3.7]
ko:K01299_E3.4.17.19; carboxypeptidase Taq [EC:3.4.17.19]
ko:K12527_ygfK; putative selenate reductase [EC:1.97.1.9]
ko:K04047_dps; starvation-inducible DNA-binding protein
ko:K06167_phnP; phosphoribosyl 1,2-cyclic phosphate phosphodiesterase [EC:3.1.4.55]

ko:K06167_phnP; phosphoribosyl 1,2-cyclic phosphate phosphodiesterase [EC:3.1.4.55]
ko:K01113_phoD; alkaline phosphatase D [EC:3.1.3.1]
ko:K00284_GLU, gltS; glutamate synthase (ferredoxin) [EC:1.4.7.1]
ko:K01265_map; methionyl aminopeptidase [EC:3.4.11.18]
ko:K02535_lpxC; UDP-3-O-[3-hydroxymyristoyl] N-acetylglucosamine deacetylase [EC:3.5.1.108]
ko:K02275_coxB, ctaC; cytochrome c oxidase subunit II [EC:1.9.3.1]
ko:K15764_tmoE, tbuA2, touE; toluene monooxygenase system protein E [EC:1.14.13.236 1.14.13.-]
ko:K07043_K07043; uncharacterized protein
ko:K00449_pcaH; protocatechuate 3,4-dioxygenase, beta subunit [EC:1.13.11.3]
ko:K18912_egtB; gamma-glutamyl hercynylcysteine S-oxide synthase [EC:1.14.99.50]
ko:K03418_E3.5.1.56; N,N-dimethylformamidase [EC:3.5.1.56]
ko:K01114_plc; phospholipase C [EC:3.1.4.3]
ko:K01682_acnB; aconitate hydratase 2 / 2-methylisocitrate dehydratase [EC:4.2.1.3 4.2.1.99]
ko:K18028_nicX; 2,5-dihydroxypyridine 5,6-dioxygenase [EC:1.13.11.9]
ko:K03268_todC1, bedC1, tcbAa; benzene/toluene/chlorobenzene dioxygenase subunit alpha [EC:1.1
ko:K03268_todC1, bedC1, tcbAa; benzene/toluene/chlorobenzene dioxygenase subunit alpha [EC:1.1
ko:K14579_nahAc, ndoB, nbzAc, dntAc; naphthalene 1,2-dioxygenase subunit alpha [EC:1.14.12.12 1.
ko:K14579_nahAc, ndoB, nbzAc, dntAc; naphthalene 1,2-dioxygenase subunit alpha [EC:1.14.12.12 1.
ko:K07306_dmsA; anaerobic dimethyl sulfoxide reductase subunit A [EC:1.8.5.3]
ko:K17050_clrA, serA; complex iron-sulfur molybdoenzyme family reductase subunit alpha
ko:K14441_rimO; ribosomal protein S12 methylthiotransferase [EC:2.8.4.4]
ko:K02274_coxA, ctaD; cytochrome c oxidase subunit I [EC:1.9.3.1]
ko:K06168_miaB; tRNA-2-methylthio-N6-dimethylallyladenosine synthase [EC:2.8.4.3]
ko:K14977_ylbA, UGHY; (S)-ureidoglycine aminohydrolase [EC:3.5.3.26]
ko:K03147_thiC; phosphomethylpyrimidine synthase [EC:4.1.99.17]
ko:K00526_E1.17.4.1B, nrdB, nrdF; ribonucleoside-diphosphate reductase beta chain [EC:1.17.4.1]
ko:K00526_E1.17.4.1B, nrdB, nrdF; ribonucleoside-diphosphate reductase beta chain [EC:1.17.4.1]
ko:K04069_pflA, pflC, pflE; pyruvate formate lyase activating enzyme [EC:1.97.1.4]
ko:K15634_gpmB; probable phosphoglycerate mutase [EC:5.4.2.12]
ko:K15634_gpmB; probable phosphoglycerate mutase [EC:5.4.2.12]
ko:K17825_FTMF; verruculogen synthase [EC:1.14.11.38]
ko:K01462_PDF, def; peptide deformylase [EC:3.5.1.88]
ko:K05297_rubB, alkT; rubredoxin---NAD+ reductase [EC:1.18.1.1]
ko:K00348_nqrC; Na+-transporting NADH:ubiquinone oxidoreductase subunit C [EC:7.2.1.1]
ko:K07464_cas4; CRISPR-associated exonuclease Cas4 [EC:3.1.12.1]
ko:K04564_SOD2; superoxide dismutase, Fe-Mn family [EC:1.15.1.1]
ko:K04564_SOD2; superoxide dismutase, Fe-Mn family [EC:1.15.1.1]
ko:K13590_dgcB; diguanylate cyclase [EC:2.7.7.65]
ko:K01258_pepT; tripeptide aminopeptidase [EC:3.4.11.4]
ko:K00457_HPD, hppD; 4-hydroxyphenylpyruvate dioxygenase [EC:1.13.11.27]
ko:K00380_cysJ; sulfite reductase (NADPH) flavoprotein alpha-component [EC:1.8.1.2]
ko:K09825_perR; Fur family transcriptional regulator, peroxide stress response regulator
ko:K18029_nicA; nicotinate dehydrogenase subunit A [EC:1.17.2.1]
ko:K14051_gmr; c-di-GMP phosphodiesterase Gmr [EC:3.1.4.52]
ko:K02291_crtB; 15-cis-phytoene synthase [EC:2.5.1.32]
ko:K00455_hpaD, hpcB; 3,4-dihydroxyphenylacetate 2,3-dioxygenase [EC:1.13.11.15]
ko:K00351_nqrF; Na+-transporting NADH:ubiquinone oxidoreductase subunit F [EC:7.2.1.1]
ko:K16969_msmB; methanesulfonate monooxygenase subunit beta [EC:1.14.13.111]
ko:K00446_dmpB, xylE; catechol 2,3-dioxygenase [EC:1.13.11.2]

ko:K00368_nirK; nitrite reductase (NO-forming) [EC:1.7.2.1]
ko:K00368_nirK; nitrite reductase (NO-forming) [EC:1.7.2.1]
ko:K04098_chqB; hydroxyquinol 1,2-dioxygenase [EC:1.13.11.37]
ko:K01673_cynT, can; carbonic anhydrase [EC:4.2.1.1]
ko:K16845_suyA; (2R)-sulfolactate sulfo-lyase subunit alpha [EC:4.4.1.24]
ko:K15512_boxB; benzoyl-CoA 2,3-epoxidase subunit B [EC:1.14.13.208]
ko:K15512_boxB; benzoyl-CoA 2,3-epoxidase subunit B [EC:1.14.13.208]
ko:K00366_nirA; ferredoxin-nitrite reductase [EC:1.7.7.1]
ko:K18054_IDS3_2; 2'-deoxymugineic-acid 2'-dioxygenase / mugineic-acid 3-dioxygenase [EC:1.14.11.
ko:K01007_pps, ppsA; pyruvate, water dikinase [EC:2.7.9.2]
ko:K08641_vanX; zinc D-Ala-D-Ala dipeptidase [EC:3.4.13.22]
ko:K00504_PAM, PHM; peptidylglycine monooxygenase [EC:1.14.17.3]
ko:K03885_ndh; NADH dehydrogenase [EC:1.6.99.3]
ko:K17489_E2.1.3.1-12S; methylmalonyl-CoA carboxyltransferase 12S subunit [EC:2.1.3.1]
ko:K10944_pmoA-amoA; methane/ammonia monooxygenase subunit A [EC:1.14.18.3 1.14.99.39]
ko:K10944_pmoA-amoA; methane/ammonia monooxygenase subunit A [EC:1.14.18.3 1.14.99.39]
ko:K00801_FDFT1; farnesyl-diphosphate farnesyltransferase [EC:2.5.1.21]
ko:K00500_phhA, PAH; phenylalanine-4-hydroxylase [EC:1.14.16.1]
ko:K12267_msrAB; peptide methionine sulfoxide reductase msrA/msrB [EC:1.8.4.11 1.8.4.12]
ko:K12503_E2.5.1.68; short-chain Z-isoprenyl diphosphate synthase [EC:2.5.1.68]
ko:K01737_queD, ptpS, PTS; 6-pyruvoyltetrahydropterin/6-carboxytetrahydropterin synthase [EC:4.2.
ko:K03150_thiH; 2-iminoacetate synthase [EC:4.1.99.19]
ko:K18707_mtaB; threonylcarbamoyladenosine tRNA methylthiotransferase MtaB [EC:2.8.4.5]
ko:K18967_dge1; diguanylate cyclase [EC:2.7.7.65]
ko:K02488_pleD; two-component system, cell cycle response regulator [EC:2.7.7.65]
ko:K00349_nqrD; Na+-transporting NADH:ubiquinone oxidoreductase subunit D [EC:7.2.1.1]
ko:K00350_nqrE; Na+-transporting NADH:ubiquinone oxidoreductase subunit E [EC:7.2.1.1]
ko:K03738_aor; aldehyde:ferredoxin oxidoreductase [EC:1.2.7.5]
ko:K05550_benB-xylY; benzoate/toluate 1,2-dioxygenase subunit beta [EC:1.14.12.10 1.14.12.-]
ko:K01752_E4.3.1.17, sdaA, sdaB, tdcG; L-serine dehydratase [EC:4.3.1.17]
ko:K01843_kamA; lysine 2,3-aminomutase [EC:5.4.3.2]
ko:K00508_E1.14.19.3; linoleoyl-CoA desaturase [EC:1.14.19.3]
ko:K00451_HGD, hmgA; homogentisate 1,2-dioxygenase [EC:1.13.11.5]
ko:K00404_ccoN; cytochrome c oxidase cbb3-type subunit I [EC:1.9.3.1]
ko:K00507_SCD, desC; stearoyl-CoA desaturase (Delta-9 desaturase) [EC:1.14.19.1]
ko:K00347_nqrB; Na+-transporting NADH:ubiquinone oxidoreductase subunit B [EC:7.2.1.1]
ko:K00346_nqrA; Na+-transporting NADH:ubiquinone oxidoreductase subunit A [EC:7.2.1.1]
ko:K15983_kshB; 3-ketosteroid 9alpha-monooxygenase subunit B [EC:1.14.15.30]
ko:K15983_kshB; 3-ketosteroid 9alpha-monooxygenase subunit B [EC:1.14.15.30]
ko:K05587_hoxF; bidirectional [NiFe] hydrogenase diaphorase subunit [EC:7.1.1.2]
ko:K18331_hndC; NADP-reducing hydrogenase subunit HndC [EC:1.12.1.3]
ko:K18331_hndC; NADP-reducing hydrogenase subunit HndC [EC:1.12.1.3]
ko:K18331_hndC; NADP-reducing hydrogenase subunit HndC [EC:1.12.1.3]
ko:K00469_MIOX; inositol oxygenase [EC:1.13.99.1]
ko:K11942_icmF; isobutyryl-CoA mutase [EC:5.4.99.13]
ko:K04072_adhE; acetaldehyde dehydrogenase / alcohol dehydrogenase [EC:1.2.1.10 1.1.1.1]
ko:K04072_adhE; acetaldehyde dehydrogenase / alcohol dehydrogenase [EC:1.2.1.10 1.1.1.1]
ko:K18365_bphI, xylK, nahM, tesG; 4-hydroxy-2-oxovalerate/4-hydroxy-2-oxohexanoate aldolase [EC:
ko:K14048_ureAB; urease subunit gamma/beta [EC:3.5.1.5]

ko:K02586_nifD; nitrogenase molybdenum-iron protein alpha chain [EC:1.18.6.1]
ko:K08660_CNDP2; cytosolic nonspecific dipeptidase [EC:3.4.13.18]
ko:K03735_eutB; ethanolamine ammonia-lyase large subunit [EC:4.3.1.7]
ko:K03780_ttdB; L(+)-tartrate dehydratase beta subunit [EC:4.2.1.32]
ko:K16363_lpxC-fabZ; UDP-3-O-[3-hydroxymyristoyl] N-acetylglucosamine deacetylase / 3-hydroxyacy
ko:K00518_sodN; nickel superoxide dismutase [EC:1.15.1.1]
ko:K00518_sodN; nickel superoxide dismutase [EC:1.15.1.1]
ko:K00505_TYR; tyrosinase [EC:1.14.18.1]
ko:K06201_cutC; copper homeostasis protein
ko:K00491_nos; nitric-oxide synthase, bacterial [EC:1.14.14.47]
ko:K05299_fdhA; formate dehydrogenase (NADP+) alpha subunit [EC:1.17.1.10]
ko:K07213_ATOX1, ATX1, copZ, golB; copper chaperone
ko:K19701_ywaD; aminopeptidase YwaD [EC:3.4.11.6 3.4.11.10]
ko:K04100_ligA; protocatechuate 4,5-dioxygenase, alpha chain [EC:1.13.11.8]
ko:K00452_HAAO; 3-hydroxyanthranilate 3,4-dioxygenase [EC:1.13.11.6]
ko:K01666_mhpE; 4-hydroxy 2-oxovalerate aldolase [EC:4.1.3.39]
ko:K03381_catA; catechol 1,2-dioxygenase [EC:1.13.11.1]
ko:K03831_mogA; molybdopterin adenylyltransferase [EC:2.7.7.75]
ko:K17838_oxa; beta-lactamase class D [EC:3.5.2.6]
ko:K00030_IDH3; isocitrate dehydrogenase (NAD+) [EC:1.1.1.41]
ko:K00456_CDO1; cysteine dioxygenase [EC:1.13.11.20]
ko:K00476_ASPH; aspartate beta-hydroxylase [EC:1.14.11.16]
ko:K00461_ALOX5; arachidonate 5-lipoxygenase [EC:1.13.11.34]
ko:K18793_blaOXA-23; beta-lactamase class D OXA-23 [EC:3.5.2.6]
ko:K18794_blaOXA-51; beta-lactamase class D OXA-51 [EC:3.5.2.6]
ko:K18973_blaOXA-50; beta-lactamase class D OXA-50 [EC:3.5.2.6]
ko:K18976_blaOXA-48; beta-lactamase class D OXA-48 [EC:3.5.2.6]
ko:K19212_blaOXA-63; beta-lactamase class D OXA-63 [EC:3.5.2.6]
ko:K19318_blaOXA-213; beta-lactamase class D OXA-213 [EC:3.5.2.6]
ko:K19321_blaOXA-214; beta-lactamase class D OXA-214 [EC:3.5.2.6]
ko:K15916_pgi-pmi; glucose/mannose-6-phosphate isomerase [EC:5.3.1.9 5.3.1.8]
ko:K11645_fbaB; fructose-bisphosphate aldolase, class I [EC:4.1.2.13]
ko:K00367_narB; ferredoxin-nitrate reductase [EC:1.7.7.2]
ko:K11991_tadA; tRNA(adenine34) deaminase [EC:3.5.4.33]
ko:K05577_ndhF; NAD(P)H-quinone oxidoreductase subunit 5 [EC:7.1.1.2]
ko:K15746_crtZ; beta-carotene 3-hydroxylase [EC:1.14.15.24]
ko:K07181_cdgJ; c-di-GMP phosphodiesterase [EC:3.1.4.52]
ko:K19215_blaACT_MIR; beta-lactamase class C ACT/MIR [EC:3.5.2.6]
ko:K13831_hps-phi; 3-hexulose-6-phosphate synthase / 6-phospho-3-hexuloisomerase [EC:4.1.2.43 5
ko:K02217_ftnA, ftn; ferritin [EC:1.16.3.2]
ko:K13624_CP; ceruloplasmin [EC:1.16.3.1]
ko:K02277_coxD, ctaF; cytochrome c oxidase subunit IV [EC:1.9.3.1]
ko:K15635_apgM; 2,3-bisphosphoglycerate-independent phosphoglycerate mutase [EC:5.4.2.12]
ko:K15635_apgM; 2,3-bisphosphoglycerate-independent phosphoglycerate mutase [EC:5.4.2.12]
ko:K01674_cah; carbonic anhydrase [EC:4.2.1.1]
ko:K10208_crtM; 4,4'-diapophytoene synthase [EC:2.5.1.96]
ko:K00474_TMLHE; trimethyllysine dioxygenase [EC:1.14.11.8]
ko:K01399_lasB; pseudolysin [EC:3.4.24.26]
ko:K21020_siaD; diguanylate cyclase [EC:2.7.7.65]

ko:K08604_hap, nprV; vibriolysin [EC:3.4.24.25]
ko:K01401_aur; aureolysin [EC:3.4.24.29]
ko:K08603_npr; thermolysin [EC:3.4.24.27]
ko:K14415_RTCB, rtcB; tRNA-splicing ligase RtcB (3'-phosphate/5'-hydroxy nucleic acid ligase) [EC:6.5.
ko:K03737_por, nifJ; pyruvate-ferredoxin/flavodoxin oxidoreductase [EC:1.2.7.1 1.2.7.-]
ko:K07752_CPD; carboxypeptidase D [EC:3.4.17.22]
ko:K08605_gelE; coccolysin [EC:3.4.24.30]
ko:K04561_norB; nitric oxide reductase subunit B [EC:1.7.2.5]
ko:K17836_penP; beta-lactamase class A [EC:3.5.2.6]
ko:K01400_nprE; bacillolysin [EC:3.4.24.28]
ko:K21024_bifA; c-di-GMP phosphodiesterase [EC:3.1.4.52]
ko:K01387_colA; microbial collagenase [EC:3.4.24.3]
ko:K05996_cpt; carboxypeptidase T [EC:3.4.17.18]
ko:K01818_fucI; L-fucose/D-arabinose isomerase [EC:5.3.1.25 5.3.1.3]
ko:K15059_amnB; 2-aminophenol/2-amino-5-chlorophenol 1,6-dioxygenase subunit beta [EC:1.13.11
ko:K04034_bchE; anaerobic magnesium-protoporphyrin IX monomethyl ester cyclase [EC:1.21.98.3]
ko:K15750_bphAb, bphA2, bphE; biphenyl 2,3-dioxygenase subunit beta [EC:1.14.12.18]
ko:K16268_todC2, bedC2, tcbAb; benzene/toluene/chlorobenzene dioxygenase subunit beta [EC:1.14
ko:K16268_todC2, bedC2, tcbAb; benzene/toluene/chlorobenzene dioxygenase subunit beta [EC:1.14
ko:K13243_dos; c-di-GMP-specific phosphodiesterase [EC:3.1.4.52]
ko:K00376_nosZ; nitrous-oxide reductase [EC:1.7.2.4]
ko:K01517_ADPRM; manganese-dependent ADP-ribose/CDP-alcohol diphosphatase [EC:3.6.1.13 3.6.1
ko:K01517_ADPRM; manganese-dependent ADP-ribose/CDP-alcohol diphosphatase [EC:3.6.1.13 3.6.1
ko:K11784_mqnC; cyclic dehypoxanthinyl futalosine synthase [EC:1.21.98.1]
ko:K00448_pcaG; protocatechuate 3,4-dioxygenase, alpha subunit [EC:1.13.11.3]
ko:K04114_bcrA, badF; benzoyl-CoA reductase subunit A [EC:1.3.7.8]
ko:K04114_bcrA, badF; benzoyl-CoA reductase subunit A [EC:1.3.7.8]
ko:K04115_bcrD, badG; benzoyl-CoA reductase subunit D [EC:1.3.7.8]
ko:K04115_bcrD, badG; benzoyl-CoA reductase subunit D [EC:1.3.7.8]
ko:K00473_PLOD1; procollagen-lysine,2-oxoglutarate 5-dioxygenase 1 [EC:1.14.11.4]
ko:K01569_oxdD; oxalate decarboxylase [EC:4.1.1.2]
ko:K13647_PLODN; procollagen-lysine,2-oxoglutarate 5-dioxygenase, invertebrate [EC:1.14.11.4]
ko:K04035_E1.14.13.81, acsF, chlE; magnesium-protoporphyrin IX monomethyl ester (oxidative) cycla
ko:K14735_HEPH; hephaestin [EC:1.16.3.1]
ko:K15862_ccoNO; cytochrome c oxidase cbb3-type subunit I/II [EC:1.9.3.1]
ko:K01264_APE3; aminopeptidase Y [EC:3.4.11.15]

padj (<0.05)	L2FC >1
*	>1
*	>1
*	>1
	>1
	>1
	>1
	>1
	>1

se [EC:2.7.7.60 4.6.1.12]

>1
>1
>1
>1
>1
>1
>1

	>1
	>1
	>1
	>1
	>1
*	>1
*	>1
*	>1
*	>1
	>1
	>1
	>1
	>1
	>1
	>1
	>1
*	>1
	>1
*	>1
*	>1
*	>1
*	>1
*	>1
*	>1
*	>1
*	>1
*	>1
	>1
*	>1
	>1
*	>1
*	>1
*	>1
	>1
*	>1
	>1
*	>1
	>1
*	>1
*	>1
*	>1
*	>1
	>1
*	>1
*	>1
*	>1
*	>1
*	>1
	>1
*	>1

*	>1
	>1
*	>1
*	>1
*	>1
*	>1
*	>1
*	>1
*	>1
*	>1
*	>1
*	>1
*	>1
	>1
*	>1
*	>1
*	>1
*	>1
*	>1
*	>1
*	>1
	>1
*	>1
*	>1
*	>1
*	>1
*	>1
*	>1
*	>1
*	>1
	>1
	>1
	>1
	>1
	>1
	>1
	>1
	>1
	>1
*	>1
*	>1
*	>1
*	>1
*	>1
*	>1
*	>1
*	>1
*	>1
*	>1
*	>1

*	>1
*	>1
*	>1
*	>1
*	>1
*	>1
*	>1
*	>1
*	>1
*	>1
*	>1
*	>1
*	>1
*	>1
*	>1
*	>1
*	>1
*	>1
*	>1
*	>1
*	>1
*	>1
*	>1
*	>1
*	>1
*	>1
*	>1
*	>1
*	>1
*	>1
*	>1
*	>1
*	>1
*	>1
*	>1
*	>1
*	>1
*	>1
*	>1
*	>1
*	>1
	>1
	>1
*	>1
*	>1
*	>1
*	>1
*	>1
*	>1

*	>1
*	>1
*	>1
*	>1
*	>1
*	>1
*	>1
*	>1
*	>1
*	>1
*	>1
*	>1
*	>1
*	>1
*	>1
*	>1
*	>1
*	>1
*	>1
*	>1
*	>1
*	>1
*	>1
*	>1
*	>1
*	>1
*	>1
*	>1
*	>1
*	>1
*	>1
*	>1
*	>1
*	>1
*	>1
*	>1
*	>1
*	>1
*	>1
*	>1
*	>1
*	>1
*	>1
*	>1
*	>1
*	>1
*	>1
*	>1
*	>1

*	>1
*	>1
*	>1
*	>1
	>1
*	>1
*	>1
	>1
	>1
*	>1
*	>1
*	>1
*	>1
*	>1
*	>1
*	>1
*	>1
*	>1
*	>1
*	>1
*	>1
*	>1
*	>1
*	>1
*	>1
*	>1
*	>1
*	>1
*	>1
*	>1
*	>1
*	>1
*	>1
*	>1
*	>1
*	>1
*	>1
*	>1
*	>1
*	>1
*	>1
*	>1
*	>1
	>1
*	>1
*	>1
*	>1
*	>1
	>1

*	>1
*	>1
*	>1
	>1
*	>1
*	>1
*	>1
*	>1
*	>1
*	>1
*	>1
*	>1
*	>1
	>1
*	>1
*	>1
*	>1
*	>1
*	>1
*	>1
*	>1
*	>1
	>1
*	>1
*	>1
*	>1
*	>1
*	>1
*	>1
*	>1
*	>1
*	>1
*	>1
	>1
*	>1
*	>1
*	>1
*	>1
*	>1
*	>1
*	>1
*	>1
*	>1
*	>1
	>1
*	>1
*	>1
	>1

*	>1
*	>1
*	>1
*	>1
*	>1
*	>1
*	>1
*	>1
*	>1
*	>1
	>1
*	>1
*	>1
*	>1
*	>1
*	>1
*	>1
*	>1
*	>1
*	>1
*	>1
*	>1
*	>1
*	>1
*	>1
*	>1
*	>1
*	>1
*	>1
*	>1
*	>1
	>1
*	>1
*	>1
*	>1
*	>1

2nd revised version

Homeostasis drives intense microbial trace metal processing on marine particles

Pavla Debeljak [1,2]†, Stéphane Blain [1], Andrew Bowie [3,4], Pier van der Merwe [4,5], Barbara Bayer[2]§, and Ingrid Obernosterer [1*]

[1]Sorbonne Université, CNRS, Laboratoire d'Océanographie Microbienne, LOMIC, F-66650 Banyuls/mer, France

[2]University of Vienna, Department of Functional and Evolutionary Ecology, A-1090 Vienna, Austria

[3]Antarctic Climate and Ecosystem Co-operative Research Centre, University of Tasmania, 20 Castray Esp. Battery Point, Tasmania, Australia, 7004

[4] Institute of Marine and Antarctic Studies, University of Tasmania, 20 Castray Esp., Battery Point, Tasmania, Australia, 7004

[5] Antarctic Gateway Partnership, University of Tasmania, 20 Castray Esp. Battery Point, Tasmania, Australia, 7004

† present address: Institut de Systématique, Évolution, Biodiversité (ISYEB), Muséum National d'Histoire Naturelle, CNRS, Sorbonne Université UMR7205, BC 50 – RdC, France

§ present address: University of California, Santa Barbara, Department of Ecology, Evolution and Marine Biology, Santa Barbara, CA 93106-9620, USA

* Ingrid Obernosterer

Email: ingrid.obernosterer@obs-banyuls.fr

Keywords: trace metals, particles, metal bioavailability, metal homeostasis, marine microbes

Running head: Microbial homeostasis and particulate metals

Abstract

As marine microorganisms and environmental conditions co-evolved over geological timescales, metals have been incorporated into all essential metabolic processes. In the modern ocean, metals are present from trace amounts limiting microbial growth to toxic concentrations. Dissolved trace metals are a major bioavailable reservoir. However, the acquisition of metals from marine particles remains largely unexplored. Here, we combined chemical characterization and a comparative metatranscriptomics approach to investigate the availability of nine metals of biological importance on particles collected in the region of Heard Island (Indian sector of the Southern Ocean). Elemental ratios identified particulate matter as a potential source of metals for prokaryotes. The expression of genes for the uptake of metals through various mechanisms demonstrated that particles are a bioavailable reservoir. But genes involved in the control of resistance to metal toxicity, storage, sensing and regulation were also highly expressed. Our observations suggest that homeostasis associated with a diverse prokaryotic community is the overarching mechanism that enhances the trace element processing on particles. These results provide clues that microbial activity on particles is critical in the redistribution of trace elements between different fractions and chemical forms in the ocean.

Introduction

Among the 20 chemical elements that are essential for life, half of them, iron (Fe), manganese (Mn), cobalt (Co), nickel (Ni), copper (Cu), zinc (Zn), cadmium (Cd), molybdenum (Mo), vanadium (V), and tungsten (W) are metals (Williams and Fraústo Da Silva 2003; Wackett et al. 2004). Metalloproteins, requiring metals as cofactors, account for one third of all proteins (Wackett et al. 2004). Free metal ions are part of the metallome and the concentration of a given metal in the cytoplasm is markedly constant among cells, but it varies by several orders of magnitudes when different elements are considered (Williams and Fraústo Da Silva 2003). This results from the co-evolution of microorganisms and environmental conditions (Silva and Williams 2001; Saito et al. 2003).

In the modern ocean, microorganisms face the challenge of acquiring enough metals to sustain their metabolic demand. The most striking case is Fe for which the low availability limits present microbial activity in large oceanic regions (Martin et al. 1992; Tagliabue et al. 2017). Moreover, once a metal has entered the cell, it is critical that it integrates to the right protein to form an active enzyme (Waldron and Robinson 2009). Because metal affinities of proteins tend to follow the Irving-Williams series (Irving and Williams 1948), populating a protein with a metal with low affinity (e.g. Fe, Mn) in the presence of others with higher affinity (e.g. Cu, Zn) requires elaborate strategies involving sensors, transporters and stores. Therefore, metal homeostasis is critical for the survival of cells (Andrews et al. 2003; Waldron and Robinson 2009; Chandrangsu et al. 2017) and drives an intense trafficking of metals inside the cell and between the cell and its micro-scale environment.

The main reservoir of metals in the ocean is the operationally defined dissolved pool, which contains chemical species with a size (< 200 nm) compatible with the physical transport capabilities of membrane proteins. Such transport modes include uptake of ions via divalent ion transporters (Andrews et al. 2003), reductive-oxidative pathways (Strzepek et al. 2011; Lis et al. 2015), endocytosis after concentration of metals at the cell surface (McQuaid et al. 2018), uptake of colloids (Rich and Morel 1990) or uptake of organic complexes via specific transporters for heme (Hogle et al. 2017) or siderophores (Sandy and Butler 2009). Particles (> 200 nm) contain metals that can quantitatively equal or exceed the dissolved pool as is the case for Fe (Boyd and Ellwood 2010; van der Merwe et al. 2019), and thus represent a potential source. Rendering particulate metals accessible for microorganisms requires, however, preliminary transformations.

The determination of the bioavailability of metals is challenging, as not all the chemical forms are equally available to microorganisms. This is well illustrated in the case of Fe, for which a careful definition and determination of the bioavailability in the dissolved form has been proposed (Shaked and Lis 2012). However, for other trace metals and notably for their particulate forms the bioavailability is still poorly constrained. To address this issue, different approaches were proposed with a focus on Fe. The geochemical perspective relies on leaching protocols that sequentially separate different fractions (Rauschenberg and Twining 2015). A more biologically oriented approach consists in following changes in the chemical composition and the microbial activity during incubations. For example, the release of Fe-binding ligands coupled with an increase in dissolved Fe was observed in incubations amended with particles (Boyd et al. 2010; Velasquez et al. 2016). A third perspective is to investigate the metabolic response of microbial cells in the presence of particles. The expression of microbial Fe transporters in the vicinity of a hydrothermal plume suggested Fe of hydrothermal origin to be bioavailable to prokaryotes (Li et al. 2014). Moreover, biologically mediated dissolution of particles has been observed during their

transit through the gut of protozoans (Barbeau et al. 1996) and assisted dissolution by siderophores of bacterial origin has also been demonstrated (Rubin et al. 2011).

The patchiness within marine particles likely renders trace element distribution and dynamics distinct from those occurring in surrounding seawater. Microbial communities inhabiting particles encounter and shape concentration gradients of various elements, including trace metals, at the micrometer scale (Azam and Malfatti 2007; Stocker et al. 2008). How diverse microbial taxa deal with these multiple challenges, such as the access to various chemical forms of metals, handling metal excess and toxicity, and how in turn they shape element composition are unanswered questions. By combining chemical characterization of marine particles and the 'metallo'-metatranscriptome of a diverse prokaryotic community, we provide here a novel view on the microbial processing of trace metals on marine particles. We show enhanced transport into and out of the cell, sensing and regulation of nine metals of biological importance, carried out by a diverse microbial community inhabiting this reservoir of trace elements in the ocean.

Materials and Methods

Collection and chemical characterization of *in situ* particulate matter

The present study was carried out during the Heard Earth-Ocean-Biosphere Interactions (HEOBI) cruise (8 January - 27 February 2016) aboard the Australian R/V *Investigator* (voyage: IN 2016-V01). For the determination of the metal to phosphorus ratios, suspended particles were collected at 8 sites in the vicinity of Heard and McDonald Island and in High-Nutrient-Low-Chlorophyll (HNLC) waters in the Indian Sector of the Southern Ocean (Fig. S1)(van der Merwe et al. 2019). For the incubation experiment, particles were collected on January 29th 2016 in shallow waters

(overall depth 210 m) in the vicinity of McDonald Island (53.03 S, 72.55 E) (Fig. S1) at 100 m. All samples were collected by McLane high volume *in-situ* pumps (WTS-LV) fitted with dual filter holders and high efficiency baffles to reduce sample wash off upon retrieval. Sample handling, collection and processing were performed in accordance with the GEOTRACES 'Cookbook' protocols (https://www.geotraces.org/methods-cookbook/). Suspended particles for the incubations and the trace metal analysis were collected using paired, acid washed, 142 mm, 0.8 µm Supor filters to obtain a 0.4 µm effective pore size. The paired filters were then subsampled into 47 mm diameter punches. For the experimental incubation (see below), concentrated particle suspensions were prepared by rinsing off particles from 2 filter punches with each 20 mL of 0.2 µm-filtered seawater per filter, collected following trace-metal clean protocols. The remaining punches served for chemical analyses of the particulate matter. A chemical leach was used to separate the chemically refractory trace metal component of marine suspended particles from the chemically labile fraction (van der Merwe et al. 2019). Both fractions were analyzed by HR-ICP-MS (Thermo-Fisher Element 2) (Bowie et al. 2010). In the present study we only considered the sum of both fractions.

Incubation experiments with prokaryotic communities and particles

To investigate prokaryotic activity and gene expression patterns on marine particles, on-board incubation experiments were performed. Batch cultures, containing the ambient prokaryotic community (< 0.8 µm size fraction) and 0.2 µm-filtered seawater in a ratio of 1:10 (final volume 2L), were amended with particles and incubated for 12 days. Particles were collected at 100 m in the vicinity of McDonald Island (Fig. S1) as described above. Seawater for the < 0.2 µm- and < 0.8 µm-size fractions was collected in HNLC waters south of Heard Island (54.17 S, 73.67 E) at 45 m depth (Fig. S1), using trace-metal clean procedures. The filtrations were performed with

polycarbonate (PC, Nuclepore, 47 mmm) filters treated with a mild HCl-wash (0.1 N) and several rinses with Milli-Q water. Particles were added to the cultures from the suspension described above (6.5 mL of suspension to 2L of batch culture). Batch cultures without particle addition served as controls. Five replicate particle-amended cultures were prepared and the control incubations were done in quadruplicates. To keep the particles in suspension, we used gentle magnetic stirring. The cultures were kept in PC carboys, in the dark in a temperature-controlled incubator at 8°C. All steps of the preparation of the cultures were done under a trace-metal clean laminar flow hood (ISO class 5).

During the 12d incubation period, the cultures were subsampled every 2-3 days for prokaryotic abundance and heterotrophic production, and the particle size distribution and enumeration of prokaryotes attached to individual particles was carried out at the beginning and the end of the incubation. Samples for metatranscriptomics and prokaryotic community composition were collected at the final time point of the incubation. For the differential expression analysis (see below), the metatranscriptomes of the prokaryotic community attached to particles (> 0.8 µm fraction in the particle-amended treatment) were compared to those obtained from prokaryotes in the < 0.8 µm fraction of the control, considered as bulk community in particle-free HNLC water.

Determination of particle size distribution and enumeration of heterotrophic prokaryotes

For microscopic observations of the particles and the enumeration of particle-attached cells (Fig. S2), 20 mL subsamples of the batch cultures were filtered onto 0.8 µm PC filters (Nuclepore, 25 mm), and the filters were placed on pads (Millipore) soaked with 5% paraformaldehyde (PFA) overnight at 4°C. The filters were then rinsed with 0.2 µm filtered Milli-Q water and dried prior to storage in petri dishes at -20°C. Back in the home laboratory, each filter was split into 6 pieces,

and stained with DAPI for microscopic observations using an Olympus AX70 epifluorescence microscope equipped with an image analyses system (Cottrell and Kirchman 2000). For each observation, two images were acquired. One image was obtained by bright-field microscopy, and another image using excitation with blue light. The images were then processed with the open platform scientific image analysis software Image J. The image obtained by excitation with blue light was used to count by eye the cells attached to the different particles. The image obtained from bright-field microscopy was split into three channels (green, blue and red) in Image J. The red image presented the best characteristics (brightness, contrast) for the determination of the surface area of the particles. The particles were contoured and the surface determined after calibration of the pixel size. For each replicate, at least 100 particles were observed on different randomly selected parts of the filter. For each particle, the surface area and the number of attached prokaryotic cells were recorded to estimate the size distribution of the particles and the areal cell abundance. Prokaryotic abundance of the bulk community and in the < 0.8 µm fraction were enumerated by flow cytometry. Subsamples (1.8 mL) were fixed with glutaraldehyde (1% final concentration), incubated for 30min at 4°C and stored at -80°C. Cells were stained with SYBRGreen I and enumerated on a BD FACS Canto flow cytometer equipped with an air-cooled laser, providing 15mW at 488 nm with the standard filter set-up as described previously (Obernosterer et al. 2008).

Prokaryotic heterotrophic production

Prokaryotic production was estimated by ^{3}H leucine incorporation applying the centrifugation method, with minor modifications (Obernosterer et al. 2008). Prokaryotic production was determined for the bulk community (unfiltered water from the batch cultures) and in the < 0.8 µm size fraction, the latter considered as free-living community. The difference in prokaryotic

heterotrophic production between these fractions was considered as particle-attached production. Prior to the incubation with leucine, subsamples of each culture were filtered through a 0.8 µm PC filter (Nuclepore, 25 mm diameter) that was treated with a mild HCl-wash (0.1 N) and several rinses with Milli-Q water. Briefly, 1.5 mL samples were incubated with a mixture of [3,4,5-^{3}H(N)] leucine (Perkin Elmer, 123.8 Ci mmol^{-1}; 7 nM final concentration) and nonradioactive leucine (13 nM final concentration). Controls were fixed with trichloroacetic acid (TCA; Sigma) at a final concentration of 5%. Samples were incubated for 2-3h in the dark. Incubations were terminated with TCA (5% final concentration). The radioactivity incorporated into prokaryotic cells was measured aboard in a HIDEX 300 SL liquid scintillation counter.

Sampling for metatranscriptomics and prokaryotic diversity

At the final time point of the experiment, 500 mL of each of three replicate cultures were sequentially filtered on 0.8 µm and 0.2 µm PC filters (Nuclepore, 47 mm), and the filters were stored at -80°C until further analysis. For metatranscriptomics and prokaryotic community composition, two separate filters for each biological replicate were used for the extraction of RNA (metatransriptomic analysis) and DNA (amplicon sequencing). Methods for nucleic acid extraction and amplicon sequencing used to describe prokaryotic community composition are provided in Supplementary Materials.

RNA Extraction with customized standards

RNA was extracted according to a previously published protocol (Angel et al. 2012) with the following modifications for the use of filters. Tubes containing the filters (2ml Eppendorf tubes)

206 were submerged in liquid nitrogen and the filters were ground into small pieces with a sterile
207 metal spatula. To each sample, 750 µL phosphate buffer (120 mM, pH 5.5) and 250 µL TNS
208 buffer (500 mM Tris base, 100 mM NaCl, 10% SDS), and customized RNA standards
209 (Supplementary Materials) were added to the filter pieces, and cells were lysed with 5x freeze and
210 thaw cycles. After centrifuging at 20 000 x g at 4°C for 3 min, the supernatant was added to a
211 fresh tube and one volume of TE saturated phenol (pH 5.5) was added. RNA was purified using
212 standard phenol/chloroform/isoamyl alcohol and chloroform/isoamyl alcohol purification, and the
213 supernatant was transferred to non-stick RNase-free microfuge tubes (Eppendorf). Nucleic acids
214 were precipitated with 30% polyethylene glycol (PEG) in 1.6 M NaCl and 2 µL glycogen
215 (Thermo Scientific), washed once with ice-cold 75% EtOH and resuspended in low TE buffer.
216 DNA was digested with TURBO DNase (Ambion) and purified using the RNeasy MinElute
217 Cleanup Kit (Qiagen). Complete DNA removal was validated via PCR amplification of 30 cycles
218 and quality of RNA was checked with Bioanalyzer RNA chip profiles (Agilent Technologies,
219 Santa Clara, CA, USA). The Ribo-Zero Gold rRNA Removal Kit (Epidemiology) was used to
220 remove cytoplasmic and mitochondrial ribosomal RNA and sequencing was performed in pair-
221 end using HiSeq (3000/4000) Illumina 2 × 150 bp chemistry on one full Illumina lane by Fasteris
222 SA. Raw sequencing reads were deposited at the European Nucleotide Archive under Project
223 number PRJEB38529.

224

225 **Metatranscriptome read processing, assembly and annotation**

226 The metatranscriptome shotgun libraries were prepared using a strand-specific protocol. An initial
227 round of read processing was provided by the company, using trimmomatic (Bolger et al. 2014),
228 an integrated quality-control tool for high-throughput Illumina NGS data. The standard Illumina
229 adapters and low-quality bases were removed with the following parameters “2:30:10

SLIDINGWINDOW:4:5", and reads without inserts or reads for which ambiguities were found were also removed, resulting in 92 - 97% of 2×150 bp paired-end reads (average 24.5 ± 4.5 Mio reads per sample). Further, we performed another round of quality control and refinement with Trim Galore v0.5.0 (https://www.bioinformatics.babraham.ac.uk/projects/trim_galore/) for automatic detection and removal of overrepresented adapters, using a phred score of 20 and a length cutoff of 50 bp. To focus on protein-coding RNAs, we computationally eliminated ribosomal RNAs and internal standards-derived reads using SortMeRNA v 2.1b (Kopylova et al. 2012). A BLASTN homology search (Altschul et al. 1990) against a custom database which consisted of representative prokaryotic rRNAs and tRNAs from NCBI RefSeq along with the template sequences of customized internal RNA standards, was also implemented using a bit score cut-off of 50 as suggested in previous studies (Satinsky et al. 2013).

Given that the same ambient prokaryotic community was used as an inoculum for all incubations, and prokaryotic genes rarely have introns, the reads from all samples were pooled together and used for co-assembly using MegaHit v1.2.7 (Li et al. 2015) with default parameters. The assembly yielded 819,328 contigs with an N50 of 577 bp. Contigs shorter than 300 bp were discarded from further analysis, and 732,369 contigs were retained. Genes were predicted using Prodigal v2.6.3(Hyatt et al. 2010). The resulting amino acid sequences (>100 aa) were taxonomically annotated by DIAMOND BLASTP against nr database (January 2019) with options "--more-sensitive -e 0.000001 -f 100 -k 1 -p 10" (Buchfink et al. 2015), and functionally annotated using eggNOG 5.0 (Huerta-Cepas et al. 2019) and GhostKOALA (Kanehisa et al. 2016b) with default parameters. The taxonomic affiliation resulted in 66% prokaryotic, 9% eukaryotic, 8% unassigned and 17% unaligned contigs. A total of 420,218 prokaryotic protein sequences were finally retrieved, among which 65 % could be assigned to KEGG orthologous (KO) groups (Kanehisa et al. 2016a).

254

255 **Gene differential expression and functional enrichment analyses**

256 Reads were mapped back to the assembled contigs using Bowtie2 (Langmead and Salzberg 2012)
257 with default parameters, resulting in an overall 54.3% recruitment rate. Reads that were aligned to
258 the selected prokaryotic gene features were counted using featureCounts
259 (http://bioinf.wehi.edu.au/featureCounts/) with the following parameters for strand specific reads
260 -F 'GTF' -t 'gene' -Q 1 -s2 -p -C (Liao et al. 2014). The R package DESeq2 (Love et al. 2014) was
261 used to perform differential expression analysis based on the count table generated by
262 'featureCounts'. One control sample had to be excluded from the further analysis as it was
263 significantly different from the triplicate set recruiting less reads than all other samples (DESeq
264 function Cooks distance). Differential expression analysis was thus calculated with a duplicate set
265 of control samples. We have used the Likelihood Ratio Test (LRT) as implemented in the
266 DESeq2 software (Love et al. 2014) to screen each gene for significant differences in normalized
267 transcript abundance between treatments (fitType: local). After adjusting for multiple testing, an
268 adjusted p-value of < 0.05 was used as threshold. The raw count data were summed by KO
269 numbers and normalized based on the count data of the internal standards by applying the
270 'controlGenes' option of the DESeq2 software to statistically test the dynamics of absolute
271 transcriptional activity as published elsewhere (Beier et al. 2018). A further normalization step
272 was performed in order to account for differences in the average feature length of each gene in
273 each sample using the 'normMatrix' option. Transcripts with a total count of less than 50 were
274 removed. Total transcripts per sample were calculated by multiplying reads of protein encoding
275 transcripts of the transcriptome library with the number of molecules of the internal standard
276 added to the samples; this value was then divided by the recovered reads of the internal standard
277 in the sequence library (Satinsky et al. 2013) as described in the Supplementary Materials.

278

279 **Metal-related transcript analysis**

280 KO numbers of metal related enzymes were retrieved by co-factor function on the bioinformatics
281 resource portal ExPASy (https://enzyme.expasy.org/enzyme-bycofactor.html). We note that this
282 co-factor function also retrieves metal transporters that are not enzymes with metals as co-factors.
283 We performed this analysis for Co^{2+}, Cob(II)alamin, cobalt cation, Cu cation, Cu^{2+}, Fe cation,
284 Fe^{2+}, Fe^{3+}, Ferriheme b, Fe-sulfur, Mo cation, Mn^{2+}, Ni^{2+}, Zn^{2+}, Cd and W. Transcripts annotated
285 for the specific KEGG were summed by treatment and relative transcript abundance was
286 calculated for taxa associated per KEGG and visualized in the R ComplexHeatmap package
287 (https://jokergoo.github.io/ComplexHeatmap-reference/book/)(Gu et al. 2016). Phylogenetic
288 groups were visualised on the family or lowest possible taxonomic level.

289

290 **Results**

291

292 Chemical analysis of the bulk particulate material collected at 8 sites in the region of Heard Island
293 (Indian sector of the Southern Ocean; Fig. S1) revealed that the ratios of Mo, Co, Cu, Ni, Zn, Mn
294 and Fe to phosphorus are in the range of or above those reported in the literature for heterotrophic
295 prokaryotes (Fig. 1a), identifying particulate matter as a potential source of these metals. The
296 particles used in the incubation experiment were sampled in the vicinity of the volcanic
297 McDonald island at 100m depth (53.03 S, 72.55 E; Fig. S1). We used microscopic observations
298 (Fig. S2) to characterize the particle surface area distribution in the range 25 to 1000 μm^2. The
299 abundance of particles decreased with surface area (Fig. 1b), while heterotrophic prokaryotes
300 determined on individual particles had an opposite trend (Fig. 1c), resulting in an overall constant
301 cell abundance per unit (μm^2) of surface area (Fig. 1d).

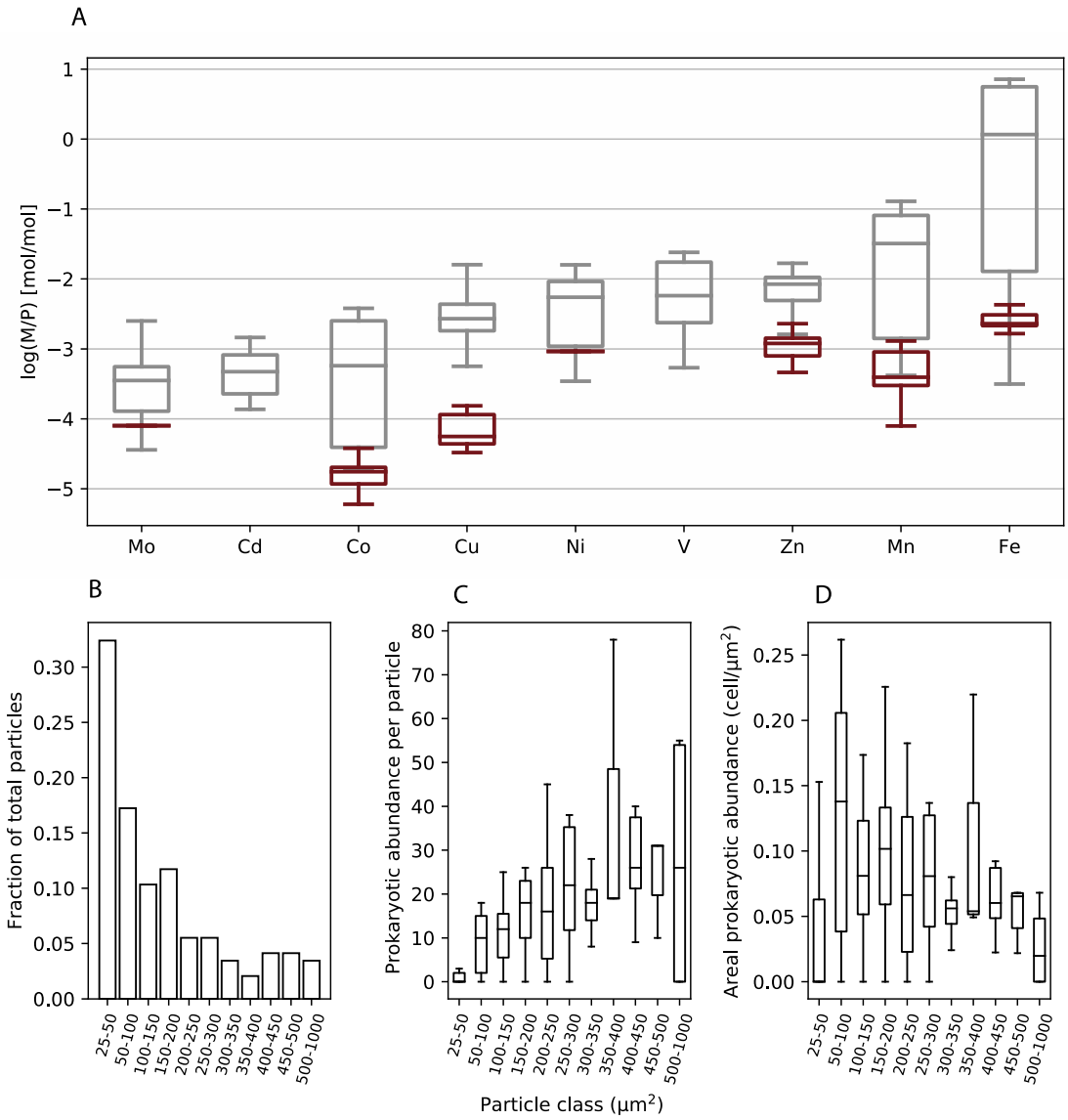

302 **Figure 1.** Particle characterization

303 Comparison of the metal to phosphorus ratios (mol/mol) between bulk marine particulate matter
304 and heterotrophic prokaryotes (a). Grey boxplots represent mean, first and third quartiles for total
305 trace metals in particles collected during the HEOBI cruise at 8 sites in the Indian Sector of the
306 Southern Ocean (n=55). Maroon boxplots represent mean, first and third quartiles for the ratio
307 measured in cultures of 5 different strains of heterotrophic prokaryotes (n=16, except for Mo and

Ni where n=1; no data for Cd and V available)(Posacka 2017; Posacka et al. 2019; Mazzotta et al. 2020). Size class distribution of particles (b), prokaryotic cell abundance on individual particles (c) and cell abundance per surface area unit (d) in the incubation experiments. Observations are from the final time point.

To investigate microbial processes on the particles, we performed an onboard experiment. The presence of particles resulted in two distinct phases of the response of the ambient prokaryotic community (< 0.8 μm size fraction). During phase 1, extending over the first 4 days of incubation, the initially high cell-specific prokaryotic production, as determined by ^{3}H leucine incorporation, decreased by 4-fold to reach values equal to those in seawater to which no particles were added (Fig. S3). Phase 1 is considered a transient microbial response to leaching products, released by particles upon their initial re-suspension in low-trace-metal seawater. During the following 8 days of the incubation (day 4 to day 12), cell-specific prokaryotic production remained stable. This second phase is considered a quasi-steady state, and was the focus of our study, including the metatranscriptomic analysis.

The particles were colonized by *in situ* prokaryotic communities and areal cell abundances did not change between the initial and the final time points of the incubation (Fig. S4). Our microscopic observations allowed us to determine the volumetric abundance of cells attached to particles of $0.61\pm0.40 \times 10^{5}$ mL^{-1}. This compares to a bulk prokaryotic cell abundance of $2.65\pm0.2 \times 10^{5}$ mL^{-1} in the particle-free control incubations. Particle-attached cells were highly active throughout the incubation period (Fig. S5), and at the final time point, cell-specific production of prokaryotes attached to particles (4.43 ± 1.03 amol leucine cell^{-1} d^{-1}) exceeded that of prokaryotes in the particle-free control (0.30 ± 0.08 amol leucine cell^{-1} d^{-1}) by 15-fold.

331 The prokaryotic community composition determined at the end of the incubations revealed that
332 *Flavobacteriaceae*, *Rhodobacteraceae* and *Oceanospirillaceae* were abundant contributors (each
333 ≈15% relative abundance on average) to the communities attached to particles (Fig. S6), and
334 other observed families were *Halieaceae*, *Porticoccaceae*, *Moritellaceae*, *Planctomycetaceae* and
335 *Verrucomicrobiaceae*. *Flavobacteriaceae* were also abundant members of the community in the
336 control incubations (≈19-21 %) and relative abundances of *Rhodobacteraceae* (≈ 5 %) and
337 *Oceanospirillaceae* (≈ 4-6 %) were lower. The higher contributions of SAR11 (15-20%), SAR92
338 (7-14%) and the OM43 clade (12 %) were distinct features of the communities in particle-free
339 control incubations.

340 To explore trace metal-related microbial processes on marine particles, we compared the gene
341 expression profiles between prokaryotic communities attached to particles and communities in the
342 control incubations. We focused on transcripts of KEGG orthologous (KO) genes related to the
343 metals Zn, Mn, Cu, Co, Ni, Cd, Mo, W, and Fe (Table S1). Of the 1125 non-redundant KO genes
344 retrieved, 476 KO gene transcripts were identified in our metatranscriptomic data set of which
345 386 KO gene transcripts were enhanced (Log2fold change > 1) in the inventory of the particle-
346 attached community as compared to that of prokaryotes in particle-free incubations (Table S2).
347 We focus in the following on the KO gene transcripts involved in metal transport into and out of
348 the cell (efflux), sensing, regulation, resistance and storage of the nine metals. The numerous KO
349 gene transcripts identified had enhanced relative (Fig. 2; Fig. S7) and absolute transcript
350 abundances (Fig. S8) in the particle-attached community as compared to that in the particle-free
351 control incubations. These included transcripts for transporters of Fe^{2+}, Fe^{3+}, Zn, Mn, Ni, Cd, Mo
352 and W. Some of these transporters are weakly selective cation carriers that cannot be associated
353 to a single metal (e.g. Mn/Zn/Fe, *tro*, *mnt*, *znu*). Transporters of organically complexed Fe

(siderophore receptors, *fiu*, Fe^{3+} dicitrate transport, *fecA*, ferric hydroxamate transport, *fhuC*) were also enhanced on particles.

Figure 2. Enrichment of trace metal related gene transcripts in particle-associated prokaryotes

Fold changes of normalized transcript counts of KEGG orthologous genes in prokaryotic communities attached to particles as compared to those in particle-free incubations (given in Log2Fold). Significantly higher expressed transcripts (adjusted p-value <0.05) are indicated by an

asterisk (*) and genes potentially implicated in the transport of multiple metals are indicated by the letter M (for multiple). Genes that are part of an ABC transporter complex are highlighted by rectangular boxes.

Genes involved in efflux and resistance (Fe, *fie*, Co, Zn, Cd, *czc*, *cus, cnr*), regulation (Fe, *fur* and Zn, *zur*), sensing (two component system, Cu, *cop*) and storage (ferritin, *ftn*, bacterioferritin, *dps* and iron storage protein, *dps*) also revealed higher transcript abundances in the particle-attached transcript inventories as compared to those in the control. A large number of genes involved in the biosynthesis of various siderophores were detected and they revealed the highest increases (Log2fold changes of 2.5 to 10) among the metal related genes.

To determine which prokaryotic taxa were associated with the trace metal processing on particles, we assigned the taxonomy of the transcripts (Fig. 3; the taxonomic assignment in the control is provided in Fig. S9). *Rhodobacteraceae* (order *Rhodobacterales*) contributed to the transport, sensing and regulation of all 9 metals, while other prokaryotes had a reduced set of trace metal transcripts. Transport of Fe^{3+} (*afuA*, *B*, *C*) was mainly associated with *Rhodobacteraceae*, and that of Fe^{2+} (*feoB*, *efeU*) with *Porticoccaceae* (*Cellvibrionales*), *Moritellaceae* (*Alteromonadales*) and *Flavobacteriaceae (Flavobacteriales)*. *Planctomycetaceae* (*Planctomycetales*) were particularly associated with Zn/Cd (*zipB*) and Mo/W (*wtpC*) transport, *Halomonadaceae* (*Oceanospiralles*) with the transport of Zn and Mn (*ABC.ZM.S*), and *Deltaproteobacteria* (not assigned to the family level) to that of Ni (*ABC.PE.P*, *P1* and *ddpD*). Transcripts involved in Co/Zn/Cd efflux (*czc*, *cus*, *cnrA, B, C*) were associated with members of the *Porticoccaceae*, *Alteromonadacaea* and *Deltaproteobacteria*, whereas *Planctomycetaceae* were associated with Cu efflux (*gesA*, *mexP*). *Deltaproteobacteria* contributed to Zn/Fe regulation (*zur, fur*) and transcripts for Cu regulation

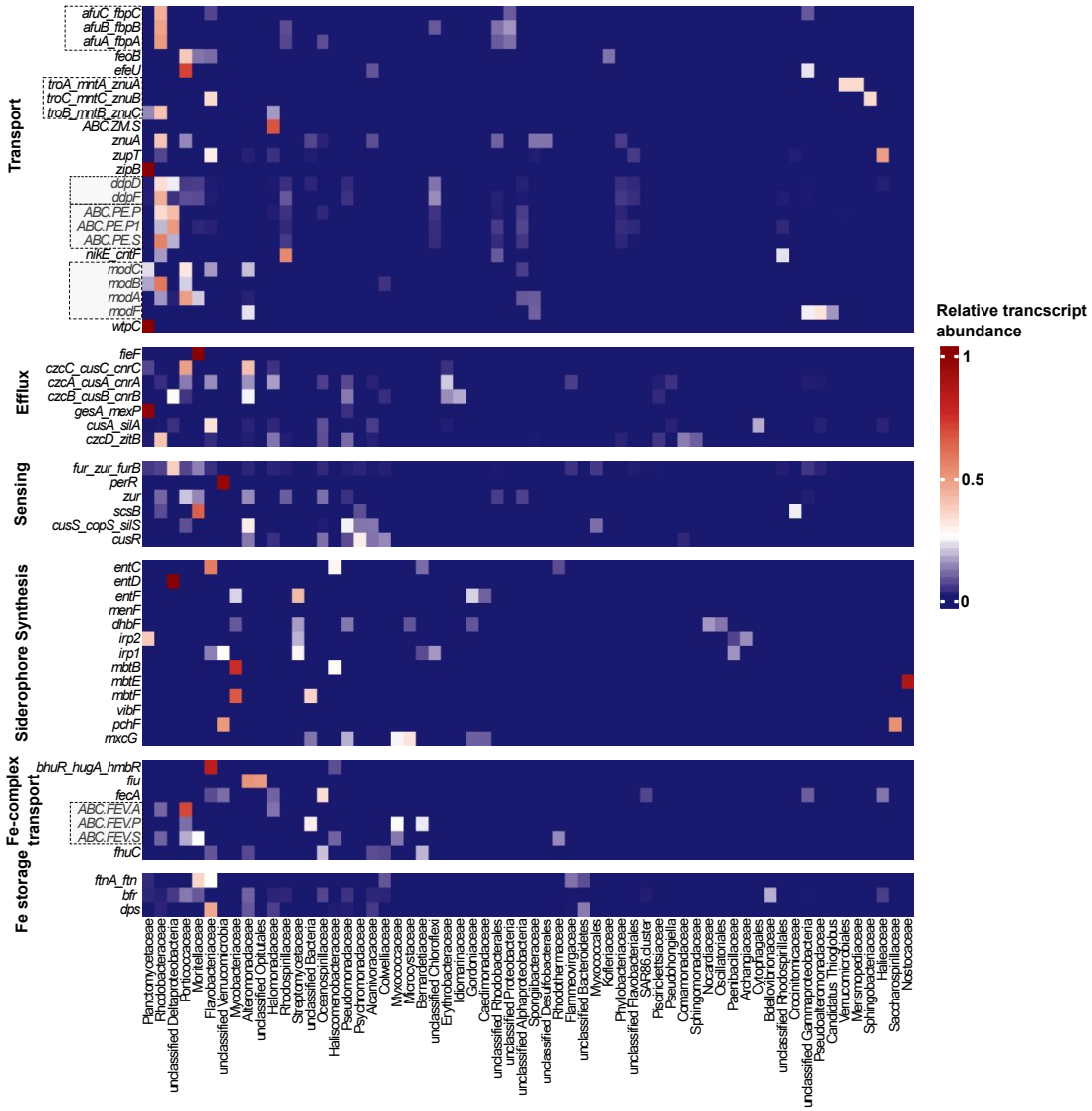

383 **Figure 3.** Taxonomic assignment of metal-related genes

384 Heatmap illustrating the relative contribution of prokaryotic groups to the expression of a given
385 KEGG orthologous (KO) gene in the particle-attached community (each KO gene sums up to 1
386 and 1 equals 100%). Phylogenetic groups are visualized on the family or lowest possible
387 taxonomic level. KO gene transcripts are grouped by function: transport, efflux and
388 sensing/regulation of 9 metals, siderophore synthesis, Fe-complex transport and Fe storage (as in
389 Fig. 2). The full description of the KEGG abbreviations is given in Fig. 2. The full gene name of

the Fe-complex transporter *bhuR_hugA_hmbR* is *tpA_hemR_IbpA_hpuB_bhuR_hugA_hmbR*. The corresponding heatmap for the control treatment is provided in Supplementary Fig. 9.

(*scsB*) were dominated by *Moritellaceae*. Relative transcript abundance could vary between subunits of the same transporter complex for a given taxonomic group, which could indicate differential regulation or the temporal decoupling of the expression of the subunits within diverse taxa.

Diverse bacterial groups contributed to siderophore biosynthesis, including *Flavobacteriaceae* (*entC*, *irp1*), *Deltaproteobacteria* (*entD*), *Mycobacteriaceae* (*mbtB, F*, *dhbF*, *entF*) and *Streptomycetaceae* (both A*ctinomycetales*)(*enFt*, *irp1,2*, *dhbF*), *Nostocaceae* (Cyanobacteria)(*mbtE*) and *Verrucomicrobia* (not assigned to the family level)(*pchF*, *irp1*). With the exception of *Flavobacteriaceae*, taxonomic groups involved in siderophore biosynthesis were distinct from those contributing to Fe-complex transport. Among these where *Rhodobacteraceae* (*ABC.FEV.A, S*), *Moritellaceae (ABC.FEV. S), Oceanospirillaceae (fecA, fhuC), Halomonadaceae (fecA, ABC.FEV.A), Alteromonadaceae (fiu, fphuc)* and *Opitutales* (*Verrucomicrobia*)(*fiu*). The taxonomic groups that contributed to metal storage and sensing belonged to *Deltaproteobacteria* (*bfr*), *Porticoccaceae* (*bfr*), *Moritellaceae* (*ftn*, *bfr*), *Flavobactericeae* (*ftn, dps*) and *Alteromonadaceae* (*bfr, dps*), while Fe efflux transcripts (*fieF*) were assigned only to *Moritellaceae*.

Discussion

The metatranscriptomic response to particulate trace metals. We observed enhanced transcript abundances of genes involved in different trace metal related processes, including transport into and out of the cell, regulation and storage in particle-associated prokaryotic

communities from the Southern Ocean. The elevated gene transcript abundances of a variety of transporters for all metals, except for Cu and Co, points to an increased uptake by particle-attached cells. In the case of Fe, the uptake was further associated with extracellular mobilization owing to the synthesis of different types of siderophores. Metal uptake was mediated by selective transporters like those involved in the internalization of Fe-siderophores, and by weakly selective cation carriers such as for Mn/Zn/Fe (*tro*, *mnt*, *znu*) and Zn/Cd (*zip*). The enhanced abundance of transcripts involved in the regulation of metal uptake like *fur* (Fe) and *zur* (Zn), and in the two-component system for Cu sensing (*cus*) suggests the requirement for a strong control of metal transport when cells are attached to particles. Transport was also directed outward from the cell as revealed by efflux pumps for Co/Zn/Cd (*czc, zit*) and Cu (*cus*), indicating the need to manage the internal excess. Transcripts dedicated to Fe storage in ferritin (*ftn*) or the Fe storage protein *dps* further point to the management of excess concentrations, or as a sparing or redistribution strategy. This concurrent enhanced transcription of distinct metal-related genes by particle-attached heterotrophic prokaryotes suggests that the involved processes are governed by an overarching biological property.

The role of metal homeostasis. Homeostasis has been defined as an ensemble of cellular processes maintaining suitable intracellular metal concentrations under changing external conditions (Waldron and Robinson 2009). As previously described, homeostasis relies on a complex network of feedbacks and feed-forwards (Williams and Fraústo Da Silva 2003) and is associated with a diverse metabolic tool box including many functions for transport (inward and outward), external mobilization, sensing, buffering, sparing, storage and regulation (Ma et al. 2009; Chandrangsu et al. 2017). This essential property further ensures the timely insertion of a required metal to the protein of interest. The present study demonstrates that multiple pathways associated with metal homeostasis are activated by prokaryotes inhabiting marine particles.

Homeostasis of heterotrophic prokaryotes has been extensively investigated for a few metals and individual strains. The classical scenario of Fe homeostasis is that cells activate different mechanisms in response to varying external conditions, and to avoid the waste of energy or toxic effects the switch between processes of uptake, storage and efflux is strongly regulated (Andrews et al. 2003). As a consequence, within a microbial cell, some processes, for example siderophore production and uptake, can be differentially regulated over others, such as Fe storage in ferritin. The description of the homeostasis of Cu (Braymer and Giedroc 2014), Zn (Braymer and Giedroc 2014), Ni (Macomber and Hausinger 2011) and Mn (Jakubovics and Jenkinson 2001) lead to the same conclusion of a simultaneous up- and down- regulation of genes that participate in distinct processes, such the acquisition and efflux of elements. Our observations of the simultaneously higher transcript abundances of genes involved in the transport and also those involved in metal efflux and regulation seems, therefore, at odds with the concept of homeostasis.

Geochemical and biological complexity of marine particles. We propose the geochemical heterogeneity of particles inhabited by a taxonomically diverse community to resolve this apparent paradox. A large variety of individual particles, each a complex mixture of biogenic and lithogenic components, make up the pool of marine particulate matter. Metals can be found deeply enclosed in a matrix or weakly adsorbed at the surface, depending on the nature of the biogenic material, such as intact cells, aggregates or fecal pellets (Blain and Tagliabue 2016). Lithogenic material contains many fractions, presented by diverse chemical composition and degrees of crystallization (van der Merwe et al. 2019). This geochemical complexity can lead to a variety of metabolic responses that likely occur either within microstructures of individual particles or in the immediately surrounding region, the particle-sphere. In the present study, gene expression was determined after 12 days of incubation in the dark, when the activity of

462 phytoplankton within these particles was strongly reduced due to the lack of light. The presence
463 of active phytoplankton cells is unlikely to change the gene expression profiles of prokaryotes
464 attached to non-living particles. Phytoplankton, notably diatoms the dominant group in the
465 Southern Ocean, have no direct access to particulate metals, excluding the possibility of
466 competition with prokaryotes for this resource. Our observations rather suggest that prokaryotes
467 render a fraction of particulate metals bioavailable that could subsequently be accessible to
468 photoautotrophs. The gene expression patterns presented here are a global response of diverse
469 prokaryotic communities to the geochemical complexity of individual particles. We illustrate
470 below the roles of some prokaryotic groups, each composed of diverse taxa with specific
471 functions in trace element processing (Sun et al. 2021), and its link to homeostasis.

472 *Rhodobacteraceae* contributed to the expression of genes involved in homeostasis of several
473 metals, pointing to their prominent role in particulate trace element cycling. The metabolically
474 diverse *Roseobacter* clade contains multiple strategies to sense and react to the environment,
475 reflected in the patch-adapted life style of many members (Luo and Moran 2014; Held et al.
476 2019). A particular feature is the large repertoire of transporters including numerous pathways for
477 the acquisition of inorganic and organically complexed metals (Newton et al. 2010; Hogle et al.
478 2016). Several *Roseobacter* harbor the Fe response regulator (*irr*) (Rodionov et al. 2006) to sense
479 Fe indirectly through heme biosynthesis (Hogle et al. 2017), and the respective gene transcripts
480 were present in both treatments in the present study. Despite the overwhelming involvement of
481 *Roseobacter* to the uptake of several trace elements and the sensing of changes in their
482 concentration, this clade had minor contributions to the uptake of organically complexed Fe
483 (*ABC.FEV*).

484 The taxonomic assignments of siderophore biosynthesis genes were overall different to those for
485 uptake, indicating that siderophore bound Fe was available to nonproducing members of the

community (Cordero et al. 2012). This cross-feeding interaction could be an efficient strategy on particles where cells are in close vicinity to each other, facilitating sensing of available Fe sources. *Flavobacteriaceae* contributed to both the production of siderophores (*ent*, *irp*) and the utilization of organically-bound Fe, while regulating excess through the Fe storage proteins ferritin (*ftn*) and *dps*. *Flavobacteriaceae* are efficient degraders of polymeric compounds (Cottrell and Kirchman 2000) enriched within particles, a functional capability that could sustain their investment to the energetically costly pathway of siderophore biosynthesis. Fe-limiting conditions (Boiteau et al. 2016; Debeljak et al. 2019) and Fe pulses (Sijerčić and Price 2015) were both associated with enhanced siderophore production, and this process appears to be regulated by cell-cell communication (McRose et al. 2018). Our observations of the various types of siderophore biosynthesis and transporter gene transcripts indicate that a fraction of the particle-bound Fe needs to be rendered bioavailable and they illustrate the key role of diverse microbes in this process.

The higher transcript abundances for Cu were exclusively associated with efflux and resistance, but not with transport into the cell. The difference in the metal to phosphorus ratio between particulate matter and prokaryotic cells was most pronounced for Cu (Fig. 1), which indicates high and thus potentially toxic Cu concentrations within some particles. Transcripts were mostly affiliated with *Planctomycetaceae (ges, mex)* and *Flavobacteriaceae (cus*) and several families belonging to *Alteromonadales, such as Alteromonadaceae, Pseudomonadaceae* and *Psychromonodaceae (cus), and Moritellaceae (scs),* suggesting these groups make intense use of this metal under a strict homeostasis control (Posacka et al. 2019), because excess of Cu is highly toxic. Cu is required for many cellular functions, including multiple extracellular or periplasmic Cu-enzymes, like multi-copper oxidases, amine oxidases or lysine oxidases, all involved in the oxidation of diverse organic substrates. *Moritellaceae* possess a range of extracellular enzymes

510 particularly adapted to low temperatures (Malecki et al. 2013), enabling them to exploit complex
511 sources of organic matter, while *Alteromonadaceae* can efficiently utilize diverse labile substrates
512 (Pedler et al. 2014). These different strategies could result in the observed higher cell-specific
513 prokaryotic production on particles as compared to the control treatment. This enhanced
514 metabolic activity is consistent with the idea of particles as "hotspots" (Grossart et al. 2003;
515 Azam and Malfatti 2007) where concentrations of organic matter can be several orders of
516 magnitude higher than in surrounding seawater. The idea that particulate organic carbon
517 stimulated bulk prokaryotic activity is further supported by dose addition experiments identifying
518 carbon as growth-limiting for the prokaryotic community in the control treatments (data not
519 shown). The intense intracellular Cu regulation and efflux could be a consequence of the
520 enhanced particulate organic matter processing by members with different strategies.

521 One consequence of prokaryotic heterotrophic activity is the consumption of oxygen and thus the
522 creation of gradients of oxygenated conditions within particles, resulting in heterogeneity within
523 the same or between particles that could impact the metal homeostatic response of prokaryotes in
524 different ways. Fe(II) is mainly present under low oxygen concentrations and the higher transcript
525 abundances of Fe^{2+} uptake genes by prokaryotes on particles suggests the presence of low oxygen
526 micro-niches. One process typical for low oxygen environments is denitrification, the step-wise
527 reduction of nitrate (NO_3^-) to nitrite (NO_2^-), nitric oxide (NO), nitrous oxide and eventually
528 dinitrogen gas (N_2). Genes encoding periplasmic nitrate reductase (*nap*), nitric oxide reductase
529 (*norB*) and copper-containing nitrous oxide reductase (*nosZ*) were higher expressed on particles
530 (Log2fold change: 5.2-6.2)(Table S3). Concurrently, a number of genes involved in aerobic
531 processes such as nitrification were significantly enhanced on particles (Log2Fold 1.8-2.9)(Table
532 S3). We also identified higher abundances of transcripts related to nitrogen fixation (e.g. *nif*) in
533 the particle-attached prokaryotic community than in the control (Log2Fold 3.6-9.3)(Table S3).

534 Mo and Fe are key elements of nitrogenase, catalyzing the reduction of atmospheric dinitrogen
535 (N_2) to ammonia (NH_3). The *nifH* gene was exclusively assigned to *Deltaproteobacteria* (Fig.
536 S10), containing members that carry out N_2 fixation under low oxygen concentrations (Farnelid et
537 al. 2011). Together, these observations suggest the presence of niches with varying micro-
538 environmental conditions that support aerobic and anaerobic microbial metabolisms. The
539 involved prokaryotes and their respective metal requirements could reflect the impact of such
540 niches on the overall transcriptional response.

541

542 **Biogeochemical lessons and perspectives of the transcriptomic view of prokaryote-particle**
543 **interactions.** The intense trace metal processing on particles is tightly linked to the fraction of
544 particulate metals that is bioavailable. In the case of Fe, prokaryotic degradation of sinking
545 particles lead to the release of dissolved Fe or weak Fe ligands and the remineralization of
546 biogenic and lithogenic Fe occurs at different length scales (Boyd et al. 2010; Bressac et al.
547 2019). Our results provide a novel perspective to this view. The expression of metal-related genes
548 suggests that diverse chemical forms of dissolved Fe, including the short-lived state Fe(II), are
549 produced and utilized by prokaryotes. Moreover, the numerous highly enriched chatecholate-type
550 siderophore synthesis transcripts point to the production of the strongest known categories of Fe
551 binding ligands. Such strong ligands which promote mineral dissolution (Kalinowski et al. 2000)
552 at high dissolution rates (Akafia et al. 2014) could be released to scavenge Fe from different types
553 of minerals, such as ilmenite as observed in the particles used here (van der Merwe et al. 2019).
554 For metals other than Fe, knowledge on trace metal release linked to prokaryotic degradation of
555 particles is limited (Twining et al. 2014). Our results provide clues that these processes should be
556 significant and require further attention and quantification.

The metal-processing on particles could impact the surrounding environment. It is unlikely that the entire outward flow resulting from efflux pumps or release of ligands was entirely captured back by attached prokaryotes before dispersion by turbulence. Particles and their plumes are likely feeding the environment with a suite of regenerated dissolved metal species (Azam and Malfatti 2007; Stocker et al. 2008). Additionally, a consequence of prokaryotic activity is the transfer of a fraction of metals from an abiotic, in the form of particles, to a biotic reservoir, a starting point for a journey of metals in the microbial loop. In the light of our findings, the concept of the ferrous wheel (Kirchman 1996; Tortell et al. 1996) could be refined to pinpoint the role of non-living particles as source of bioavailable Fe, and it could further be extended to other trace elements leading to the microbial metal wheel.

Acknowledgments

We thank M. Coffin, The PI of the Heard Earth-Ocean-Biosphere Interactions (HEOBI) voyage and the crew and scientists of the Australian R/V *Investigator* for their support during the cruise (IN 2016-V01). Thanks to the HEOBI trace-metal team for help in the collection of seawater. P. Catala carried out the flow cytometry analyses. We thank Gerhard J. Herndl for the opportunity to perform RNA extractions in the laboratory of the Microbial Oceanography Working Group in Vienna. We thank Laurie Bousquet and Sara Beier for their help and important discussions on RNA-Sequencing data analysis. The authors thank the Roscoff Bioinformatics platform ABiMS (http://abims.sb-roscoff.fr) for providing computational resources. We thank M. A. Moran and M. Landa for providing the internal standards for further *in vitro* transcription. This work was supported by the French Research program of INSU-CNRS LEFE/CYBER ("Les enveloppes fluides et l'environnement" – "Cycles biogéochimiques, environnement et ressources") of the

project PACBO, the International Collaborative Program CNRS-PICS of the project FASO, the Austrian FWF grant under the number P28781-B21. The research was also supported by the Australian Research Council (DP150100345 to ARB), the Antarctic Climate and Ecosystems CRC, and Australian Antarctic Science program (AAS4338 to ARB). The HEOBI voyage shiptime was supported by the Australian Marine National Facility. The authors declare no conflict of interest. We thank two referees whose comments and suggestions helped improve a previous version of the manuscript.

589 **References**

590 Akafia, M. M., J. M. Harrington, J. R. Bargar, and O. W. Duckworth. 2014. Metal oxyhydroxide
591 dissolution as promoted by structurally diverse siderophores and oxalate. Geochimica et
592 Cosmochimica Acta **141**: 258–269. doi:10.1016/j.gca.2014.06.024
593 Altschul, S. F., W. Gish, W. Miller, E. W. Myers, and D. J. Lipman. 1990. Basic local alignment
594 search tool. Journal of Molecular Biology **215**: 403–410. doi:10.1016/S0022-
595 2836(05)80360-2
596 Andrews, S. C., A. K. Robinson, and F. Rodrigez-Quinones. 2003. Bacterial iron homeostasis.
597 FEMS Microbiology reviews **27**: 215–237.
598 Angel, R., P. Claus, and R. Conrad. 2012. Methanogenic archaea are globally ubiquitous in
599 aerated soils and become active under wet anoxic conditions. The ISME Journal **6**: 847–
600 862. doi:10.1038/ismej.2011.141
601 Azam, F., and F. Malfatti. 2007. Microbial structuring of marine ecosystems. Nat Rev Microbiol **5**:
602 782–791. doi:10.1038/nrmicro1747
603 Barbeau, K., J. W. Moffett, D. A. Caron, P. L. Croot, and D. L. Erdner. 1996. Role of protozoan
604 grazing in relieving iron limitation of phytoplankton. Nature **380**: 61–64.
605 doi:10.1038/380061a0
606 Beier, S., P. Holtermann, D. Numberger, T. Schott, L. Umlauf, and K. Jürgens. 2018. A
607 metatranscriptomics-based assessment of small-scale mixing of sulfidic and oxic waters
608 on redoxcline prokaryotic communities. Environ Microbiol 1462-2920.14499.
609 doi:10.1111/1462-2920.14499
610 Blain, S., and A. Tagliabue. 2016. Iron cycle in oceans, ISTE Ltd/John Wiley and Sons Inc.

611 Boiteau, R. M., D. R. Mende, N. J. Hawco, and others. 2016. Siderophore-based microbial
612 adaptations to iron scarcity across the eastern Pacific Ocean. Proc Natl Acad Sci USA
613 **113**: 14237–14242. doi:10.1073/pnas.1608594113
614 Bolger, A. M., M. Lohse, and B. Usadel. 2014. Trimmomatic: a flexible trimmer for Illumina
615 sequence data. Bioinformatics **30**: 2114–2120. doi:10.1093/bioinformatics/btu170
616 Bowie, A. R., A. T. Townsend, D. Lannuzel, T. A. Remenyi, and P. van der Merwe. 2010. Modern
617 sampling and analytical methods for the determination of trace elements in marine
618 particulate material using magnetic sector inductively coupled plasma–mass
619 spectrometry. Analytica Chimica Acta **676**: 15–27. doi:10.1016/j.aca.2010.07.037
620 Boyd, P. W., and M. J. Ellwood. 2010. The biogeochemical cycle of iron in the ocean. Nature
621 Geoscience **3**: 675–682. doi:10.1038/ngeo964
622 Boyd, P. W., E. Ibisanmi, S. G. Sander, K. A. Hunter, and G. A. Jackson. 2010. Remineralization of
623 upper ocean particles: Implications for iron biogeochemistry. Limnology and
624 Oceanography **55**: 1271–1288. doi:10.4319/lo.2010.55.3.1271
625 Braymer, J. J., and D. P. Giedroc. 2014. Recent developments in copper and zinc homeostasis in
626 bacterial pathogens. Current Opinion in Chemical Biology **19**: 59–66.
627 doi:10.1016/j.cbpa.2013.12.021
628 Bressac, M., C. Guieu, M. J. Ellwood, and others. 2019. Resupply of mesopelagic dissolved iron
629 controlled by particulate iron composition. Nat. Geosci. **12**: 995–1000.
630 doi:10.1038/s41561-019-0476-6
631 Buchfink, B., C. Xie, and D. H. Huson. 2015. Fast and sensitive protein alignment using
632 DIAMOND. Nature Methods **12**: 59–60. doi:10.1038/nmeth.3176

633 Chandrangsu, P., C. Rensing, and J. D. Helmann. 2017. Metal homeostasis and resistance in
634 bacteria. Nat Rev Microbiol **15**: 338–350. doi:10.1038/nrmicro.2017.15
635 Cordero, O. X., L.-A. Ventouras, E. F. DeLong, and M. F. Polz. 2012. Public good dynamics drive
636 evolution of iron acquisition strategies in natural bacterioplankton populations.
637 Proceedings of the National Academy of Sciences **109**: 20059–20064.
638 doi:10.1073/pnas.1213344109
639 Cottrell, M. T., and D. L. Kirchman. 2000. Natural assemblages of marine proteobacteria and
640 members of the cytophaga-flavobacter cluster consuming low- and high-molecular-
641 weight dissolved organic matter. Applied environmental Microbiology **66**: 1692–1697.
642 Debeljak, P., E. Toulza, S. Beier, S. Blain, and I. Obernosterer. 2019. Microbial iron metabolism as
643 revealed by gene expression profiles in contrasted Southern Ocean regimes. Environ
644 Microbiol **21**: 2360–2374. doi:10.1111/1462-2920.14621
645 Farnelid, H., A.F. Andersson, S. Bertilsson, W.A. Al-Soud, L.H. Hansen, S. Sorensen, G.F. Steward,
646 A. Hagström, and L. Riemann. 2011. Nitrogenase gene amplifications from global marine
647 surface waters are dominated by genes of non-cyanobacteria. PLosONE **6**: e19223
648 Grossart, H.-P., T. Kiorboe, K. Tang, and H. Ploug. 2003. Bacterial Colonization of Particles:
649 Growth and Interactions. Applied and Environmental Microbiology **69**: 3500–3509.
650 Gu, Z., R. Eils, and M. Schlesner. 2016. Complex heatmaps reveal patterns and correlations in
651 multidimensional genomic data. Bioinformatics **32**: 2847–2849.
652 doi:10.1093/bioinformatics/btw313
653 Held, N. A., M. R. McIlvin, D. M. Moran, M. T. Laub, and M. A. Saito. 2019. Unique Patterns and
654 Biogeochemical Relevance of Two-Component Sensing in Marine Bacteria O. Mason

[ed.]. mSystems **4**: e00317-18, /msystems/4/1/msys.00317-18.atom. doi:10.1128/mSystems.00317-18

Hogle, S. L., B. Brahamsha, and K. A. Barbeau. 2017. Direct Heme Uptake by Phytoplankton-Associated *Roseobacter* Bacteria J. Weitz [ed.]. mSystems **2**: e00124-16, /msys/2/1/e00124-16.atom. doi:10.1128/mSystems.00124-16

Hogle, S. L., J. C. Thrash, C. L. Dupont, and K. A. Barbeau. 2016. Trace Metal Acquisition by Marine Heterotrophic Bacterioplankton with Contrasting Trophic Strategies V. Müller [ed.]. Appl. Environ. Microbiol. **82**: 1613–1624. doi:10.1128/AEM.03128-15

Huerta-Cepas, J., D. Szklarczyk, D. Heller, and others. 2019. eggNOG 5.0: a hierarchical, functionally and phylogenetically annotated orthology resource based on 5090 organisms and 2502 viruses. Nucleic Acids Res. **47**: D309–D314. doi:10.1093/nar/gky1085

Hyatt, D., G.-L. Chen, P. F. LoCascio, M. L. Land, F. W. Larimer, and L. J. Hauser. 2010. Prodigal: prokaryotic gene recognition and translation initiation site identification. BMC Bioinformatics **11**: 119. doi:10.1186/1471-2105-11-119

Irving, H., and R. J. P. Williams. 1948. Order of Stability of Metal Complexes. Nature **162**: 746–747. doi:10.1038/162746a0

Jakubovics, N. S., and H. F. Jenkinson. 2001. Out of the iron age: new insights into the critical role of manganese homeostasis in bacteria. Microbiology **147**: 1709–1718. doi:10.1099/00221287-147-7-1709

Kalinowski, B. E., L. J. Liermann, S. Givens, and S. L. Brantley. 2000. Rates of bacteria-promoted solubilization of Fe from minerals: a review of problems and approaches. Chemical Geology **169**: 357–370. doi:10.1016/S0009-2541(00)00214-X

678 Kanehisa, M., Y. Sato, M. Kawashima, M. Furumichi, and M. Tanabe. 2016a. KEGG as a reference
679 resource for gene and protein annotation. Nucleic Acids Research **44**: D457–D462.
680 doi:10.1093/nar/gkv1070
681 Kanehisa, M., Y. Sato, and K. Morishima. 2016b. BlastKOALA and GhostKOALA: KEGG Tools for
682 Functional Characterization of Genome and Metagenome Sequences. J. Mol. Biol. **428**:
683 726–731. doi:10.1016/j.jmb.2015.11.006
684 Kirchman, D. L. 1996. Microbial ferrous wheel. Nature 303–304.
685 Kopylova, E., L. Noé, and H. Touzet. 2012. SortMeRNA: fast and accurate filtering of ribosomal
686 RNAs in metatranscriptomic data. Bioinformatics **28**: 3211–3217.
687 doi:10.1093/bioinformatics/bts611
688 Langmead, B., and S. L. Salzberg. 2012. Fast gapped-read alignment with Bowtie 2. Nature
689 Methods **9**: 357–359. doi:10.1038/nmeth.1923
690 Li, D., C.-M. Liu, R. Luo, K. Sadakane, and T.-W. Lam. 2015. MEGAHIT: an ultra-fast single-node
691 solution for large and complex metagenomics assembly via succinct de Bruijn graph.
692 Bioinformatics **31**: 1674–1676. doi:10.1093/bioinformatics/btv033
693 Li, M., B. M. Toner, B. J. Baker, J. A. Breier, C. S. Sheik, and G. J. Dick. 2014. Microbial iron uptake
694 as a mechanism for dispersing iron from deep-sea hydrothermal vents. Nat Commun **5**:
695 3192. doi:10.1038/ncomms4192
696 Liao, Y., G. K. Smyth, and W. Shi. 2014. featureCounts: an efficient general purpose program for
697 assigning sequence reads to genomic features. Bioinformatics **30**: 923–930.
698 doi:10.1093/bioinformatics/btt656

699 Lis, H., C. Kranzler, N. Keren, and Y. Shaked. 2015. A Comparative Study of Iron Uptake Rates and
700 Mechanisms amongst Marine and Fresh Water Cyanobacteria: Prevalence of Reductive
701 Iron Uptake. Life **5**: 841–860. doi:10.3390/life5010841
702 Love, M. I., W. Huber, and S. Anders. 2014. Moderated estimation of fold change and dispersion
703 for RNA-seq data with DESeq2. Genome Biol **15**. doi:10.1186/s13059-014-0550-8
704 Luo, H., and M. A. Moran. 2014. Evolutionary Ecology of the Marine Roseobacter Clade.
705 Microbiol. Mol. Biol. Rev. **78**: 573–587. doi:10.1128/MMBR.00020-14
706 Ma, Z., F. E. Jacobsen, and D. P. Giedroc. 2009. Coordination Chemistry of Bacterial Metal
707 Transport and Sensing. Chem. Rev. **109**: 4644–4681. doi:10.1021/cr900077w
708 Macomber, L., and R. P. Hausinger. 2011. Mechanisms of nickel toxicity in microorganisms.
709 Metallomics **3**: 1153. doi:10.1039/c1mt00063b
710 Malecki, P. H., J. E. Raczynska, C. E. Vorgias, and W. Rypniewski. 2013. Structure of a complete
711 four-domain chitinase from *Moritella marina* , a marine psychrophilic bacterium. Acta
712 Crystallogr D Biol Crystallogr **69**: 821–829. doi:10.1107/S0907444913002011
713 Martin, J. H., M. R. Gordon, and S. E. Fitzwater. 1992. Iron limitation in Antatrctic waters. Nature
714 **345**: 156–158.
715 Mazzotta, M., M. R. McIlvin, and M. A. Saito. 2020. Characterization of the Fe Metalloproteome
716 of a Ubiquitous Marine Heterotroph, Pseudoalteromonas (BB2-AT2): Multiple
717 Bacterioferritin Copies Enable Significant Fe Storage. preprint.
718 McQuaid, J. B., A. B. Kustka, M. Oborník, and others. 2018. Carbonate-sensitive phytotransferrin
719 controls high-affinity iron uptake in diatoms. Nature **555**: 534–537.
720 doi:10.1038/nature25982

McRose, D. L., O. Baars, M. R. Seyedsayamdost, and F. M. M. Morel. 2018. Quorum sensing and iron regulate a two-for-one siderophore gene cluster in *Vibrio harveyi*. Proc Natl Acad Sci USA **115**: 7581–7586. doi:10.1073/pnas.1805791115

van der Merwe, P., K. Wuttig, T. Holmes, T. W. Trull, Z. Chase, A. T. Townsend, K. Goemann, and A. R. Bowie. 2019. High Lability Fe Particles Sourced From Glacial Erosion Can Meet Previously Unaccounted Biological Demand: Heard Island, Southern Ocean. Front. Mar. Sci. **6**: 332. doi:10.3389/fmars.2019.00332

Newton, R. J., L. E. Griffin, K. M. Bowles, and others. 2010. Genome characteristics of a generalist marine bacterial lineage. ISME J **4**: 784–798. doi:10.1038/ismej.2009.150

Obernosterer, I., U. Christaki, D. Lefèvre, P. Catala, F. Van Wambeke, and P. Lebaron. 2008. Rapid bacterial mineralization of organic carbon produced during a phytoplankton bloom induced by natural iron fertilization in the Southern Ocean. Deep Sea Research Part II: Topical Studies in Oceanography **55**: 777–789. doi:10.1016/j.dsr2.2007.12.005

Pedler, B. E., L. I. Aluwihare, and F. Azam. 2014. Single bacterial strain capable of significant contribution to carbon cycling in the surface ocean. Proceedings of the National Academy of Sciences **111**: 7202–7207. doi:10.1073/pnas.1401887111

Posacka, A. 2017. Biogeochemical cycling of copper in the Northeast Pacific Ocean : role of marine heterotrophic bacteria.doi:10.14288/1.0355246

Posacka, A. M., D. M. Semeniuk, and M. T. Maldonado. 2019. Effects of Copper Availability on the Physiology of Marine Heterotrophic Bacteria. Front. Mar. Sci. **5**: 523. doi:10.3389/fmars.2018.00523

742 Rauschenberg, S., and B. S. Twining. 2015. Evaluation of approaches to estimate biogenic
743 particulate trace metals in the ocean. Marine Chemistry **171**: 67–77.
744 doi:10.1016/j.marchem.2015.01.004
745 Rich, H. W., and F. M. M. Morel. 1990. Availability of well-defined iron colloids to the marine
746 diatom *Thalassiosira weissflogii*. Limnol. Oceanogr. **35**: 652–662.
747 doi:10.4319/lo.1990.35.3.0652
748 Rodionov, D. A., M. S. Gelfand, J. D. Todd, A. R. J. Curson, and A. W. B. Johnston. 2006.
749 Computational Reconstruction of Iron- and Manganese-Responsive Transcriptional
750 Networks in α-Proteobacteria. PLoS Comput Biol **2**: e163.
751 doi:10.1371/journal.pcbi.0020163
752 Rubin, M., I. Berman-Frank, and Y. Shaked. 2011. Dust- and mineral-iron utilization by the
753 marine dinitrogen-fixer Trichodesmium. Nature Geosci **4**: 529–534.
754 doi:10.1038/ngeo1181
755 Saito, M. A., D. M. Sigman, and F. M. M. Morel. 2003. The bioinorganic chemistry of the ancient
756 ocean: the co-evolution of cyanobacterial metal requirements and biogeochemical
757 cycles at the Archean–Proterozoic boundary? Inorganica Chimica Acta **356**: 308–318.
758 doi:10.1016/S0020-1693(03)00442-0
759 Sandy, M., and A. Butler. 2009. Microbial Iron Acquisition: Marine and Terrestrial Siderophores.
760 Chemical Reviews **109**: 4580–4595. doi:10.1021/cr9002787
761 Satinsky, B. M., S. M. Gifford, B. C. Crump, and M. A. Moran. 2013. Use of Internal Standards for
762 Quantitative Metatranscriptome and Metagenome Analysis. Microbial Metagenomics,
763 Metatranscriptomics, and Metaproteomics **531**: 237–250. doi:10.1016/B978-0-12-
764 407863-5.00012-5

765 Shaked, Y., and H. Lis. 2012. Disassembling Iron Availability to Phytoplankton. Frontiers in
766 Microbiology **3**. doi:10.3389/fmicb.2012.00123
767 Sijerčić, A., and N. Price. 2015. Hydroxamate siderophore secretion by Pseudoalteromonas
768 haloplanktis during steady-state and transient growth under iron limitation. Mar. Ecol.
769 Prog. Ser. **531**: 105–120. doi:10.3354/meps11338
770 Silva, J. J. R. F. da, and R. J. P. Williams. 2001. The biological chemistry of the elements: the
771 inorganic chemistry of life, 2nd ed. Oxford University Press.
772 Stocker, R., J. R. Seymour, A. Samadani, D. E. Hunt, and M. F. Polz. 2008. Rapid chemotactic
773 response enables marine bacteria to exploit ephemeral microscale nutrient patches.
774 Proceedings of the National Academy of Sciences **105**: 4209–4214.
775 doi:10.1073/pnas.0709765105
776 Strzepek, R. F., M. T. Maldonado, K. A. Hunter, R. D. Frew, and P. W. Boyd. 2011. Adaptive
777 strategies by Southern Ocean phytoplankton to lessen iron limitation: Uptake of
778 organically complexed iron and reduced cellular iron requirements. Limnol. Oceanogr.
779 **56**: 1983–2002. doi:10.4319/lo.2011.56.6.1983
780 Sun, Y., P. Debeljak and I. Obernosterer. 2021. Microbial iron and carbon metabolism as
781 revealed by taxonomy-specific functional diversity in the Southern Ocean. ISMEJ. doi:
782 10.1038/s41396-021-00973-3
783 Tagliabue, A., A. R. Bowie, P. W. Boyd, K. N. Buck, K. S. Johnson, and M. A. Saito. 2017. The
784 integral role of iron in ocean biogeochemistry. Nature **543**: 51–59.
785 Tortell, P. D., M. T. Maldonado, and N. M. Price. 1996. The role of heterotrophic bacteria in iron-
786 limited ocean ecosystems. Nature **383**: 330–332. doi:10.1038/383330a0

787 Twining, B. S., S. D. Nodder, A. L. King, and others. 2014. Differential remineralization of major
788 and trace elements in sinking diatoms. Limnology and Oceanography **59**: 689–704.
789 Velasquez, I. B., E. Ibisanmi, E. W. Maas, P. W. Boyd, S. Nodder, and S. G. Sander. 2016.
790 Ferrioxamine Siderophores Detected amongst Iron Binding Ligands Produced during the
791 Remineralization of Marine Particles. Front. Mar. Sci. **3**. doi:10.3389/fmars.2016.00172
792 Wackett, L. P., A. G. Dodge, and L. B. M. Ellis. 2004. Microbial Genomics and the Periodic Table.
793 Applied and Environmental Microbiology **70**: 647–655. doi:10.1128/AEM.70.2.647-
794 655.2004
795 Waldron, K. J., and N. J. Robinson. 2009. How do bacterial cells ensure that metalloproteins get
796 the correct metal? Nat Rev Microbiol **7**: 25–35. doi:10.1038/nrmicro2057
797 Williams, R. J. . P., and J. J. R. Fraústo Da Silva. 2003. Evolution was Chemically Constrained.
798 Journal of Theoretical Biology **220**: 323–343. doi:10.1006/jtbi.2003.3152
799
800

Response to Reviewers

Reviewer(s):

Reviewer: 1

Comments to the Author
My concerns have been fully addressed in this revision.

Minor points:
Line 444, the sentence beginning with "We propose the geochemical...": I can't figure out exactly what this sentence means. Perhaps give a bit more detail here of the proposed resolution.

Authors response : This part of the Discussion has now been modified ; we describe in a different manner our idea.

Line 516: Planctomycetaceae is misspelled.

Authors response : Thank you, this has been corrected.

Reviewer: 2

Comments to the Author
The revisions addressed many of the concerns raised by the reviewers and have resulted in a better paper. The authors still focus, however, on “homeostasis” and I still wonder if that’s the best strategy. I do understand more clearly than before what the authors mean by the term, but I think they could do more to help the reader see their argument. Are all metals and all organisms in equal homeostasis? What would the metatranscriptome data look like if an organism wasn’t in homeostasis?

Authors response : We would like to thank the Reviewer for another round of careful reading of our manuscript. To help the reader better understand why we use the concept of homeostasis to explain our results, we have now modified the start of the Discussion Section (p. 21-23). We first discuss the main finding that is the observation of the simultaneously higher transcript abundances of genes involved in different trace metal related processes, including transport into and out of the cell, regulation and storage (p. 21-22). We then intrododuce the concept of homeostasis (line 429-437), and illustrate this concept based on previous studies carried out for a single metal and in individual strains (line 439-450). In this paragraph, we have added a few more explanatory sentences to help understand why our observations appear at a first glance ‘at odds’ with the conclusions from these previous studies.

Our observations are a global response from a highly diverse prokaryotic community inhabiting different types of particles. All prokaryotic cells need to maintain suitable intracellular metal concentrations, but the requirements vary among taxa and metals. A given prokaryotic taxon could be actively taking up a given metal (in our case Rhodobacterales and Fe^{3+}), while another taxon transports the same metal out of the cell (Fe efflux, in our case Moritellaceae). Both processes are part of homeostasis. These taxa could deal with Fe in such a different way, because either they have very different Fe requirements or tolerances, or they are located in distinct particles with different Fe concentrations. Due to the geochemical complexity of our particles and the prokaryotic diversity, not all cells are regulating metal-related processes in the same way. Beceause metal homeostasis is an inherent biological property, the scenario of cells that are not regulating their metal requirements is unlikely to occur in the marine environment.

Regardless, the data are interesting and important even if a reader doesn't buy the homeostasis argument.

Authors response : Thank you for this supportive feedback. We hope our MS will stimulate the discussion and new research on this topic.

The paper has several simple mistakes in English and a few sentences that don't make sense. I wouldn't count on the copyeditor to correct these. I pointed out only some of the problems below.

Authors response : Thank you, we have carefully gone through the MS once more.

Specific comments

L27: The opening phrase of the Abstract ("Alongside the co-evolution of marine microorganisms and biogeochemical cycles…") is a bit clunky. I think the authors should try again. Maybe something like "As marine microorganisms and biogeochemical cycles evolved…." Not sure though if cycles "evolve" though.

Authors response : This sentence has been changed (line 28-29).

L54-55: The concluding phrase ("as determined by the different chemical composition…) doesn't make sense here—it's unclear to me. The easiest solution is to just delete it.

Authors response : This part of the sentence has been deleted.

L80: The authors here mean "constrained", not "constraint."

Authors response : Thank you, this has been corrected.

L100: Rather than “inside and out of the cell”, I think the authors mean “into and out of the cell.”

Authors response : Thank you, this has been corrected.

L157: “PFA” needs to be defined here, when it’s first used, I believe.

Authors response : Thank you, PFA has been written out.

L162: I don’t think the author mean that they did a type of epifluorescence microscopy in which they excited the sample with white light and looked at the resulting emission of green, blue and red light. I suspect they did “bright-field” microscopy (the colors are reflected from the sample, not emitted like from DAPI) and epifluorescence microscopy with blue-light excitation.

Authors response : We have added more details to this description (line 163-169).

L276: “KO” needs to be defined when first used.

Authors response : KO is first used on line 253 where it is written out

L297: Per surface “area”, not per surface “unit.”

Authors response : We have modified this to « ..cell abundance per unit (μm^2) of surface area » (line 301)

L298: Figure 1B x-axis label should be “particle class” not “surface class”. It should be under Figure 1C, implying it applies to panels B, C, and D. Or perhaps the label should be put under all three panels. For the Figure 1C y-axis label, “Prokaryote” should be capitalized.

Authors response : These modifications have been made on Fig. 1

L327: The Methods section in the main text should point out that the supplemental materials described the amplicon sequencing approach used to identify the bacterial taxa.

Authors response : We have added this information in the Material and Methods Section in the paragraph « Sampling for metatranscriptomics and prokaryotic diversity » (line 199-201).

L347: I think the authors mean “weakly” selective, not “poorly” selective.

Authors response : Thank you, this has been corrected.

L354: The authors need to define what ** means.

Authors response : There are not two stars (**), but one star (*) and a (+) sign. To differentiate these symbols better, we now use a * and M, the latter indicating genes potentially implicated in the transport of multiple metals.

L364: The authors make an important observation about the transcripts for siderophore synthesis compared with others. More information should be given and data mentioned. For example, it’s not clear if the “up to 10” is about the enhanced siderophore synthesis or about the difference between siderophore synthesis and expression of other genes. Also, I wonder if a statistical test should be done. But maybe more info about the differences, more than just “up to 10”, would be sufficient.

Authors response : These aspects are described in the manuscript. As for all transcripts considered in our study, the Log2-fold change has been calculated with respect to the control incubations. This is explained in the starting sentence of this paragraph (line 340-341). The differences in the transcript abundances were tested statistically and all significantly different transcript abundances are indicated by an asterisk(*) on Fig. 2.

We appreciate the Reviewers interest in this particular observation. We think that Fig. 2 presents all these data in a detailed manner, providing the KO gene name, its abbreviation and the respective Log2-fold changes. Our main message here is that prokaryotes on particles are expressing a lot more (Log2Fold 2.5 to 10) genes for siderophore biosynthesis than prokaryotes in the absence of particles.

We describe siderophore biosynthesis genes in detail also in the context of the respective taxonomic assignations (line 484-498).

L397: Not clear what “these latter” refers to.

Authors response : We eliminated the « latter » to clarify the sentence.

L438: What “switch” are the authors talking about here?

Authors response : We refer here to the switch between cellular processes that are activated when a cell needs to take up Fe and those when a cell needs to store or transport Fe out of the cell to avoid any toxic effect. This is now clarified in the text (line 439-450).

L444: It’s not clear to me why the authors’ results are “at odds” with the conclusion of a previous study about the “simultaneous up- and down- regulation of participating systems.”

Authors response : Homeostasis has been extensively investigated for a few metals (Fe, Cu, Zn and Ni) and individual bacterial strains. These previous studies lead to the same conclusion : genes that participate to distinct metal related processes, e.g. uptake vs efflux of a given metal, are simultaneously up- and down-regulated. Our data, however, suggest that the genes related to these distinct processe are all upregulated in prokaryotes inhabiting particles. This observations appears at odds with the previous findings.

In response to the Reviewers’ question, we have modified this part of the discussion (line 439-450).

L477: So, if Roseobacter didn’t contribute much to organic Fe uptake, any evidence that it did more with inorganic Fe?

Authors response : Our results indeed show that Rhodobacteraceae dominated the Fe(III) uptake transcripts, suggesting this form of iron to be the preferred source for this bacterial group. This information is shown by the high relative transcript abundances assigned to Rhodobacteraceae of the afu, fbp A, B, C on Fig. 3. The KO genes are explained in Fig. 2 : iron (III) transport system ATP-binding protein, ABC type.

We describe this observation in the Results Section (line 374) and we refer to it in the Discussion Section, on line 472-483, in combination with other metals.

L479: This paragraph about Roseobacter and organic Fe use is very interesting and important. It would be also interesting and important to hear about taxa active in taking up Fe+2 vs. Fe+3.

Authors response : The transcripts for Fe(III) uptake were dominated by Rhodobacteraceae, while *Porticoccaceae* (*Cellvibrionales*), *Moritellaceae* (*Alteromonadales*) and *Flavobacteriaceae (*Flavobacteriales contributed to those of Fe(II) uptake (feoB, efeU). This information is illustrated in Fig. 3 and described in the Results Section (line 372-376).

L520: At first, I thought that there is highly unlikely that Cu is at toxic levels in this very pristine ocean, and still think it's unlikely. But the authors could point out that Cu levels in particular matter were higher than that required by cells (Fig 1) and the difference between particular matter and cellular Cu levels is greater, I believe, than for other metals.

Authors response : We thank the Reviewer for pointing this out, this is indeed an interesting link between the chemical analyses and our metatranscriptomic observations. We have added a sentence in the revised version of the MS (line 500-502).